Check for updates

Geochemistry, Geophysics, Geosystems

RESEARCH ARTICLE
10.1029/2020GC009466

Special Section:
Tethyan dynamics: from rifting to collision

The Deep Structure of the Alps Based on the CIFALPS Seismic Experiment: A Synthesis

M. G. Malusà[1,2], S. Guillot[3], L. Zhao[4], A. Paul[3], S. Solarino[2], T. Dumont[3], S. Schwartz[3], C. Aubert[3], P. Baccheschi[5], E. Eva[2], Y. Lu[3], C. Lyu[4], S. Pondrelli[5], S. Salimbeni[5], W. Sun[7], and H. Yuan[8,9,10]

[1]Department of Earth and Environmental Sciences, University of Milano-Bicocca, Milan, Italy, [2]Istituto Nazionale di Geofisica e Vulcanologia, ONT, Genova, Italy, [3]University of Grenoble Alpes, University of Savoie Mont Blanc, CNRS, IRD, IFSTTAR, ISTerre, Grenoble, France, [4]State Key Laboratory of Lithospheric Evolution, Institute of Geology and Geophysics, Chinese Academy of Sciences, Beijing, China, [5]Istituto Nazionale di Geofisica e Vulcanologia, Bologna, Italy, [7]Key Laboratory of Earth and Planetary Physics, Institute of Geology and Geophysics, Chinese Academy of Sciences, Beijing, China, [8]Department of Earth and Planetary Sciences, ARC Centre of Excellence for Core to Crust Fluids Systems, Macquarie University, North Ryde, Australia, [9]Centre for Exploration Targeting, University of Western Australia, Perth, Australia, [10]Geological Survey of Western Australia, Perth, Australia

Key Points:

- Summary of the main results of the CIFALPS seismic experiment provides new insights on the deep tectonic structure of the Alpine region
- Application of a wide range of tomographic methods and joint interpretation with geological and petrophysical data
- Interpretive geologic cross-sections at the scale of the lithosphere and the upper mantle

Correspondence to:
M. G. Malusà
marco.malusa@unimib.it

Citation:
Malusà, M. G., Guillot, S., Zhao, L., Paul, A., Solarino, S., Dumont, T., et al. (2021). The deep structure of the Alps based on the CIFALPS seismic experiment: A synthesis. *Geochemistry, Geophysics, Geosystems*, *22*, e2020GC009466. https://doi.org/10.1029/2020GC009466

Received 6 OCT 2020
Accepted 4 FEB 2021

© 2021. American Geophysical Union. All Rights Reserved.

Abstract The European Alps are the site where classic geologic concepts such as nappe theory, continental subduction and slab breakoff have been first proposed. However, the deep tectonic structure of the Alps has long been poorly constrained by independent geophysical evidence. This review paper summarizes the main results of the CIFALPS passive seismic experiment, that was launched by Chinese, French and Italian scientists in the 2010s to provide new insights on the deep tectonic structure of the Alpine region. The application of a wide range of tomographic methods to the analysis of a single fossil subduction zone makes the CIFALPS experiment a potential reference case for the analysis of other orogenic belts. Major results include: (i) the first seismic evidence of European continental crust subducted into the Adriatic upper mantle, beneath the place where coesite was first recognized in continental (U)HP rocks in the Alps; (ii) evidence of a major involvement of the mantle wedge during (U)HP rock exhumation; (iii) evidence of a serpentinized plate interface favoring continental subduction; (iv) evidence of a continuous slab beneath the Western and Central Alps, ruling out the classic model of slab breakoff magmatism; (v) evidence of a polyphase development of anisotropic fabrics in the Alpine mantle, either representing active mantle flows or fossil fabrics inherited from previous rifting stages. Detection of these major tectonic features allows to propose interpretive geologic cross-sections at the scale of the lithosphere and upper mantle, providing a baseline for future analyses of active continental margins.

Plain Language Summary The European Alps are the site where classic geologic concepts such as nappe theory, continental subduction, and slab breakoff have been first proposed. However, the deep tectonic structure of the Alps has long been poorly constrained by independent geophysical evidence. This review paper summarizes the main results of the CIFALPS passive seismic experiment, which allows us to propose an updated image of the deep structure of the Alps at the scale of the lithosphere and the upper mantle. The concepts and ideas summarized in this article provide a baseline for further advances in the fields of Alpine tectonics and in the analysis of active continental margins more generally.

1. Introduction

The European Alps are one of the best studied orogenic belts in the world, and the site where classic concepts of major relevance for the development of Earth Sciences have been first proposed. Beside the nappe theory (Argand, 1911; Lugeon, 1901), these include the concept of continental subduction, that was considered as impossible until the discovery of coesite in eclogite-facies rocks of the Dora-Maira massif (Chopin, 1984), and the concept of slab breakoff that was first proposed by Davies and von Blanckenburg (1995) to explain the enigmatic Cenozoic magmatism in the Alps and that was subsequently applied to many other orogenic belts worldwide (Garzanti et al., 2018). Despite the relevance of these processes at a broader scale, the deep tectonic structure of the Alps has long been poorly constrained by independent geophysical evidence. The active seismic experiments launched in the 1980s (e.g., Frei et al., 1990; Nicolas et al., 1990b;

Roure et al., 1996) even failed to clearly detect the Moho beneath the Internal Alps, and the travel-time tomography models available since the 2000s (e.g., Lippitsch et al., 2003; Piromallo & Morelli, 2003) did provide first-order constraints to the deep Alpine structure although they were not invariably consistent.

Within this framework, the aim of the CIFALPS passive seismic experiment, launched in the 2010s through a collaboration among Chinese, French, and Italian scientists (Zhao et al., 2016a) was to provide new insights on the deep tectonic structure of the Alpine region, based on recent developments in the fields of seismic data acquisition and tomography model computation, through a full collaboration between geologists and geophysicists. The main geophysical results provided by the CIFALPS experiment have been already published in international journals (Beller et al., 2018; Lyu et al., 2017; Malusà et al., 2017; Salimbeni et al., 2018; Solarino et al., 2018; Sun et al., 2019; Zhao et al, 2015, 2016a, 2020). In this review paper, mainly aimed at a geologic audience, we summarize the main results of the CIFALPS experiment that are discussed within the framework of available geologic and geodynamic constraints to provide an updated image of the deep structure of the Alps at the scale of the lithosphere and the upper mantle. We hope that the concepts and ideas summarized in this article will help provide a baseline for further advances in the fields of Alpine tectonics and in the analysis of active continental margins more generally.

2. Tectonic Setting

The European Alps are the result of oblique subduction of the Alpine Tethys under the Adriatic microplate since the Late Cretaceous, followed by diachronous continental collision between the Adriatic and European paleomargins during the Cenozoic (e.g., Handy et al., 2010; Coward & Dietrich, 1989; Dal Piaz, 2001; Pfiffner, 2014; Schmid et al., 2004; Trümpy, 1960) (Figure 1a). In the western segment of the orogen, European basement rocks and associated Helvetic-Dauphinois cover sequences that have partly escaped Alpine metamorphism are exposed in the External zone, to the west of the Frontal Pennine Fault (FPF in Figure 1b) (e.g., Bellahsen et al., 2014; Dumont et al., 2011, 2012). To the east of the Frontal Pennine Fault, the subduction wedge formed atop the European slab is still largely preserved (e.g., Beltrando et al., 2010; Lardeaux et al., 2006) and chiefly includes rocks derived from the Alpine Tethys and the distal European paleomargin (Lemoine et al., 1986; Tricart, 1984), the so-called Penninic units (Argand, 1911) (shades of blue in Figure 1b). Rocks derived from the Adriatic paleomargin (brown in Figure 1b), classically referred to as the Austroalpine-Southalpine units (e.g., Bernoulli et al., 1979; Mohn et al., 2010), are exposed north of the Po Plain on the upper-plate side of the orogen. There, the Ivrea gravity anomaly (Closs & Labrouste 1963) reveals the occurrence of mantle rocks exhumed at shallow depth that may mark the lithospheric necking zone of the southern Tethyan margin (Nicolas et al., 1990a). Eclogitized mantle rocks are exposed in the Lanzo massif to the west of the Insubric Fault (IF in Figure 1b) (Boudier, 1978; Piccardo et al., 2007). South of the Po Plain, the complex transition zone between the Western Alps and the Apennines involves rotated fragments of the Alpine subduction wedge (Eva et al., 2015; Maffione et al., 2008) and is mainly covered by thick Cenozoic sedimentary successions (Malusà & Balestrieri, 2012; Rossi et al., 2009).

The subduction wedge of the Western Alps includes two main tectono-metamorphic domains (e.g., Malusà et al., 2011, 2015): (i) an Eocene eclogite belt consisting of (ultra) high pressure—(U)HP continental crust domes of European derivation (DM, GP, and MR in Figure 1b) (e.g., Dal Piaz & Lombardo, 1986; Henry et al., 1993) tectonically enveloped by (U)HP metaophiolites (e.g., Lombardo et al., 1978; Schwartz et al., 2000); and (ii) a doubly vergent Frontal wedge consisting of lower-pressure metamorphic units exposed closer to the European mainland (e.g., Caby, 1996; Michard et al., 2004). The (U)HP rocks of the Eclogite belt reached the pressure peak in the late Eocene (e.g., Gabudianu Radulescu et al., 2009; Rubatto & Hermann, 2001) and were rapidly exhumed to Earth's surface by the early Oligocene, when they were unconformably covered by syntectonic sediments still preserved in the Tertiary Piedmont Basin (Federico et al., 2004; Malusà et al., 2015) (Figure 1b). Quartz-eclogite assemblages prevail, but rock slivers with coesite-eclogite assemblages are found in the Dora-Maira dome (Chopin et al., 1991; Groppo et al., 2019) and on top of the Monte Rosa dome (Lapen et al., 2003; Reinecke, 1991). The lower-pressure metamorphic units of the Frontal wedge include blueschist-to-(sub)greenschist facies cover sequences and basement slivers that underwent subduction starting from the Paleocene, and were later exhumed in the Eocene—early Oligocene (e.g., Agard et al., 2002; Ganne et al., 2007; Lanari et al., 2014). Different tectonostratigraphic

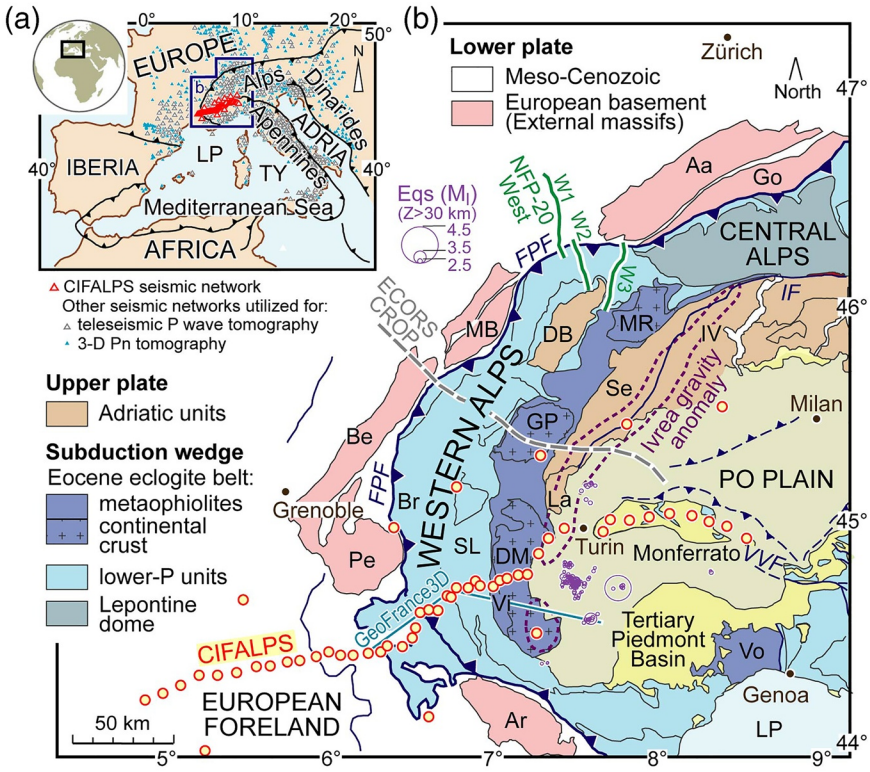

Figure 1. Tectonic setting of the study area. (a) Tectonic sketch map of the Adria-Europe plate boundary zone, and distribution of seismic stations of the CIFALPS experiment and other networks used for the teleseismic P-wave and 3D Pn tomographies of Zhao et al. (2016b) and Sun et al. (2019). (b) Geologic map of the Western Alps (modified after Bigi et al., 1990; Malusà et al., 2015), with location of previous geophysical transects indicated (ECORS CROP, NFP-20 West, GeoFrance 3D) and CIFALPS temporary stations. The Ivrea gravity anomaly (0 mGal isoline, in purple, after Bigi et al., 1990) and the locations of anomalously deep earthquakes beneath the Po Plain (Eva et al., 2015; Malusà et al., 2017) are also indicated. Acronyms: Aa, Aar; Ar, Argentera; Be, Belledonne; Br, Briançonnais; DB, Dent Blanche; DM, Dora-Maira; FPF, Frontal Pennine Fault; Go, Gotthard; GP, Gran Paradiso; IF, Insubric Fault; IV, Ivrea-Verbano; La, Lanzo; LP, Ligurian-Provençal; MB, Mont Blanc; MR, Monte Rosa; Pe, Pelvoux; Se, Sesia-Lanzo; SL, Schistes lustrés; TY, Tyrrhenian; Vi, Viso; Vo, Voltri; VVF, Villalvernia-Varzi Fault.

domains are exposed in different segments of the Frontal wedge, likely reflecting the obliquity of the Alpine trench relative to the European paleomargin. In the northern part of the Western Alps, the Frontal wedge includes Valaisan metasediments with minor metaophiolites and upper Paleozoic continental metaclastics (Bertrand et al., 1998; Masson et al., 2008; Polino et al., 2012), juxtaposed against Briançonnais (Br in Figure 1b) basement units in the rear part of the wedge (Bergomi et al., 2017; Malusà et al., 2005). In the southern part of the Western Alps, the Frontal wedge includes turbidites and Briançonnais cover sequences (Barfety et al., 1996; Kerckhove, 1969) juxtaposed against the oceanic metasediments of the Schistes lustrés (SL in Figure 1b) (Agard et al., 2002; Polino & Lemoine, 1984; Schwartz et al., 2009). Progressively more distal facies are thus accreted in the Frontal wedge moving from the North toward the South, but the effects of oblique subduction are also observed in the Eclogite belt, where the relative amount of oceanic crust comprised within the eclogitic tectonic domes increases toward the south and is dominant in the Voltri massif (Capponi & Crispini, 2002; Forcella et al., 1973). The well preserved domal shape of the Dora-Maira and Gran Paradiso massifs (Figure 1b) suggests only minor late-stage indentation of the Adriatic upper plate beneath the southern segments of the Alpine subduction wedge, whereas farther north the Monte Rosa dome is evidently backfolded (Keller et al., 2005), and the Adriatic lower crust has been deeply indented beneath the Lepontine dome during the latest stages of hard continent-continent collision (Liao et al., 2018a; Pfiffner et al., 2002).

3. State of Knowledge Before the CIFALPS Experiment

Since the pioneering studies of Dolomieu (1791), Kilian and Revil (1903), Lugeon (1901, 1902), and Argand (1911, 1916), the reconstruction of the deep tectonic structure of the Alps has long been based on field geology data, including the vergence of regional folds (e.g., Milnes, 1974; Ramsay, 1963) and the polarity of metamorphic field gradients (e.g., Ernst, 1971, 1973). Following this approach, the occurrence of higher-pressure rocks toward the Po Plain (e.g., Bocquet, 1971; Frey et al., 1974) and the first radiometric constraints to the age of Alpine metamorphism (e.g., Bocquet et al., 1974; Ferrara et al., 1962) have generally suggested an Alpine evolution driven by European subduction beneath Adria, and a progressive deformation propagation toward the European foreland (e.g., Dewey et al., 1973; Hawkesworth et al., 1975; Laubscher, 1974; Martini, 1972). However, based on the same data sets, alternative interpretations invoking Adriatic subduction were also proposed (e.g., Caby, 1975; Oxburg, 1972).

Starting from the 1980s, independent constraints to the deep structure of the Alps were provided by active seismic experiments launched in the Western and the Central Alps. They include the joint French-Italian ECORS-CROP experiment across the northern Western Alps (Nicolas et al., 1990b; Roure et al., 1996) and the NFP-20 research program in the Swiss Alps (Frei et al., 1990) (see locations in Figure 1b). The ECORS-CROP vertical seismic reflection profile (Figure 2a) has successfully imaged the SE-dipping European lower crust beneath the European foreland (ELC in Figure 2a), the SE-dipping Frontal Pennine Fault (FPF in Figure 2a), the top of the Adriatic mantle beneath the Ivrea gravity anomaly (AM in Figure 2a) and the Po Plain basin fill (Nicolas et al., 1990b). However, it failed to image the European Moho beneath the Alpine subduction wedge, as underlined by the question mark in Figure 2a. Additional constraints indicating European subduction beneath Adria were anyway provided by a complementary wide-angle reflection profile (Thouvenot et al., 1990) showing SE-dipping Moho-like surfaces beneath the frontal part of the Alpine metamorphic wedge and beneath the Gran Paradiso dome (Figure 2b). A migrated ECORS-CROP vertical seismic reflection profile (Figure 2c) was later reinterpreted by Schmid and Kissling (2000), who suggested that the strong reflectors at ∼20 km depth beneath the Gran Paradiso would mark the top of a slice of European lower crust (ELC in Figure 2c), rather than the top of a mantle slice as originally proposed by Nicolas et al. (1990a) and Polino et al. (1990) (Figure 2a). According to Schmid and Kissling (2000), the reflectors located at 10–15 km depth beneath the Gran Paradiso would mark the suture zone of the Valaisan ocean, a controversial paleogeographic feature (e.g, Masson et al., 2008; Stampfli et al., 2002) potentially documented only in the Central Alps and in the northernmost Western Alps (Liati and Froitzheim, 2006). Information provided by the NFP-20 West profile (Frei et al., 1990) is even more limited. In fact, this profile (in green in Figure 1b) is limited to the frontal part of the Alpine subduction wedge and to the nearby External zone. The classic geologic cross-sections proposed by Schmid et al. (2004) along the ECORS-CROP and NFP-20 traverses, which are shown in Figures 2d and 2f, are thus constrained only to a limited extent by geophysical data (the masked areas in Figures 2d and 2f indicate regions not constrained by vertical reflection seismic data). In the absence of further independent constraints, these cross-sections have reproduced the nappe structure proposed by Argand (1911) (Figure 2e), which was conceived well before the advent of plate tectonics.

Since the late 1990s, independent geophysical constraints on the deep Alpine structure were also provided for the southern Western Alps (Tardy et al., 1999) thanks to the GeoFrance 3D project (Groupe de Recherche Géofrance 3D, 1997). A local earthquake tomography model (Paul et al., 2001) was able to resolve the deep tectonic structure beneath the Dora-Maira down to depths of 15–20 km (Figure 2g), leading to the detection of mantle rocks at depths as shallow as ∼10 km (AM in Figure 2g) and to a geologic interpretation (Lardeaux et al., 2006) that was still largely based on field geology data (right panel in Figure 2g). Geologic cross-sections of the southern Western Alps were also presented by Schmid et al. (2017), who suggested an East-vergent backfold at the scale of the entire Eclogite belt and the occurrence, beneath the Dora-Maira massif, of Briançonnais crust slivers down to depths >30 km (see Schmid et al., 2017, their Figure 2). However, the Dora-Maira dome shows no cartographic evidence for such a backfold (Figures 1b and 2g), and the Schmid et al. (2017)'s interpretation was not consistent with seismic velocity constraints provided by the GeoFrance 3D experiment (Paul et al., 2001).

Starting from the 2000s, travel-time tomography studies (e.g., Giacomuzzi et al., 2011; Lippitsch et al., 2003; Piromallo & Morelli, 2003) have provided further constraints on the deep structure of the Alpine region,

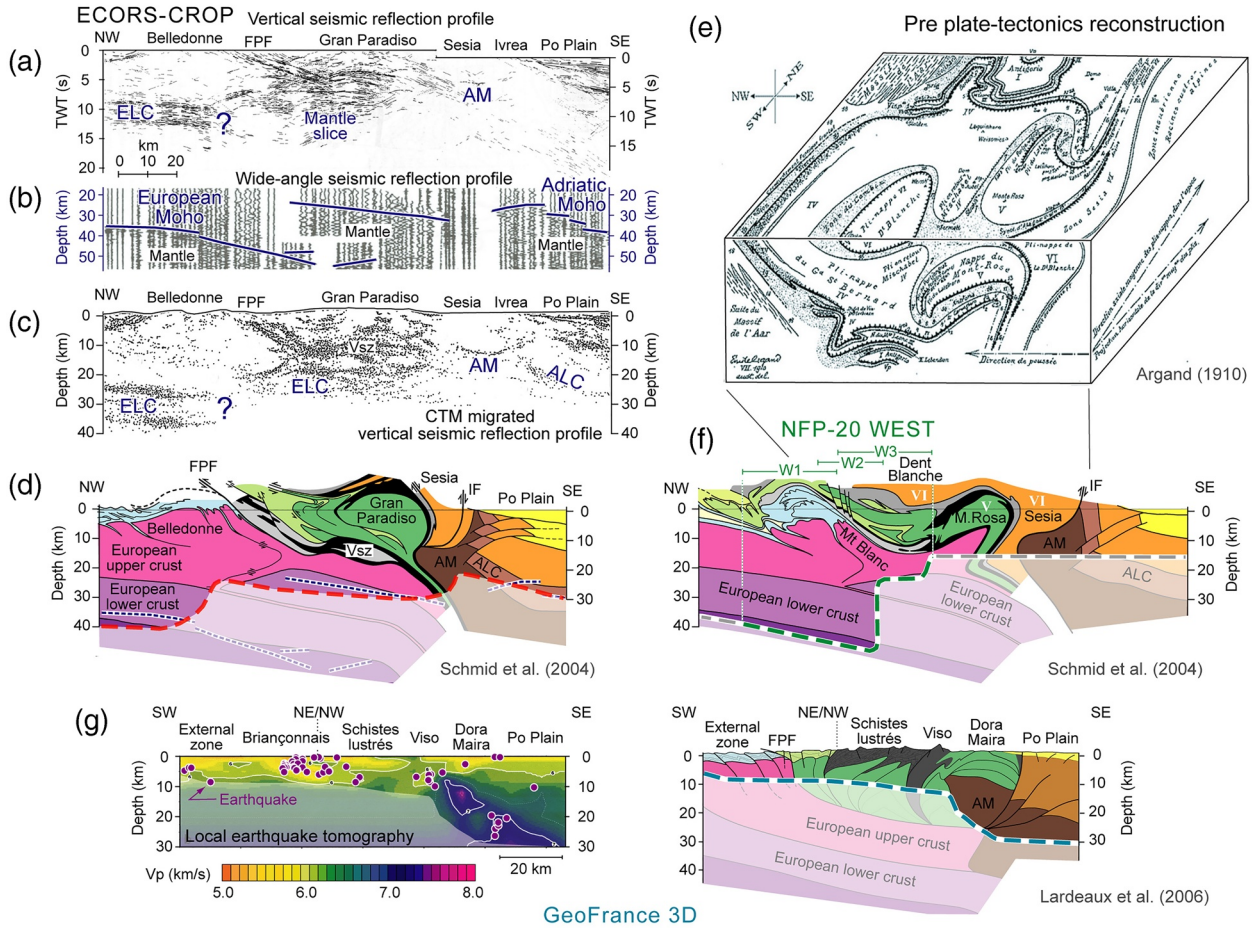

Figure 2. Crustal structure of the northern Western Alps as imaged prior to the CIFALPS passive seismic experiment. (a) Line drawing of the ECORS-CROP vertical seismic reflection profile (after Nicolas et al., 1990; see location in Figure 1b) (TWT = two-way travel time). The European lower crust (ELC) beneath the European foreland, and the top of the Adriatic mantle (AM) beneath the Ivrea zone are clearly imaged, as well as the SE-dipping Frontal Pennine Fault (FPF) and the Po Plain basin fill. To the east of the FPF, no European Moho is imaged beneath the Alpine subduction wedge. (b) ECORS-CROP wide-angle reflection seismic profile (same location as profile in "a") and inferred Moho-like reflectors (thick blue lines, after Thouvenot et al., 1990). Note the reflector with Moho characteristics imaged beneath the Gran Paradiso at ∼25–35 km depth, and the European Moho imaged farther west beneath the frontal part of the Alpine metamorphic wedge. (c) Migrated ECORS-CROP seismic reflection profile based on the common tangent method (CTM, after Thouvenot et al., 1996) as reinterpreted by Schmid and Kissling (2000): the reflectors at ∼25–35 km depth beneath the Gran Paradiso dome would not mark the top of a mantle slice, as proposed by Nicolas et al. (1990), but the interface between upper and lower European crust; the reflectors located at 10–15 km depth beneath the Gran Paradiso would mark the Valais suture zone (Vsz). ALC = top of the Adriatic lower crust beneath the Po Plain. (d) Geologic cross-section along the ECORS-CROP traverse as proposed by Schmid et al. (2004), compared with the main interfaces detected by the wide-angle seismic experiment (dashed blue lines). Below the dashed red line, where the cross-section proposed by Schmid et al. (2004) is masked, no constraint is provided by vertical reflection seismics. (e) Nappe structure in the northern Western Alps according to the pre-plate-tectonics reconstruction of Argand (1911), showing six major and laterally continuous recumbent folds-nappes (Roman numbers) with crystalline rocks enveloped by Mesozoic metasediments. (f) Geologic cross-section including the area investigated by the composite NFP-20 West traverse (Frei et al., 1990, see location in Figure 1b) as proposed by Schmid et al. (2004). Roman numbers (in white) indicate the fold-nappes of Argand (1911). Note the similarities between pre-plate-tectonics (e) and recent (f) tectonic interpretations proposed before the CIFALPS experiment. (g) P-wave velocity structure (Paul et al., 2001) and geologic cross-section (Lardeaux et al., 2006) along the GeoFrance 3D profile. No constraint was provided by local earthquake tomography below the dashed blue line. See locations in Figure 1.

revealing high-velocity anomalies in the Alpine upper mantle (Figures 3a and 3b) that were readily interpreted as traces of subducting slabs (e.g., Kissling et al., 2006; Piromallo & Faccenna, 2004; Spakman & Wortel, 2004). However, some of these models showed high-velocity anomalies in areas where no slab was expected based on geologic evidence (e.g., the Provençal margin of SE France, see Figure 3a), and different models were not invariably consistent. For example, Piromallo and Morelli (2003) imaged a continuous high-velocity anomaly beneath the Western Alps (cross-section A-A′ in Figure 3a) at the very same location where Lippitsch et al. (2003) proposed a shallow slab breakoff (cross-section C-C′ in Figure 3b). The

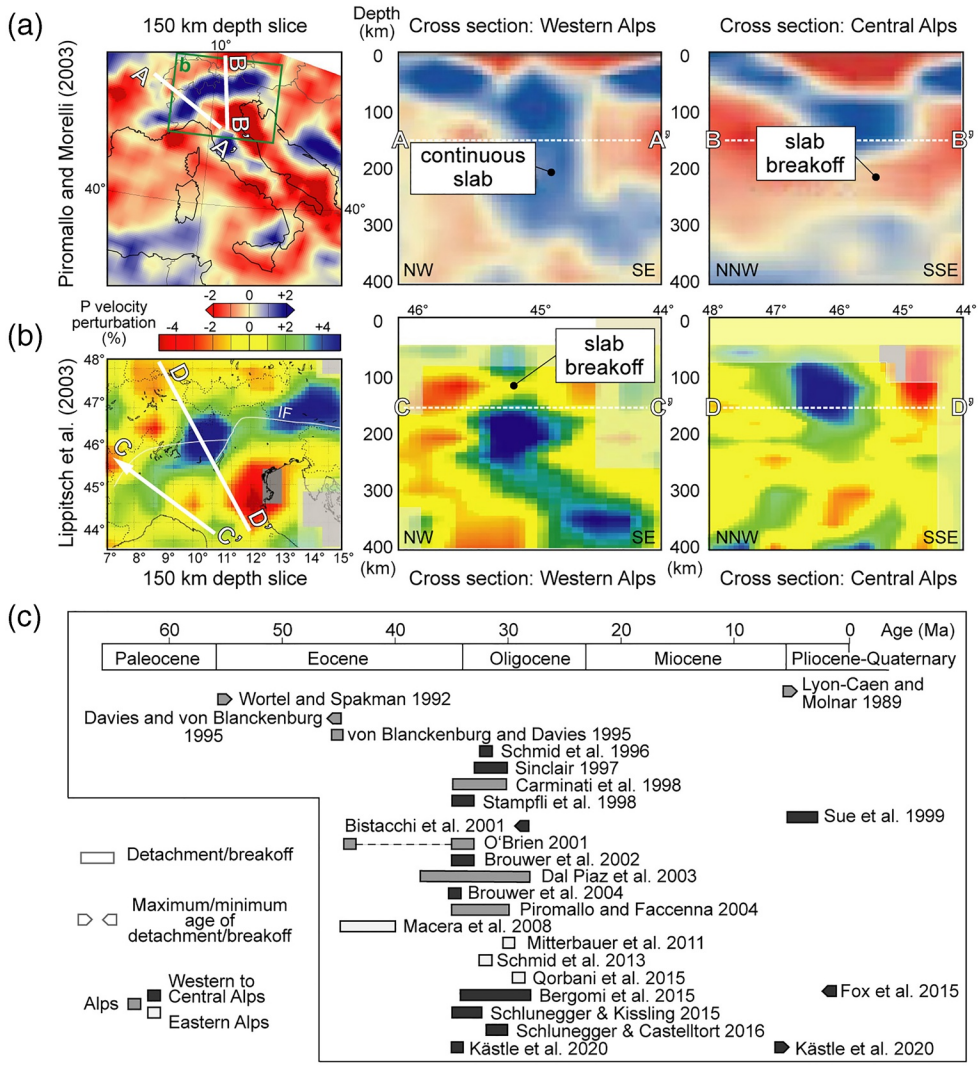

Figure 3. Slab breakoffs beneath the Alps as proposed by previous work. (a) Teleseismic P-wave tomography model by Piromallo and Morelli (2003), suggesting a continuous slab beneath the Western Alps (A-A′) and potential slab breakoff beneath the Central Alps (B-B′) (modified after Piromallo & Faccenna, 2004; Malusà et al., 2015). (b) Teleseismic P-wave tomography model by Lippitsch et al. (2003), suggesting shallow slab breakoff beneath the Western Alps (C-C′) and a more continuous slab beneath the Central Alps possibly affected by a deeper slab breakoff (D-D′) (modified after Schmid et al., 2004); IF, Insubric Fault. (c) Different ages and sites of slab breakoff/detachment events envisaged in publications on the Alpine region since the late 1980s (modified after Garzanti et al., 2018). Based on: Lyon-Caen and Molnar (1989), Wortel and Spakman (1992), Davies and von Blanckenburg (1995), von Blanckenburg and Davies (1995), Schmid et al. (1996), Sinclair (1997), Carminati et al. (1998), Stampfli et al. (1998), Sue et al. (1999), Bistacchi et al. (2001), O'Brien (2001), F. Brouwer et al. (2002), Dal Piaz et al. (2003), F. M. Brouwer et al. (2004), Piromallo and Faccenna (2004), Macera et al. (2008), Mitterbauer et al. (2011), Schmid et al. (2013), Bergomi et al. (2015), Fox et al. (2015), Qorbani et al. (2015), Schlunegger and Kissling (2015), Schlunegger and Castelltort (2016), and Kästle et al. (2020).

identification of a possibly missing section of the Alpine slab beneath the Central Alps (B-B′ and D-D′ in Figure 3) was held to be supportive of the slab-breakoff model first proposed by Davies and von Blanckenburg (1995), which was conceived to explain Alpine magmatism and exhumation of high-pressure rocks. Despite geophysical evidence was not unequivocal, the slab-breakoff model has been applied to the Alps by several studies since then (Figure 3c). However, unlike the original formulation of von Blanckenburg and Davies (1995) who suggested an Eocene slab breakoff (Figure 3c), most subsequent authors have either proposed an Oligocene slab breakoff (e.g., Bistacchi et al., 2001; Schlunegger & Castelltort, 2016; Schlunegger

Table 1
Summary Table of the CIFALPS Geophysical Approaches and Main Information Retrieved

Method	Main information retrieved	Reference
Receiver function analysis	Moho imaging beneath the subduction wedge	Zhao et al. (2015)
Teleseismic P-wave tomography	Upper mantle velocity structure and slab configuration	Zhao et al. (2016b)
Array analysis of surface waves	Lithosphere-asthenosphere boundary beneath the European plate	Lyu et al. (2017)
HypoDD earthquake relocation	Detection of lithospheric faults	Malusà et al. (2017)
Receiver function azimuthal harmonic decomposition	Detection of anisotropic rocks in the lithosphere	Piana Agostinetti et al. (2017)
Teleseismic full-waveform inversion	Moho imaging and detection of velocity anomalies in the Alpine subduction channel	Beller et al. (2018)
Local earthquake tomography	Moho imaging and absolute P-wave velocity structure of the European and Adriatic crust, the uppermost Adriatic mantle and the subduction wedge	Solarino et al. (2018)
SKS splitting measurement	Seismic anisotropy due to lattice preferred orientation of olivine crystals in the upper mantle	Salimbeni et al. (2018)
S wave splitting of intermediate-depth earthquakes	Seismic anisotropy in the crust and lithospheric mantle	Baccheschi et al. (2019)
3-D Pn tomography	Seismic signature of continental subduction	Sun et al. (2019)
TransD inversion of Rayleigh wave dispersion data	Moho imaging and absolute S wave velocity structure of the European and Adriatic lithosphere, the subduction wedge and the subduction channel	Zhao et al. (2020)

& Kissling, 2015; Schmid et al., 1996) or an even younger Pliocene-Quaternary breakoff event (e.g., Fox et al., 2015; Kästle et al., 2020; Sue et al., 1999), even though no orogenic magmatism and no exhumation event occurred at that time in the Alps.

4. The CIFALPS Experiment

The CIFALPS experiment (Zhao et al., 2016a) is the first passive seismic survey that crosscuts the entire Western Alps across the Dora Maira massif. It involves scientists and institutions from China, Italy, and France. Geophysicists and geologists have worked side by side during the project, starting from the early steps of the experiment set up to the final steps of geologic interpretation. The temporary seismic network includes 46 broadband seismic stations operating from July 2012 to September 2013, deployed along a linear WSW-ESE transect from the European foreland to the western Po Plain, and nine additional stations installed to the north and to the south of the main profile (red yellow-filled dots in Figure 1b). Stations located along the main profile, which was chiefly conceived for receiver function analysis (Zhao et al., 2015), have spacing ranging from ~5 km in the Alpine mountain range to ~10 km in the European foreland and the western Po Plain. Off-profile stations were installed to improve the crossing of seismic rays for local earthquake tomography (Solarino et al., 2018) and to build mini-arrays for surface wave tomography (Lyu et al., 2017). Some of the analyses performed during the CIFALPS experiment (e.g., Lyu et al., 2017; Sun et al., 2019; Zhao et al., 2016b, 2020) also exploited data sets from permanent broadband networks and benefitted from the recent opening of the European seismic databases. A dataset of anomalously deep earthquakes (purple circles in Figure 1b) recorded in the western Po Plain during the past 25 years (Eva et al., 2015) was extremely useful to extend local earthquake tomography analysis toward greater depths and analyze the seismic anisotropy in the crust and the lithospheric mantle.

Most of the analyses presented in this summary work have been published in international journals. The reader is referred to the original publications (see Table 1) for a more detailed discussion of the procedures followed for the different types of tomography models and for an estimate of their resolution. Different tomographic methods allow to illuminate different levels of the crust and the mantle, and at different locations with respect to the Alpine slab (Table 1). It should be remembered that a tomographic model is not a true image of the Earth subsurface. It shows the projection of a data set onto a model space controlled by

simplifying assumptions. Its accuracy is limited by the seismic data availability and quality, the type of wave used, and the assumptions made. Moreover, solutions are not unique. For example, in teleseismic body wave tomography the ray geometry tends to induce vertical smearing, whereas in surface wave tomography the accuracy of the model degrades with depth. Imaging the Alpine subduction system requires the integration of different tomographic methods through interpretive steps that should avoid any over-interpretations of observed features. A close collaboration between geophysicists and geologists is thus particularly important. The series of independent tomographies presented in this summary paper, despite their numerous limitations, converge toward a coherent geologic model, which attests to the robustness of our geologic interpretation of the deep structure of the Alps. The application of a wide range of tomographic methods to the analysis of a single fossil subduction zone (Table 1) makes the CIFALPS experiment a reference case that could be exported to other orogenic belts.

5. Seismic Velocities of Rocks Involved in the Alpine Orogeny

The geologic interpretation of geophysical information provided by the CIFALPS experiment requires independent knowledge of seismic velocities of rocks possibly involved in the Alpine subduction zone. Various proportions of serpentinized mantle, basalts, and sedimentary rocks were subducted at the Alpine trench since the Cretaceous during the oceanic subduction stage (Agard et al., 2009; Dal Piaz & Ernst, 1978; Deville et al., 1992; Guillot et al., 2009a). Due to the low spreading rates characterizing the Alpine Tethys in the Jurassic, exhumed mantle rocks were dominant on the Tethys seafloor compared to pillow basalts (Lagabrielle & Cannat, 1990; Lagabrielle & Lemoine, 1997; Manatschal, 2004; Piccardo, 2003). Rocks from the Tethys seafloor were initially subducted together with slivers of granitic and (meta)sedimentary rocks from the hyperextended Adriatic paleomargin (Rubatto et al., 1998; Thöni, 2006; Zanchetta et al., 2012), whereas granitic and (meta)sedimentary rocks from the European paleomargin were later involved in the subduction zone during the main stage of continental subduction in the Paleogene (Lanari et al., 2012; Malusà et al., 2011; Rubatto & Hermann, 2001).

P-wave and S-wave velocities for all of these lithologies are provided by several laboratory experiments (e.g., Bezacier et al., 2010, 2013; S. Ji et al. 2013, 2015; Kern et al., 2002; Khazanehdari et al., 2000; Pera et al., 2003; Reynard, 2013; Rudnick & Fountain, 1995; Watanabe et al., 2011; Weiss et al., 1999) and are summarized in the diagrams of Figure 4. The ellipse size in these diagrams is proportional to the maximum and minimum seismic velocities. The ellipse location depends on the pressure-temperature range at equilibrium for each rock type. As shown in Figure 4, for a given bulk composition, rocks generally display a progressive increase in P and S velocities with depth (i.e., pressure) and metamorphic grade (i.e., temperature). For a specific rock type, the effects of increasing pressure with depth, which would imply an increase in seismic velocity, are partly compensated by the effects of increasing temperature that would conversely imply a seismic velocity decrease. As a result, for a given bulk composition (indicated by ellipses of the same color) major changes in V_p and V_s are mainly due to changes in metamorphic mineral assemblages with depth. For example, V_p values in metapelites (brown in Figure 4) progressively increase, according to laboratory experiments from 5.3–6.4 km s^{-1} in low-grade metapelites to 6.5–6.7 km s^{-1} in medium-grade metapelites, reaching values as high as 7.2 km s^{-1} in high-grade metapelites with minor variability depending on rock composition (S. Ji et al., 2015; Khazanehdari et al., 2000; Weiss et al., 1999). In the same rocks, V_s values progressively increase from 3.3–3.8 km s^{-1} in low-grade metapelites (S. Ji et al., 2015) to 3.8–4.1 km s^{-1} in high-grade metapelites (Khazanehdari et al., 2000; Weiss et al., 1999). A similar progressive increase in seismic velocity with depth is also observed in mafic (blue in Figure 4) and granitic (purple in Figure 4) rocks.

In fully hydrated ultramafic rocks (green in Figure 4), measured V_p values increase from 4.5 to 6.0 km s^{-1} in low-temperature lizardite serpentinite to 6.3–7.0 km s^{-1} in high-temperature antigorite serpentinite (Bezacier et al., 2013; S. Ji et al., 2013). In the same rocks, V_s values increase from 2.4–3.0 km s^{-1} in lizardite serpentinite to 3.4–3.8 km s^{-1} in antigorite serpentinite, but V_s as low as 3.2 km s^{-1} can be observed in antigorite mylonites (Watanabe et al., 2011). A sharp change in seismic velocities toward values that are typical of peridotite (V_p = 7.7–9.0 km s^{-1}, V_s = 4.4–5.1 km s^{-1}) (Bezacier et al., 2010; Khazanehdari et al., 2000; Pera et al., 2003) is expected across the antigorite-out curve (Hilairet et al., 2006). In partly serpentinized peridotites (inset of Figure 4), V_p values linearly increase for decreasing volume fractions of

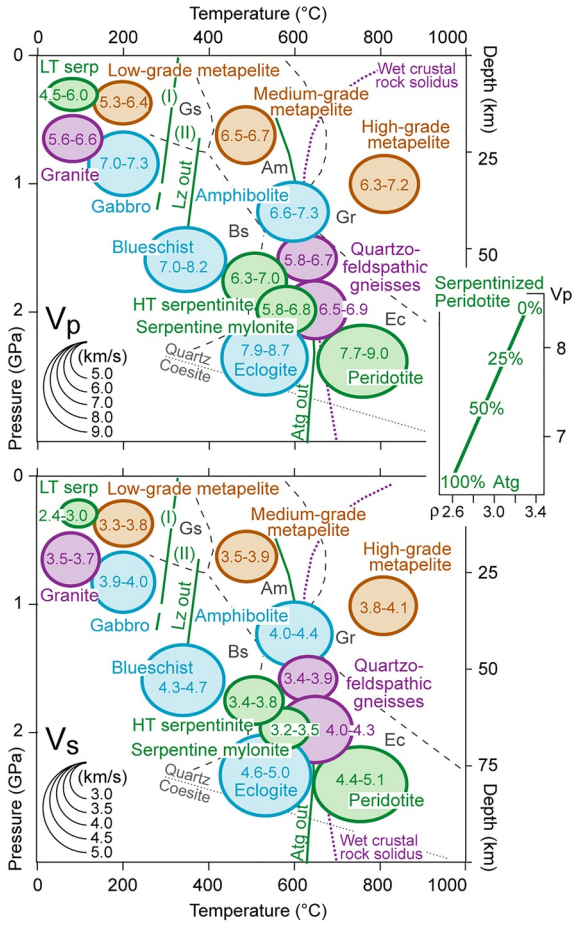

Figure 4. Measured V_p and V_s (km s^{-1}) for different rock types possibly involved in the Alpine subduction zone (green = ultramafic; blue = mafic; purple = granitic; brown = pelitic) at ambient conditions. The size of the ellipses is proportional to the maximum and minimum seismic velocities; ellipse location depends on the pressure-temperature range at equilibrium for each rock type. The dashed gray lines indicate the metamorphic facies boundaries (Am = Amphibolite; Bs = Blueschist; Ec = Eclogite; Gr = Granulite; Gs = Greenschist). Antigorite (Atg) stability fields after Hilairet et al. (2006); lizardite (Lz) stability fields after Evans et al. (2004) (I—Onset of Lz destabilization into Atg) and Schwartz et al. (2013) (II—maximal stability limit of Lz observed in natural serpentinites); wet crustal-rock solidus after Schmidt et al. (2004). Note the progressive increase in V_p and V_s with depth and metamorphic grade in pelitic, granitic and mafic rocks, and the sharp change in V_p and V_s across the Atg-out curve in ultramafic rocks. V_p variations for partially serpentinized peridotite at depths greater than 15–20 km, where Atg is stable, are shown on the right (after Reynard, 2013). Data sources: LT and HT serpentinite after S. Ji et al. (2013) (the V_s lower bound for antigorite serpentinite is calculated from single-crystal elastic data, and is referred to Reuss approximation and 2 GPa, Bezacier et al., 2013); HT serpentine mylonite after Watanabe et al. (2011); peridotite after Khazanehdari et al. (2000) and Pera et al. (2003), as compiled by Bezacier et al. (2010); gabbro, blueschist and eclogite after Bezacier et al. (2010); amphibolite after Brownlee et al. (2011); granite after Rudnick and Fountain (1995) and Khazanehdari et al. (2000); quartzo-feldspathic gneiss after Kern et al. (2002) and Brownlee et al. (2011) (the V_p and V_s ranges of 6.5–6.9 and 4.0–4.3 km s^{-1} are based on calculations for modeled rocks at 700°C and 2 GPa); low-grade metapelite after S. Ji et al. (2015); medium-grade metapelite (kinzigite) after Khazanehdari et al. (2000); high-grade metapelite after Weiss et al. (1999) and (stronalite) Khazanehdari et al. (2000).

antigorite (Reynard, 2013). Correlation between seismic velocities and lithology is particularly challenging in subduction wedges, former subduction channels and the nearby upper mantle, because subducted rocks are generally heterogeneous and display anisotropic fabrics and velocity variations as a function of direction (e.g., Bezacier et al., 2013; Rudnick & Fountain, 1995; Weiss et al., 1999), and V_s values are strongly reduced in the presence of fractures, fluids or partial melts. As demonstrated by laboratory studies (e.g., Yoshino et al., 2007), if melt completely wets grain boundaries, even a small amount of melt (e.g., 1%) can produce remarkable velocity drops of 20%–30% (Karato, 2010; Malusà et al., 2018).

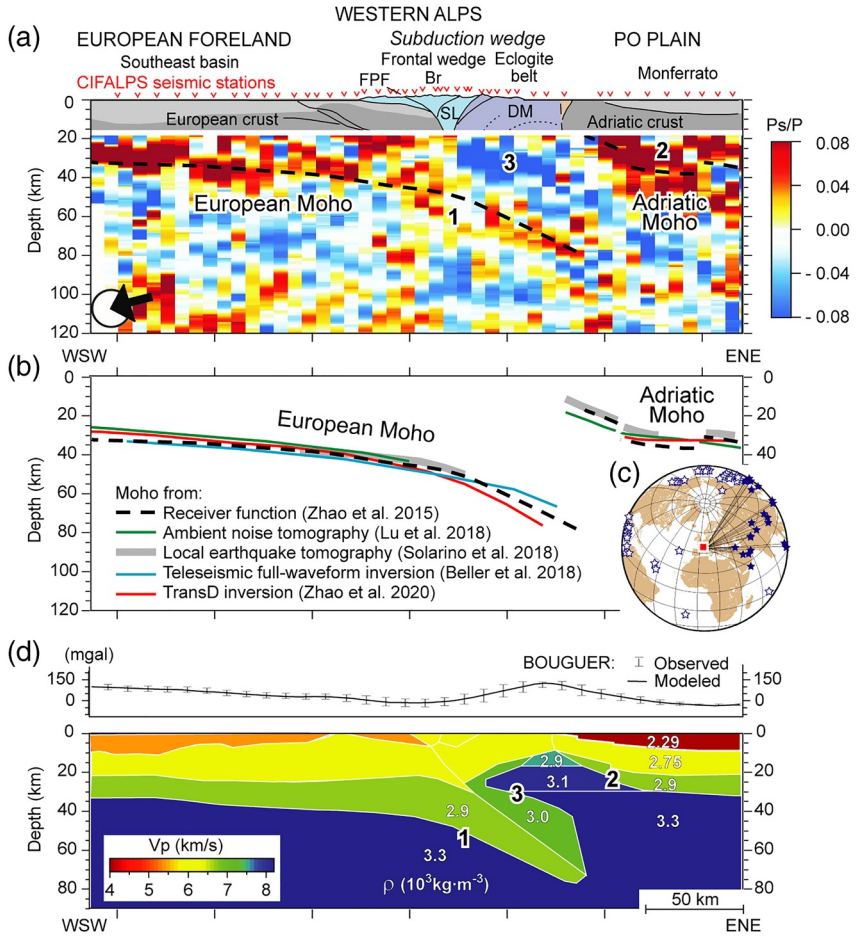

Figure 5. Moho imaging by receiver function (RF) analysis. (a) Raw migrated CCP (common conversion point) depth section without horizontal smoothing, using receiver functions corresponding to ENE back-azimuths (28°–118°, black arrow on the bottom-left) (after Zhao et al., 2015), and inferred Moho depth (dashed black lines). The European Moho (1) is continuously marked by Ps-conversions with positive polarity (red to yellow colors), dipping toward the east from ∼40 km depth beneath the Frontal Pennine Fault (FPF) to ∼75 km depth beneath the westernmost Po Plain (note the progressive weakening, from red to yellow colors, of this converted phase beneath the Alpine subduction wedge). The Adriatic Moho (2) is marked by shallower positive-polarity Ps-conversions from 10 to 15 km depth to the west to 20–30 km depth to the east. The negative polarity conversions beneath the Dora-Maira (3, in blue) mark a downward velocity decrease at 20–40 km depth. Acronyms as in Figure 1. (b) Comparison with Moho depths as later constrained by other geophysical methods: ambient noise tomography—Lu et al., 2018; local earthquake tomography—Solarino et al., 2018 (see Figure 6); teleseismic full-waveform inversion—Beller et al., 2018; transdimensional inversion of Rayleigh wave dispersion data—Zhao et al., 2020 (see Figure 7). Note the good consistency of the results despite the different techniques and datasets used. (c) Locations of teleseismic events used in RF analysis (the blue stars mark events with ENE back-azimuths considered for image (a)). (d) Velocity and gravity model of the CIFALPS cross-section (density values in white) utilized by Zhao et al. (2015) to test the interpretation of the CCP section that fits the Bouguer anomaly data.

6. Seismic Evidence of Continental Subduction in the Western Alps

6.1. Moho Imaging by Receiver Function Analysis

The first output of the CIFALPS experiment (Zhao et al., 2015) is based on the application of the receiver function (RF) technique (Figure 5). The RF technique exploits the P-to-S (Ps) conversion of seismic waves at velocity interfaces beneath an array of seismic stations (Langston, 1979; Ligorría & Ammon, 1999). It allows detection of interfaces with downward velocity increase, for example the Moho, and interfaces with downward velocity decrease possibly expected within a subduction wedge, because the polarity of the converted

signal depends on the sign of the velocity change. In the Western Alps, application of the RF approach to teleseismic earthquakes (Zhao et al., 2015) has provided the first seismic evidence of European crust subducted into the Adriatic upper mantle, right beneath the place where coesite was first recognized in continental (U)HP rocks by Chopin (1984).

The RF image of Figure 5a is based on teleseismic events with ENE back-azimuths and magnitude Mw ≥ 5.5 (the location of events is shown in Figure 5c). In order to produce a depth image beneath the CIFALPS transect, Zhao et al. (2015) migrated the time data to depth and stacked the radial receiver functions using the common conversion point method (L. Zhu, 2000). The resulting image shows two main velocity interfaces marked by positive-polarity Ps-conversions (red-to-yellow regions in Figure 5a), corresponding to downward velocity increase at the European and Adriatic Mohos (thick dashed lines 1 and 2 in Figure 5a) and a main blue spot of negative-polarity Ps-conversions located beneath the Dora-Maira (3 in Figure 5a).

The eastward-dipping European Moho (1 in Figure 5a) can be recognized in the RF image from ∼40 km depth beneath the Frontal Pennine Fault (FPF in Figure 5a) to ∼75 km depth beneath the Po Plain. In the European foreland, the velocity interface marked by positive-polarity Ps-conversions is located at ∼30–40 km depth and is clearly connected with the European Moho imaged by previous work (e.g., Thouvenot et al., 2007). According to Zhao et al. (2015), the eastward weakening of this converted phase beneath the Alpine subduction wedge, as highlighted by the progressive change in color from red to yellow in Figure 5a, may be due to eclogitization of the European lower crust at depth >40 km, and consequent reduction of the density (and velocity) contrast with the underlying lithospheric mantle.

The Adriatic Moho (2 in Figure 5a) can be recognized in the RF image from 10–15 km depth, to the West, to 20–30 km depth to the East, where it is connected with the Adriatic Moho imaged beneath the Po Plain by independent studies (e.g., Molinari et al., 2015). In the westernmost Po Plain, this velocity interface coincides with the top of the so-called "Ivrea body" (Closs & Labrouste, 1963), classically interpreted as a slice of Adriatic upper mantle (Kissling, 1993; Nicolas et al., 1990a; Paul et al., 2001; Scafidi et al., 2009) exhumed at shallow crustal depth during Tethyan rifting (Malusà et al., 2015; Manatschal & Bernoulli, 1999).

The main spot of negative-polarity Ps-conversions (3 in Figure 5a) is located between 20 and 40 km depth beneath the Dora-Maira massif. It likely marks a downward velocity decrease from mantle rocks to (U)HP rock slivers and/or associated serpentinites of the suture zone (Zhao et al., 2015; Malusà et al., 2017). The hypothesis of dominant (U)HP continental slivers would be consistent with the predictions of numerical models of synconvergent exhumation (e.g., Jamieson & Beaumont, 2013), whereas the hypothesis of dominant serpentinites would be in line with the predictions of numerical models of exhumation triggered by divergence between upper plate and accretionary wedge (e.g., Liao et al., 2018b), which are more consistent with the geologic record available for the Western Alps (Malusà et al., 2011, 2015). Constraints provided by RF allowed to define preliminary two-dimensional models of layer boundaries and velocity contrasts along the CIFALPS profile, which were tested by Zhao et al. (2015) for compatibility with available Bouguer anomaly data by gravity modeling (Figure 5d). However, Zhao et al. (2015) could not assess the relative proportion of serpentinites and (U)HP rock slivers in the region marked by negative polarity conversions. Such evaluation requires absolute V_p and V_s constraints that were provided, at a later stage of the CIFALPS project, by local earthquake tomography (Solarino et al., 2018) and TransD inversion of surface-wave data (Zhao et al., 2020) as described in Sect. 7.

6.2. Moho Imaging by Other Tomographic Methods

Breakthroughs provided by RF analysis using teleseismic events have been subsequently confirmed, along the CIFALPS transect, by different seismic data sets and tomographic methods (Figure 5b). These methods include: (i) tomography from ambient seismic noise (Lu et al., 2018); (ii) local earthquake tomography (Solarino et al., 2018); (iii) tomography from teleseismic full-waveform inversion (Beller et al., 2018); and (iv) tomography from Bayesian transdimensional inversion of Rayleigh wave group velocity dispersion data (Zhao et al., 2020).

Ambient noise tomography (ANT) is particularly efficient to image the velocity structure of the crust and uppermost mantle, provided that continuous noise records are available at dense arrays of seismic stations

(Shapiro et al., 2005). Rayleigh waves between stations can be reconstructed from the cross-correlation of recorded seismic noise, basically turning each station to a source of seismic waves (e.g., Campillo & Paul, 2003; Larose et al., 2006). In the Alpine region, Lu et al. (2018) used noise correlations to compute Rayleigh wave phase and group velocity and derive a high-resolution 3-D S-wave velocity model. Their dispersion dataset took advantage of the large number of seismic stations in Europe, particularly the great Alpine region with the high-density CIFALPS (Zhao et al., 2016a) and AlpArray (Hetényi et al., 2018) temporary experiments. The depth to the European Moho estimated from ANT beneath the Frontal Pennine Fault and surroundings (green line in Figure 5b) (Lu et al., 2018) is in good agreement with the Moho depth estimated from RF. At the western end of the profile, the ANT Moho beneath the Southeast Basin is shallower than the RF Moho by 5–8 km, which could be due to an inappropriate velocity model for the migration of RF. Beneath the Po Plain, and on top of the Ivrea body, the Adriatic Moho estimated from ANT correlates well with the RF Moho (Figure 5b).

Moho constraints are also provided by local earthquake tomography (LET). The LET method is based on the analysis of earthquakes within the model volume (Kissling, 1988). The maximum depth of the resolved model is thus limited by the depth of occurrence of the deepest seismic events. The investigated volume needs to be adequately sampled by a dense set of crossing rays, depending on the distribution of both earthquakes and receivers, in order to resolve the inherent trade-off between variations in velocity structure and hypocenter locations. Along the CIFALPS transect, the P-wave velocity structure provided by LET can be locally resolved down to 50–60 km depth (Solarino et al., 2018) using the anomalously deep earthquakes recorded in the western Po Plain (Eva et al., 2015; Malusà et al., 2017). The Adriatic Moho estimated from LET beneath the Po Plain and on top of the Ivrea body (thick gray line in Figure 5b) confirms the results of RF analysis, providing an even more reliable estimate of Moho depth compared to previous results based on RF alone (see Section 7.1 for more details). Only part of the European Moho, i.e., the part located beneath the External Zone, lays within the resolved LET model volume. There, the LET Moho confirms the location of the RF Moho as revealed by analysis of teleseismic events (Solarino et al., 2018).

A further independent image of the European Moho along the CIFALPS transect is based on full-waveform inversion (FWI) of selected teleseismic events recorded during the CIFALPS experiment (Beller et al., 2018). By FWI is meant the inversion of the full seismogram including phase and amplitude effects, within a time window following the first arrival up to a frequency of 0.2 Hz. Based on FWI, Beller et al. (2018) built 3-D models of density and P- and S-wave velocities, and detected the European Moho (blue line in Figure 5b) at depths ranging from ~30 km beneath the Southeast Basin to ~65 km beneath the Dora-Maira massif, which confirms previous results based on RF.

A more recent Moho image along the CIFALPS transect is based on a Bayesian transdimensional (TransD) inversion of the Rayleigh wave group velocity dispersion data of Lu et al. (2018), as performed by Zhao et al. (2020) according to the procedure described in Bodin et al. (2014) and Yuan and Bodin (2018). TransD inversion provides absolute S-wave velocity information and treats the model parameterization (e.g., the number of velocity layers) as an unknown in the inversion to be determined by the data, thus yielding more robust velocity amplitude estimates (Bodin, Sambridge, Rawlinson, & Arroucau, 2012; Bodin, Sambridge, Tkalčić, et al., 2012). The resulting image presented by Zhao et al. (2020) provides compelling evidence of European continental-crust subduction into the Adriatic upper mantle (see Section 7.2 for more details), thus confirming the main findings of RF analysis. The eastward-dipping TransD European Moho (red line in Figure 5b) is located at ~30 km depth beneath the Southeast Basin, getting progressively deeper from ~45 km depth beneath the Frontal Pennine Fault to ~75 km depth beneath the Dora-Maira massif. On the eastern side of the CIFALPS transect, the TransD Moho overlaps with the Adriatic Moho as imaged by RF, ANT and LET (Figure 5b).

7. Absolute Velocity Structure of the Crust and the Mantle Wedge

A more detailed geologic interpretation of the crustal structure along the CIFALPS transect requires absolute P-wave and S-wave velocity constraints. These constraints are provided by LET (Solarino et al., 2018) and TransD inversion of Rayleigh wave dispersion data (Zhao et al., 2020) and are illustrated below.

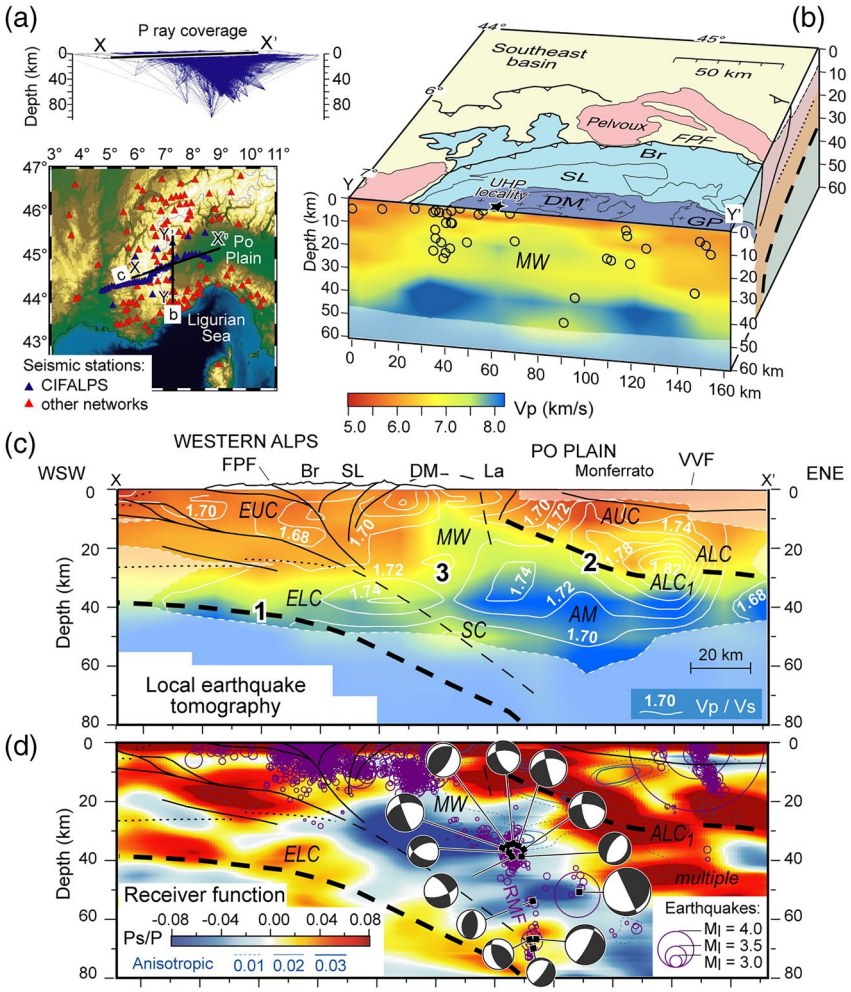

Figure 6. Crustal and mantle-wedge P velocity structure by local earthquake tomography (LET) (after Solarino et al., 2018). (a) P ray coverage and location of stations used for LET. (b) Absolute V_p along a N-S tomographic cross-section across the Dora-Maira UHP locality (black star). Note the high-velocity body interpreted as serpentinized mantle wedge (MW); the black circles are projected hypocenters located within ±3 km distance off the profile (masked areas have resolution diagonal elements <0.1). (c) WSW-ENE tomographic cross-section along the CIFALPS transect (white lines are isolines of equal V_p/V_s). The black lines indicate tectonic features previously inferred from receiver function (RF) analysis and already indicated in Figure 5a. Acronyms in italics indicate regions of the model discussed in the main text: ALC and ALC_1, Adriatic lower crust; AM, Adriatic mantle; AUC, Adriatic upper crust; ELC, European lower crust; EUC, European upper crust; MW, serpentinized mantle wedge. (d) Smoothed RF cross-section for the same transect shown in (c), also including the amplitude of RF anisotropic component from azimuthal harmonic decomposition (blue contours, Piana Agostinetti et al., 2017), earthquakes (in purple) plotted from ±20 km distance off the profile, and focal solutions for events deeper than 30 km (beach balls in gray, after Malusà et al., 2017). Note the consistency between structures imaged by the analysis of local (c) and teleseismic (d) events. RMF, Rivoli-Marene Deep Fault. Other acronyms as in Figure 1.

7.1. Absolute P-Wave Velocity Structure From LET

The absolute P-wave velocity structure revealed by LET in the southern Western Alps (Solarino et al., 2018) is shown in Figure 6. In order to improve ray crossing (Figure 6a) and better constrain the bottom part of the study volume, Solarino et al. (2018) have integrated recordings of the CIFALPS stations with recordings of permanent stations operating during the CIFALPS experiment, and have also considered the intermediate depth earthquakes that occurred before the experiment (Eva et al., 2015). The well-resolved regions of the resulting LET model include the European crust to the west, the Adriatic crust and uppermost Adriatic mantle to the east, and the Alpine subduction wedge (Solarino et al., 2018) (Figures 6b and 6c).

The European upper crust (EUC in Figure 6c) shows V_p values < 6.4 km s^{-1} and rather constant V_p/V_s ratios ~1.70 ± 0.02, consistent with a mainly granitic continental crust (cf. Figure 4). V_p values increase in the European lower crust (ELC in Figure 6c) from V_p ~6.7 km s^{-1}, at depth of ~25 km, to V_p ~7.6 km s^{-1} at depth > 40 km (i.e., beneath the Alpine subduction wedge), under rather constant V_p/V_s ratios of 1.70–1.72. The observed velocity structure suggests a relatively homogeneous lower crust at the scale of seismic observations along the CIFALPS profile. V_p values ~6.7 km s^{-1} in the lower crust are consistent with granulitic rocks of felsic to intermediate compositions (Goffé et al., 2003; Rudnick & Fountain, 1995; Mechie et al., 2012; Wang et al., 2005; Weiss et al., 1999). Major occurrence of granulitic metapelites can be excluded in the light of their higher P-wave velocities (up to 7.2 km s^{-1}; see Figure 4), which is not observed in the western part of the CIFALPS profile. The progressive increase in P-wave velocities at depth > 40 km may mirror the progressive eclogitization of the European lower crust (Solarino et al., 2018), as eclogitization of a felsic granulite strongly increases the garnet content and consequently the rock density (from 2.90 to 3.30 10^3 kg m^{-3}) and P-wave velocity (up to 7.6 km s^{-1}) (e.g., Christensen, 1989; De Paoli et al., 2012; Hacker & Abers, 2004; Hacker et al., 2015, 2003; Hetényi et al., 2007). Alternatively, the increase in P-wave velocity in the European lower crust may indicate an increase in mafic component beneath the Alpine subduction wedge. However, V_p values provided by LET are far too low for a pure mafic eclogite (7.9–8.7 km s^{-1}; Bezacier et al., 2010; Reynard, 2013) (Figure 4). Zhao et al. (2015) and Solarino et al. (2018) have thus favored the hypothesis of a progressive change in metamorphic assemblages during continental subduction rather than a change in bulk composition from west to east. The progressive P-wave velocity increase in the European lower crust at depth >40 km, as documented by LET, provides an explanation for the eastward weakening of RF converted phases along the European Moho described by Zhao et al. (2015) (see Figure 6d).

On the eastern side of the CIFALPS transect, the LET model shows a sharp downward P-wave velocity increase across the Adriatic Moho (thick dashed line two in Figure 6c). Above the Adriatic Moho, the Adriatic upper crust (AUC in Figure 6c) shows V_p values < 6.4 km s^{-1} and V_p/V_s ratios ~1.70–1.74. The Adriatic lower crust (ALC in Figure 6c) shows a more complex velocity structure than the European lower crust, likely reflecting a more heterogeneous composition at the scale of seismic observations. Local spots with V_p ~7.2 km s^{-1} and low V_p/V_s ratios may suggest, according to Solarino et al. (2018), local occurrences of granulite-facies metapelites (V_p = 6.3–7.2 km s^{-1}, V_s = 3.8–4.1 km s^{-1}; Weiss et al., 1999; Khazenehdari et al., 2000). North of the Po Plain, similar granulite facies metapelites are also exposed at Earth's surface (e.g., Ewing et al., 2014). In the region labeled as ALC_1 (Figure 6c), the locally high V_p/V_s ratios >1.8 associated to V_p ~7.0–7.3 km s^{-1} may be interpreted as gabbro underplated at the base of the Adriatic lower crust. Permian gabbros are indeed exposed at Earth's surface north of the Po Plain, and intrude lower crustal rocks belonging to the Adriatic (Southalpine) basement (Quick et al., 1994; Schaltegger & Brack, 2007). Below the Adriatic Moho, seismic velocities provided by LET are consistent with dry to partly serpentinized peridotites of the Adriatic lithospheric mantle (AM in Figure 6c), as indicated by V_p values ~7.5–8.0 km s^{-1} and V_p/V_s ratios ~1.70–1.72. Peridotites are found at depth > 30 km beneath the Monferrato, and at much shallower depth (10–15 km) in correspondence with the Ivrea positive gravity anomaly, in line with results of previous tomography models (Diehl et al., 2009; Paul et al., 2001; Scafidi et al., 2006, 2009; Solarino et al., 1997; Wagner et al., 2012).

In the central part of the CIFALPS transect, the uppermost part of the Alpine subduction wedge shows V_p values invariably <6.5 km s^{-1} (Figure 6c). The structural variability in this region is mirrored by the variability in V_p/V_s ratios. V_p/V_s > 1.75 in the Briançonnais and Schistes Lustrés units likely reflect low S-wave velocities resulting from a widespread network of mesoscale faults developed in these units during the Neogene (Sue et al., 2007; Malusà et al., 2009). In the western flank of the Dora-Maira massif, V_p/V_s < 1.66 likely reflect high S-wave velocities, possibly due to the presence of poorly fractured granitic gneisses that are also exposed at Earth's surface (Brossasco granite; Lenze & Stöckhert, 2007; Paquette et al., 1999). A prominent feature highlighted by the LET model in this part of the transect is the high velocity body (V_p ~7.5 km s^{-1}, V_p/V_s = 1.70–1.72) imaged at depths from ~10 km to >30 km (MW in Figures 6b and 6c). This body is exclusively found beneath the Dora-Maira massif, as highlighted by the N-S cross-section of Figure 6b. It was already imaged with similar velocities by previous work (V_p ~7.4–7.7 km s^{-1}; Béthoux et al., 2007; Paul et al., 2001) but was only resolved down to depths of 15–20 km (cf. Figure 2g). Its P-wave velocity is not consistent with dry mantle peridotite or imbricated continental crust rocks as suggested for example by Schmid et al. (2017). Instead, it suggests mantle rocks with variable degrees of serpentinization (Reynard, 2013)

ranging from <30%, at depth greater than 30 km, to >90% in the uppermost part of the body (see Figure 4). According to Solarino et al. (2018), this high velocity body may include mantle-wedge rocks exhumed in the late Eocene together with the (U)HP rocks of the Dora-Maira massif, as a result of divergent motion between the Alpine slab and the Adriatic upper plate (Liao et al., 2018b; Malusà et al., 2011). In the southern Western Alps, these mantle-wedge rocks may contribute, together with the Adriatic mantle rocks exhumed during Tethyan rifting, to the positive gravity anomaly classically referred to as the Ivrea gravity anomaly due to the high-density "Ivrea body" (Closs & Labrouste, 1963; Nicolas et al., 1990a) (see Figure 5d).

The bottom part of the LET model of Solarino et al. (2018) provides absolute P-wave velocity constraints to the uppermost part of the Alpine subduction channel (SC in Figure 6c). At depth ~50 km, in the region located beneath the thick blue spot of RF negative polarity conversions (3 in Figure 6c), P-wave velocity is lower than in the nearby Adriatic upper mantle (~7.0–7.5 km s^{-1} vs. ~8.0 km s^{-1}). This region may include serpentinites or other lithologies possibly found in a high-pressure mélange zone (Marschall & Schumacher, 2012), such as eclogitic metasediments and mafic eclogites. However, the observed velocities (V_p ~7.0–7.5 km s^{-1}; $V_p/V_s < 1.70$) are consistent with ultramafic rocks with a degree of serpentinization ranging between 50% and 75% (according to Reynard, 2013), but they are neither consistent with eclogitic metasediments (V_p ~7.0 km s^{-1}; V_p/V_s ~1.75) nor with mafic eclogite ($V_p > 7.9$; V_p/V_s ~1.73) (Reynard, 2013; Weiss et al., 1999). V_p/V_s ratios ~1.74 indicate that slivers of eclogitic metasediments could be present instead at ~40 km depth beneath the western flank of the Dora-Maira massif.

In general terms, velocity changes evidenced by LET (Solarino et al., 2018) match with those highlighted by RF analysis (Zhao et al., 2015), despite the different techniques and datasets used (i.e., local vs. teleseismic events). Not only do the European and Adriatic Mohos detected by these different techniques show a remarkable fit (see Section 6.2), but also the downward velocity decrease revealed by LET from the exhumed mantle wedge to the underlying subduction channel is consistent with the spot of negative-polarity Ps-conversions provided by RF (3 in Figure 6c). A good match is also observed for local anomalies, e.g., the high V_p/V_s ratios in region ALC_1 (Figure 6c) corresponding to a major break in the alignment of positive-polarity Ps-conversions in the RF image (Figure 6d).

The shape of the high-velocity region corresponding to the exhumed mantle wedge is mirrored by the distribution of seismic events (Figure 6d) (Eva et al., 2015; Malusà et al., 2017). The exhumed mantle wedge is virtually aseismic, consistent with the fact that serpentinization promotes aseismic deformation (Hilairet et al., 2007; Peacock & Hyndman, 1999). Earthquakes are mainly located in the surrounding regions. To the east, the anomalously deep earthquakes ($30 < Z < 75$ km) recorded beneath the western Po Plain (Cattaneo et al., 1999; Eva et al., 2015) are aligned along an active lithospheric strike-slip fault referred to as the Rivoli-Marene deep fault (RMF in Figure 6d). Results provided by LET confirm that this left-lateral fault (see focal mechanisms in Figure 6d) is located in the mantle beneath the Adriatic Moho, as first proposed by Malusà et al. (2017) based on RF results. V_p/V_s values > 1.74, beside V_p ~8.0 km s^{-1} at depth around 25–35 km (Figure 6c) may reflect low S-wave velocities due to the impact of the Rivoli-Marene deep fault on the fabric of Adriatic-mantle peridotite (Solarino et al., 2018). In the same region, the azimuthal harmonic decomposition of RF reveals the occurrence of anisotropic rocks (Piana Agostinetti et al., 2017) (Figure 6d). High-amplitude anisotropic components of RF are observed in places also within the Adriatic crust and along the Adriatic Moho.

7.2. Absolute S-wave Velocity Structure From TransD Inversion

The shear wave velocity model of the Western Alps based on TransD inversion of Rayleigh wave group velocity dispersion data (Zhao et al., 2020) is shown in Figure 7. It provides absolute V_s constraints to the European and Adriatic crust, and a high-resolution image of the velocity structure of the Alpine subduction zone. Figures 7c–7e show three cross-sections of the inverted velocity model down to 90 km depth, in different sites of the Western Alps corresponding to the NFP-20 West, ECORS-CROP, and CIFALPS profiles. Along these cross-sections, the European lithospheric mantle (in blue on the left) is clearly underthrust beneath the Adriatic mantle on the eastern part of each profile (in blue on the right). A major Moho step of ~8 km, first highlighted by Lu et al. (2018), is detected along the ECORS-CROP profile beneath the Belledonne massif (Figure 7d). A similar Moho step is observed along the NFP-20 West profile (Figure 7c) north of the Frontal Pennine Fault. No Moho step is observed along the CIFALPS profile (Figure 7e).

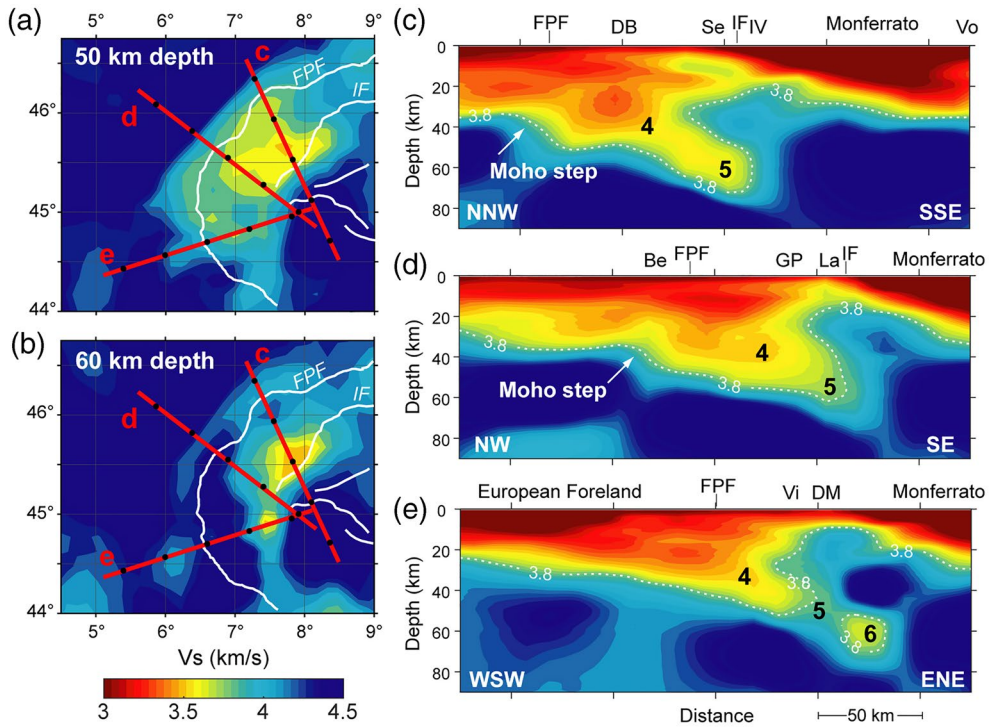

Figure 7. S velocity structure of the crust and the mantle wedge as revealed by Bayesian transdimensional (TransD) inversion of Rayleigh wave dispersion data (after Zhao et al., 2020). (a and b) Depth slices of the V_s tomography model at 50 and 60 km depth. (c and e) Inversion results showing absolute V_s in the 0–90 km depth range along the NFP-20 West (c), ECORS-CROP (d), and CIFALPS (e) cross-sections. The white dashed isovelocity lines indicate $V_s = 3.8$ km s^{-1}. Numbers 4-to-6 indicate regions of the model discussed in the text (acronyms as in Figure 1). The white arrow in (d) indicates a major (~8 km) Moho step beneath the western front of the Belledonne massif (Be), first highlighted by Lu et al. (2018). A similar Moho step is observed in (c) in correspondence with the Frontal Pennine Fault (FPF). Note the sharp V_s decrease at ~60 km depth along cross-section (e), which is not observed along cross-sections (c) and (d).

In the shear wave velocity model of Zhao et al. (2020), the Alpine subduction wedge exhibits a "normal" velocity structure in all three profiles, from Earth's surface to regions four and 5 (Figures 7c–7e). V_s values progressively increase with depth from ~3.3 km s^{-1} (red to orange colors) in the uppermost levels of the subduction wedge, to >3.6 km s^{-1} (yellow to green colors) at depth > 40 km. This normal velocity structure is consistent with expected V_s values in metapelites and gneisses exposed in the Alpine belt, and with a progressive V_s increase with depth. Very low V_s regions (dark red) correspond to the main sedimentary basins formed atop the European and Adriatic crusts (Southeast basin and Po Plain, respectively). The lateral extent of the low V_s material ascribed to the subduction wedge can be evaluated in the horizontal slices of the tomography model at 50 and 60 km depth (Figures 7a and 7b). The region with $V_s < 3.8$ km s^{-1} (green to yellow colors), detected all along the arc of the Western Alps at 60 km depth (Figure 7b), is apparently thicker in the northern Western Alps compared to the southern Western Alps.

On the eastern side of each cross-section, the culmination of the region with $V_s > 4.0$ km s^{-1} (marked by blue colors) invariably matches with the location of the Ivrea gravity anomaly shown in Figure 1b. A region with $V_s > 3.8$ km s^{-1} is imaged beneath the Dora-Maira starting from ~10 km depth. This region has a similar shape, with a near-vertical western boundary, as the high V_p anomaly imaged beneath the Dora-Maira by LET along the same profile (Figure 6c). A similar high-velocity region is not observed beneath the eclogitic domes farther north (Figures 7c and 7d), in line with results provided by LET (Solarino et al., 2018). At 50–70 km depth along the CIFALPS profile, the inverted model also shows a region with $V_s < 3.7$ km s^{-1} (green to yellow colors) that is interposed between the European lithospheric mantle and the overlying Adriatic mantle (6 in Figure 7e). This low-velocity region, which reverts a trend of progressively increasing V_s with depth, is not observed along the ECORS-CROP and NFP-20 West profiles (cf. Figures 7c and 7d). It has been interpreted by Zhao et al. (2020) as the evidence of serpentinites preserved along the Alpine subduction

channel. In fact, the decreasing V_s values from region five to region six cannot be explained by metamorphic phase changes in metapelites and gneisses. The only rock characterized by V_s values of ~3.6 km s^{-1} in the 55–70 km depth range is serpentinite (Figure 4). Alternatively, the low V_s values in region 6 may be due to high pore-fluid pressures, which would in turn promote serpentinization. A sharp V_s increase, observed at depth >70 km along the Alpine subduction channel, may reflect destabilization of antigorite and transformation of subduction-channel serpentinite into peridotite (e.g., Reynard, 2013).

8. Velocity Structure in the Upper Mantle Along the CIFALPS Profile

For a reliable geologic interpretation of the upper mantle structure along the CIFALPS profile, seismic velocity constraints of the slab structure and the mantle flow in the surrounding asthenosphere are required. Crucial for the interpretation of seismic velocities in the Alpine upper mantle is also the location of the lithosphere-asthenosphere boundary beneath the European foreland and the Alpine subduction wedge. Within the framework of the CIFALPS experiment, this information is provided by array analysis of seismic surface waves (Lyu et al., 2017). Information concerning the deeper slab structure is provided by teleseismic P-wave tomography (Zhao et al., 2016b), whereas clues on asthenospheric mantle flow are provided by the analysis of seismic anisotropy (Salimbeni et al., 2018).

8.1. The Lithosphere-Asthenosphere Boundary Beneath the Alpine Foreland Areas

The depth of the lithosphere-asthenosphere boundary beneath the Alpine region has been investigated by Lyu et al. (2017) using a combination of CIFALPS and permanent seismic station data. Lyu et al. (2017) inverted the fundamental mode Rayleigh wave dispersion curves for V_s using the crustal interfaces imposed from RF (Zhao et al., 2015). The resulting V_s values, derived from independent measurements in each mini-array, are shown in Figure 8a. V_s values vary smoothly across the profile length. The decrease in S-wave velocity below ~110 km depth in the western part of the profile (Figure 8a) has been interpreted by Lyu et al. (2017) as the lithosphere-asthenosphere boundary beneath the European foreland. The top of this low-velocity layer, marked by a thick dashed line in Figure 8a, is approximately parallel to the eastward dipping European Moho as detected by RF and other methods, which suggests a ~110 km thick and eastward-dipping European lithosphere. These findings are consistent with the lithospheric thickness generally observed in Phanerozoic Europe using surface waves (e.g., Cotte et al., 2002; Dost, 1990) and S-receiver functions (Geissler et al., 2010). S-wave velocities retrieved by Lyu et al. (2017) in the European upper mantle are overall low, at least when compared with velocities of the AK135 model (Kennett et al., 1995). S-wave velocities are much higher in the Adriatic lithosphere (~5 km s^{-1}, dark blue colors in Figure 8a), and consistent with a lithosphere-asthenosphere boundary located at ~100 km depth beneath the Po Plain, as proposed by Brandmayr et al. (2010) and Malusà et al. (2018).

8.2. Velocity Structure Beneath the Alpine Subduction Wedge

According to Lyu et al. (2017), very low V_s values < 4 km s^{-1} are found at the base of the European lithosphere in the central part of the CIFALPS profile, at depth ~120 km beneath the Alpine subduction wedge (7 in Figure 8a). In that region, the high-velocity anomaly imaged by teleseismic P-wave tomography is strongly attenuated (Lippitsch et al., 2003; Zhao et al., 2016b; see Section 8.3), and a low-V_s anomaly has been also detected by FWI (Beller et al., 2018) (7 in Figure 8b). This is illustrated in the composite cross-section of Figure 8b, which combines in the upper panel the results of TransD inversion of surface-wave dispersion data (Zhao et al., 2020), and in the lower panel the V_p perturbations based on teleseismic P-wave tomography (Zhao et al., 2016b). The V_s anomaly derived from FWI and described by Beller et al. (2018) is shown as purple isolines (Figure 8b). Note that these different models are based on different data, obtained by means of different techniques and their resolving power is also different. Beller et al. (2018) have suggested that the low-V_s anomaly detected in their S-wave velocity model may be supportive of a slab detachment beneath the Western Alps, an interpretation recently reintroduced by Dal Zilio et al. (2020) and Kästle et al. (2020). However, when the low-V_s anomaly detected by Beller et al. (2018) is analyzed in more detail and compared with information provided by independent tomographic methods along the CIFALPS profile (Fig. 8b), a different scenario emerges. The anomaly shows in fact two peaks, a weaker one at the base of the

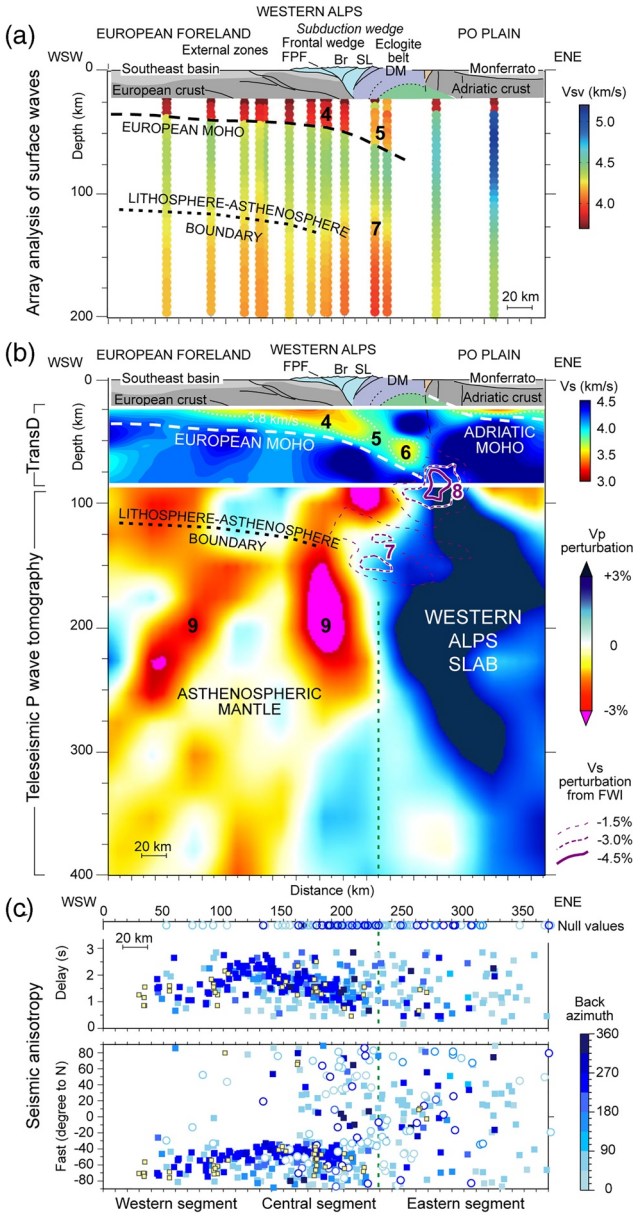

Figure 8. Upper mantle velocity structure along the CIFALPS transect. (a) Absolute V_s based on array analysis of seismic surface waves (after Lyu et al., 2017); numbers in bold indicate regions of the model discussed in the main text. Acronyms as in Figure 1. (b) Composite cross-section showing, in the upper panel (20–90 km depth), the absolute V_s values (in km s^{-1}) based on Bayesian TransD inversion of surface-wave dispersion data (Zhao et al., 2020) and, in the lower panel (90–400 km depth), the V_p perturbations (in %) based on teleseismic P-wave tomography (Zhao et al., 2016b); lithosphere-asthenosphere boundary as in (a). Purple lines are isolines of equal V_s anomaly (relative to the preliminary reference Earth model of Dziewonski & Anderson, 1981) as derived from teleseismic full-waveform inversion (FWI, Beller et al., 2018). Numbers 4-to-9 indicate regions of the model discussed in the main text. All of the anomalies discussed in the original publications are indicated. The European lithosphere in the upper panel is directly connected with the steeply dipping Western Alps slab (in blue) in the lower panel. A prominent low-velocity anomaly (yellow to red colors in the lower panel) is located to the west of the Western Alps slab, beneath the core of the Western Alps and the European foreland. (c) Distribution of delay times and fast axis orientations of SKS splitting measured in a 60-km wide swath profile along the CIFALPS transect. In blue are splitting measurements from Salimbeni et al. (2018) (color coded according to the back-azimuth), in yellow are splitting measurements pre-dating the CIFALPS experiment (from Barruol et al., 2004, 2011; Salimbeni et al., 2008, 2013). Null measurements (empty circles) are plotted as fast axes parallel to the back-azimuth and dt > 3 s. Note the sharp change in fast axis orientation and delay time across the dashed green line, which reflects a major change in upper mantle structure as shown in (b). In the western and central segments of the CIFALPS profile, delay times are lower in correspondence of stronger low-V_p perturbations.

European lithosphere (7 in Figures 8band 8a) stronger one at ∼75–95 km depth along the subduction channel above the European slab (8 in Figure 8b). The anomaly (8) is not present in the TransD inversion model of Zhao et al. (2020) because it lays in a region where the model is not well resolved (cf. Zhao et al., 2020, their Figure S9). Along the subduction channel, low V_s values in the 55–70 km depth range (6 in Figure 8b) likely mark the occurrence of serpentinite (see Section 7.2). Given the sharp V_s increase at depth >70 km along the subduction channel (Figure 8b), interpreted by Zhao et al. (2020) as due to transformation of serpentinite into peridotite after destabilization of antigorite (cf. Figure 4), the low V_s anomaly detected by Beller et al. (2018) at 75–95 km depth (8 in Figure 8b) may also indicate a metasomatized mantle peridotite due to infiltration of slab fluids. We conclude that comparison among different techniques underlines that the results provided by Beller et al. (2018) are not supportive of European slab detachment. Instead, they are consistent with the results provided by other tomography approaches that have been applied during the CIFALPS experiment (e.g., Lyu et al., 2017; Zhao et al., 2020).

8.3. Slab Structure From Teleseismic P-Wave Tomography

Previous seismic tomography models of the Alpine upper mantle have revealed more or less discontinuous P-wave velocity anomalies interpreted as the seismic signature of subducted lithospheric slabs (e.g., Lippitsch et al., 2003; Piromallo & Faccenna, 2004; Wortel & Spakman, 2000). However, interpretations in terms of slab length and lateral or vertical slab continuities strongly depend on the resolution of seismic tomography models. The Zhao et al. (2016b)'s tomography study performed within the framework of the CIFALPS experiment first benefited from the recent opening of the European seismic databases and improvement of the permanent broadband network. It is based on a much denser station coverage than any previous work, especially in the Western Alps. Data were recorded by 527 broadband seismic stations: 449 from permanent networks, 23 from the PYROPE temporary experiment (Chevrot et al., 2014), and 55 from the CIFALPS experiment. In order to avoid interference of upper mantle tomography by crustal anomalies, Zhao et al. (2016b) used the EPcrust reference model to correct for traveltime residuals within the crust (Molinari & Morelli, 2011). Although the EPcrust model does not include all the details of the most recent Moho maps (e.g., Lu et al., 2020; Spada et al., 2013), and the approach chosen by Zhao et al. (2016b) does not include the effects of 3-D propagation of nonvertical rays from different azimuths in the heterogeneous crust (e.g., Waldhauser et al., 2002), synthetic tests performed by Zhao et al. (2016b) indicate that their tomography model of V_p perturbations is not significantly affected by smearing of crustal anomalies to mantle depth.

Teleseismic tomography models of V_p perturbations display lateral P-wave velocity changes with respect to the horizontally averaged V_p in the region crossed by incident P waves. They are not associated to a reference model. The lower panel of Figure 8b shows a cross-section of the Zhao et al. (2016b)'s model along the CIFALPS profile down to 400 km depth. The cross-section includes strong low-velocity anomalies (9 in Figure 8b) at 100–250 km depth beneath the Frontal wedge and the European foreland, and an E-dipping high-velocity anomaly (blue in Figure 8b) beneath the Eclogite belt and the western Po Plain. This high-velocity anomaly, likely marking the European slab beneath the Western Alps, is continuous from the uppermost mantle where it links with the lithosphere-asthenosphere boundary detected by array analysis of seismic surface waves (Lyu et al., 2017) and with the European Moho recognized by RF and TransD inversion (Zhao et al., 2015, 2020). Specific resolution tests suggest that any major slab gap should be revealed by the model, if present. According to the tomography model, the inferred length of the Western Alps slab may reach ∼300 km (cf. Malusà et al., 2015, their Figure 6), but such estimate should be taken with caution due to the potential vertical smearing typical of teleseismic body-wave tomography images. The Zhao et al. (2016b)'s model also shows a weakening of the high-velocity anomaly at the base of the European lithosphere (7 in Figure 8b), supported by the results of subsequent work by Lyu et al. (2017) and Beller et al. (2018) discussed in Sections 8.1 and 8.2. Such weakening affects part, but not the entire thickness of the Western Alps slab.

8.4. Comparison With Other Tomography Models

The continuity of the high-velocity anomaly in the Zhao et al. (2016b)'s model along the CIFALPS profile contrasts with those interpretations (e.g., Fox et al., 2015; Kissling & Schlunegger, 2018; Kästle et al., 2020)

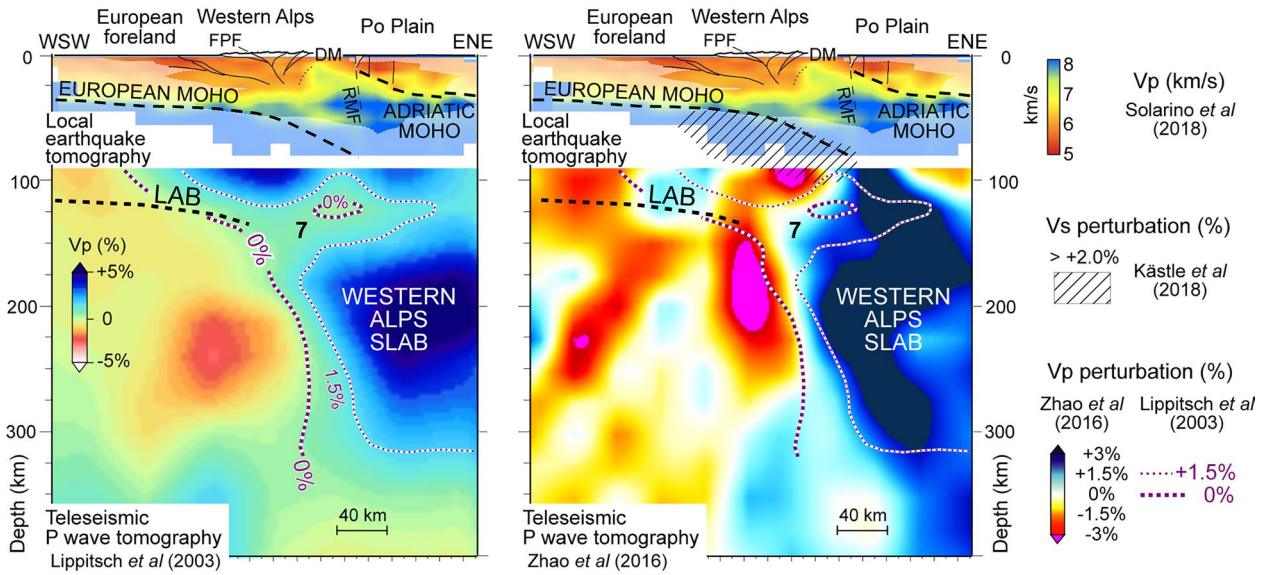

Figure 9. Comparison of upper mantle V_p perturbations beneath the CIFALPS transect according to the teleseismic P-wave tomography models of Lippitsch et al. (2003) (left) and Zhao et al. (2016b) (right). Absolute V_p values in the 0–60 km depth range are from Solarino et al. (2018) (see Figure 6). Note the good correspondence between the high velocity anomaly detected by Zhao et al. (2016b) (in blue on the panel to the right) and the first-order features of the Lippitsch et al. (2003) model as highlighted by isolines of equal V_p anomaly (in purple, also reported in the panel to the right for the sake of clarity). Despite the broadly similar velocity structures, either a continuous or broken-off slab was proposed (see text for discussion). The region of positive V_s perturbation (>+2% relative to the preliminary reference Earth model of Dziewonski & Anderson, 1981) proposed by Kästle et al. (2018) is also reported (black hatched area to the right). Acronyms: DM, Dora-Maira; FPF, Frontal Pennine Fault; LAB, lithosphere-asthenosphere boundary; RMF, Rivoli-Marene Deep Fault.

based on the Lippitsch et al. (2003)'s model that have suggested slab breakoff beneath the Western Alps (see also Figure 3c). Kissling and Schlunegger (2018) rejected the Zhao et al. (2016b)'s interpretation of a continuous slab in the Western Alps using the arguments that the Zhao et al. (2016b)'s model would be mainly based on 2-D information and poor quality data, which is incorrect as it is based on data from >500 stations distributed in the entire Alpine region (gray triangles in Figure 1a), including 29 months of data at 449 high-quality broadband permanent stations. Cross-sections of these different tomographic models are compared in Figure 9: the Lippitsch et al. (2003)'s ray-based model (on the left in Figure 9) has a horizontal grid size of 50 km, it is based on ~4,200 traveltime measurements and it was the first to suggest a slab breakoff beneath the Western Alps; the Zhao et al. (2016b)'s kernel-based model (on the right in Figure 9) has a denser horizontal grid size of 25 km, it is based on ~42,000 traveltime measurements and was the first to explicitly propose a continuous slab under the Western Alps, although similar evidence is also provided by teleseismic tomography models from other working groups (e.g., Giacomuzzi et al., 2011; Hua et al., 2017; Koulakov et al., 2009; Paffrath et al., 2020; Piromallo & Morelli, 2003). As shown in Figure 9, the first-order features of the Lippitsch et al. (2003)'s and Zhao et al. (2016b)'s models are remarkably similar, despite interpretations that are quite different (for the sake of clarity, the contours of equal V_p anomaly in the Lippitsch et al. (2003)'s model are also plotted onto the Zhao et al. (2016b)'s model to the right). Both models show low-V_p anomalies located beneath the European foreland and a high-V_p anomaly under the western Po Plain that becomes weaker at ~120 km depth (7 in Figure 9). The 0% anomaly isoline in the Lippitsch et al. (2003)'s model largely matches the boundary between high-V_p and low-V_p perturbations in the Zhao et al. (2016b)'s model. The observed differences in the amplitudes of V_p perturbations between models are not informative, because the kernel-based models (e.g., the finite frequency method used in Zhao et al., 2016b) generally yield higher root-mean square amplitudes for V_p perturbations than the ray-based method (e.g., Lippitsch et al., 2003).

Evidence of potential slab breakoff and associated passive asthenospheric upwelling along the breakoff gap should include, in a teleseismic P-wave tomography model, a low-velocity anomaly cutting across the high-velocity anomaly representing the broken slab. However, the shape of the anomaly is generally retrieved much better than its amplitude. Within the framework of the CIFALPS experiment, Zhao et al. (2016b) performed a series of tests, e.g., by replacing part of the high-velocity slab with a low-velocity

body extending from 80 to 140 km depth, in order to mimic a possible slab breakoff beneath the CIFALPS profile. They found that the shape of a low-velocity body, if present, would be well recovered as a low-velocity anomaly by the inversion, albeit with attenuated amplitude (see Zhao et al., 2016b, their Figure 5). They also demonstrated that a strong high-velocity anomaly in the crust like the Ivrea body does not smear to mantle depth and could by no way erase or attenuate a possible low-velocity anomaly in the mantle related to slab breakoff (see Zhao et al., 2016b, their Figure 6). Within this framework, it is worth noting that the small low-velocity anomaly at ∼120 km depth detected by Lippitsch et al. (2003) under the Dora-Maira is not connected, in their model, with the main low-velocity anomaly beneath the European foreland (see the left panel in Figure 9). In fact, the two regions are separated by a region with V_p (%) > 0. Based on these considerations, the Lippitsch et al. (2003)'s model may provide no clear support to the hypothesis of a slab detachment along the CIFALPS profile, which would also imply a much stronger and continuous negative anomaly beneath the Dora-Maira.

The right panel of Figure 9 also includes the fast V_s anomaly imaged by Kästle et al. (2018) by analysis of surface wave dispersion data from ambient noise and earthquakes (black hatched area in Figure 9). The Kästle et al. (2018)'s model is sometimes invoked, together with the Lippitsch et al. (2003)'s and the Beller et al. (2018)'s models, to support the hypothesis of a detached slab beneath the Western Alps (see discussion in Kästle et al., 2020). However, the recent review paper by Kästle et al. (2020) may suggest that the Kästle et al. (2018)'s model does not provide an accurate image of the subducted lithosphere beneath the Western Alps. Indeed, the body-wave tomography models compared by Kästle et al. (2020) in their Figure 2 (Koulakov et al., 2009; Lippitsch et al., 2003; Zhao et al., 2016b) invariably include an ENE-WSW trending high-V_p anomaly located to the south and well outside the Switzerland borders in the 120 and 200 km depth slices, whereas the Kästle et al. (2018)'s model, by contrast, shows an E-W trending high-V_s anomaly that is located more to the north and within the Switzerland borders.

8.5. Seismic Anisotropy

The birefringence of core-refracted shear waves (SKS phase) and associated transverse anisotropy of seismic velocities (Mainprice et al., 2000; Savage, 1999) can provide information on the lattice-preferred-orientation of olivine crystals in the mantle. Salimbeni et al. (2018) analyzed the seismic anisotropy properties beneath seismic stations of the CIFALPS profile using the waveforms of 40 teleseismic events with Mw > 5.8, considering the azimuth of the fast axis (φ) and the delay time (dt) as proxies for the preferred orientation of olivine a axes and the thickness of the anisotropic layer (Silver et al., 1999). The resulting distributions of delay times and fast axis orientations are plotted in Figure 8c using different colors according to the back-azimuth of the seismic events.

Three different segments of the CIFALPS profile (western, central and eastern segments) are distinguished by Salimbeni et al. (2018) based on seismic anisotropy data. The western segment shows quite homogeneous fast-axis directions in the range of $-60° \pm 20°$, with minor differences depending on the back-azimuth. Along the western segment, ray paths coming from the West (dark blue marks in Figure 8c) show increasing delay times from ∼1 s (at abscissae ∼40 km) to ∼2.4 s (at abscissae ∼140 km). In the central segment, ray paths coming from the West (dark blue marks) define a trend of linearly decreasing delay times from ∼2.4 s (at abscissae ∼140 km) to ∼1.0 s (at abscissae ∼220 km). No such trend is observed in the eastern segment of the profile, where the fast-axis directions are much more dispersed and the delay time is strongly scattered in a range from <1 to 2.8 s. The abrupt change in seismic anisotropy pattern between the central and the eastern segments of the CIFALPS profile occurs in correspondence with the transition (green dashed line in Figures 8b and 8c) between the high-velocity anomaly marking the Western Alps slab and the low velocity anomaly detected to the west. West of the green dashed line, delay time variations for ray paths coming from the west show some correlation with the low P-wave velocity perturbations shown in Figure 8b (red to yellow colors): higher delay times are found where the low-velocity anomaly in the mantle is weaker (i.e., at abscissae ∼140 km), whereas lower delay times are found where the low-velocity anomaly in the mantle is stronger. A geologic interpretation of this seismic anisotropy pattern requires a 3-D analysis of delay times and fast-axis directions with respect to the slab structure of the entire Alpine region, which is presented in Section 9.

9. Slab Structure of the Broader Alpine Region

The complex slab structure of the broader Alpine region is still actively debated (e.g., Handy et al., 2015; W. Q. Ji et al. 2019; Kästle et al., 2020; Rosenberg et al., 2018; Schmid et al., 2013). Within the framework of the CIFALPS experiment, useful pinpoints are provided by teleseismic P-wave tomography (Zhao et al., 2016b) and 3-D Pn tomography (Sun et al., 2019).

9.1. Continental Subduction From 3-D Pn Tomography

Sun et al. (2019) mapped the seismic velocity signature of continental subduction in the broader Alpine region by inversion of Pn phase traveltimes, using data recorded by permanent and temporary stations since the 1960s (Figure 1a). Pn phases, i.e., the first arrivals at regional distance, propagate through the crust, penetrate the uppermost mantle and are finally refracted at the Moho and return to the free surface (Hearn, 1999). The tomography model of Sun et al. (2019) is based on a three-step 3-D approach (Sun & Kennett, 2016a, 2016b) applied to a dataset of >395,000 Pn arrivals for >9,500 events and 1,080 stations, and provides absolute P-wave velocities in the uppermost 80 km of the Alpine lithosphere. In their model, the expected seismic velocity signature of continental subduction is given by P-wave velocities lower than those expected for upper-mantle peridotites (i.e., $V_p < 7.7$ km s^{-1}, see Figure 4). Oceanic subduction should remain undetected using the Sun et al. (2019)'s approach, because the high V_p values of the oceanic crust after eclogitization ($V_p > 7.9$ km s^{-1} for mafic eclogites) are undistinguishable from the high V_p values of upper-mantle peridotites (Figure 4).

The P-wave velocity structure retrieved by Sun et al. (2019) is illustrated in the 50-km depth slice of Figure 10a. It shows elongated regions characterized by $V_p < 7.7$ km s^{-1} (yellow-to-red colors) all along the northeastern, northwestern and southwestern boundaries of the Adriatic microplate, providing evidence for continental subduction along the Dinaric, Alpine and Apenninic subduction zones, respectively. The low-velocity belt corresponding to Dinaric subduction displays a remarkable continuity from Austria to Albania. The Dinaric low-velocity belt terminates at high-angle (1 in Figure 10a) against the low-velocity belt of the Eastern Alps, which shows an ENE–WSW trend consistent with major thrust faults formed during Alpine subduction. In the western Alpine region, the low-velocity belts provided by 3-D Pn tomography show an abrupt change in orientation (2 in Figure 10a) likely marking the boundary between the Alpine and Apenninic subduction zones. Underthrusting of continental material by Apenninic subduction can be detected as far north as near Genoa. Prominent breaks (3 and 4 in Figure 10a) are also observed in the Northern and Central Apennines. Higher V_p values in the Southern Apennines suggest that subduction in southern Italy was dominantly oceanic, as also indicated by the geochemistry of subduction-related magmatism (Peccerillo & Frezzotti, 2015).

9.2. Slab Structure From V_p Anomalies in Teleseismic Tomography Models

The previously mentioned P-wave tomography model of Zhao et al. (2016b) provides constraints for the upper-mantle velocity structure of the broader Alpine region down to 600 km depth. The main features of the model are illustrated in Figure 10 by three horizontal slices at 100, 200 and 300 km depth (Figures 10b–10d) and by four cross-sections (Figure 10e). Salient features of the model include the lateral continuity, from the Central Alps to the Western Alps, of the high-velocity anomaly ascribed to the Alpine slab, and the lateral continuity of the high-velocity anomaly ascribed to the Apenninic slab that is particularly evident in the Northern Apennines. In the 100-km depth slice (Figure 10b), at the transition between the Northern and the Southern Apennines, the model shows a major gap in the Apenninic high-velocity anomaly that was already detected by previous work and interpreted as a potential slab window (Amato et al., 1998; Faccenna et al., 2014). Another important feature of the model is the step between the ENE-WSW trending high-velocity anomaly ascribed to the Alpine slab beneath the Central Alps, and the NW-SE trending high-velocity anomaly detected beneath the Eastern Alps (Hua et al., 2017; Zhao et al., 2016b). The latter is shifted northward and forms an angle of 30°–60° (depending on the depth range) relative to the strike of the Alpine frontal thrusts. The model also shows two main low-velocity anomalies (yellow-to-red colors in Figures 10b–10e), labeled as "low V_p anomaly A" and "low V_p anomaly B″ in Figures 10b–10e. The former is located in the upper mantle of the Western Alps at 100–300 km depth, and does not extend east of 8°E.

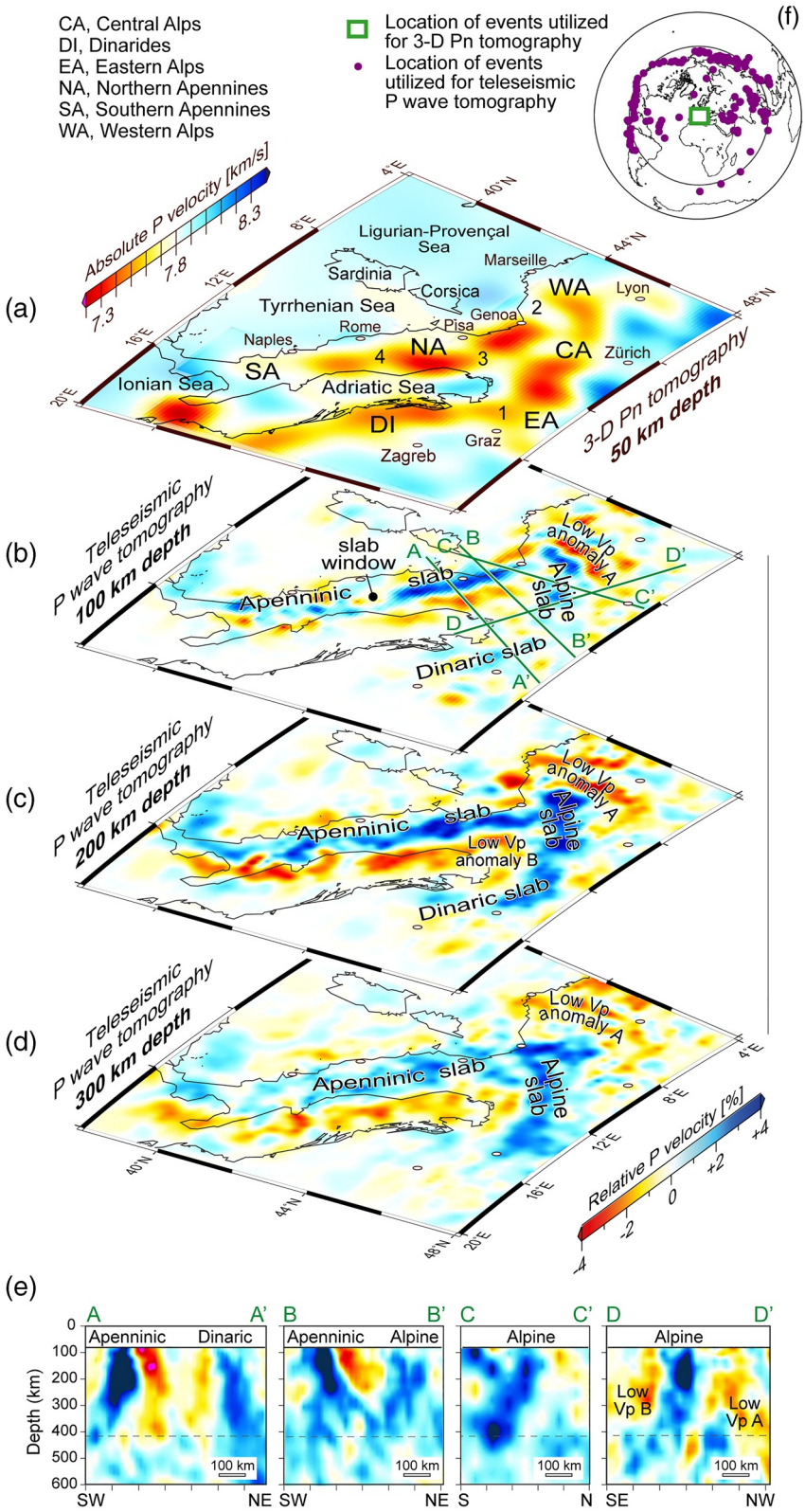
CA, Central Alps
DI, Dinarides
EA, Eastern Alps
NA, Northern Apennines
SA, Southern Apennines
WA, Western Alps
Location of events utilized for 3-D Pn tomography
Location of events utilized for teleseismic P wave tomography
(f)
(a)
Absolute P velocity [km/s]
7.3
7.8
8.3
Ligurian-Provençal Sea
Marseille
Sardinia
Corsica
Tyrrhenian Sea
Genoa
Pisa
Rome
Naples
Lyon
Zürich
Ionian Sea
Adriatic Sea
Graz
Zagreb
WA
NA
CA
SA
DI
EA
3-D Pn tomography
50 km depth
(b)
Teleseismic P wave tomography
100 km depth
slab window
Apenninic slab
Alpine slab
Low Vp anomaly A
Dinaric slab
(c)
Teleseismic P wave tomography
200 km depth
Apenninic slab
Low Vp anomaly B
Alpine slab
Low Vp anomaly A
Dinaric slab
(d)
Teleseismic P wave tomography
300 km depth
Apenninic slab
Alpine slab
Low Vp anomaly A
Relative P velocity [%]
(e)
Depth (km)
Apenninic
Dinaric
Alpine
Low Vp B
Low Vp A
100 km
SW
NE
S
N
SE
NW

The latter is located in the Adriatic upper mantle beneath the Po Plain, and lays above the Alpine slab (see Figure 10e, cross-section D-D′).

In cross-section, the Zhao et al. (2016b)'s tomography model shows a steep SW-dipping high-velocity anomaly beneath the northern Tyrrhenian region corresponding to the Apenninic slab, and an even steeper NE-dipping high-velocity anomaly beneath the Eastern Alps and the northernmost Dinarides (A-A′ in Figure 10e). The origin of this latter anomaly, also detected by several other tomography models (e.g., Dando et al., 2011; Hua et al., 2017; Lippitsch et al., 2003; Mitterbauer et al., 2011), is still debated. It is either interpreted as due to continental Dinaric subduction during the Neogene (Handy et al., 2015; Schmid et al., 2013), as stemming from an oceanic and detached Alpine slab (Rosenberg et al., 2018), or as resulting from a more complex interaction between the Alpine and Dinaric slabs (W. Q. Ji et al., 2019; Kästle et al., 2020; Sun et al., 2019) as discussed in more detail in Sect. 9.3. The relationships between the Alpine and Apenninic slabs are clearer. In cross-section B-B′ (Figure 10e), the Alpine slab dips toward the SW and the steeply dipping Apenninic slab is almost overturned to a northeastward dip. The down-dip continuity of the Alpine slab in the Central Alps is as debated as in the Western Alps (e.g., W. Q. Ji et al., 2019; Kissling & Schlunegger, 2018; Kästle et al., 2020). The Zhao et al. (2016b)'s model shows a remarkable down-dip continuity of the high-velocity anomaly in the Central Alps (see cross-sections B-B′, C-C′, and D-D′ in Figure 10e) that conflicts with the hypothesis of slab breakoff (e.g., Kissling & Schlunegger, 2018; von Blanckenburg & Davies, 1995). The amount of subducted lithosphere shown in cross-section D-D′ is consistent with the amount of subduction predicted by paleomagnetic and geologic constraints (Handy et al., 2010; Malusà et al., 2015). About 450 km subduction took place in the Central Alps based on geologic evidence (Malusà et al., 2016a), which is also the amount that can be inferred from the length of the high-velocity anomaly in cross-section D-D′.

9.3. Interpretive Slab Structure Beneath the Alpine Region

Constraints on the slab structure provided by teleseismic P-wave and 3-D Pn tomography (Sun et al., 2019; Zhao et al., 2016b) are summarized in Figure 11. Outside of the well-resolved areas of the Zhao et al. (2016b)'s model, slab traces (thick blue lines in Figure 11a) are based on a previous, lower-resolution tomography model by Piromallo and Morelli (2003). In general terms, there is a good match between the sites of continental subduction documented by 3-D Pn tomography (thick brown lines in Figure 11a) and the slab structure inferred from teleseismic P-wave tomography, in spite of the different techniques and data sets used (see event locations in Figure 10f). As shown in the cartoon of Figure 11b, two opposite-dipping slabs are attached to the southwestern and northeastern boundaries of the Adriatic microplate, forming a reversed U-profile in cross-section (Salimbeni et al., 2013; Sun et al., 2019; Vignaroli et al., 2008; Zhao et al., 2016b). To the southwest, the segmented low-V_p belt attesting to subduction of Adriatic crust beneath the Northern Apennines matches with the Apenninic slab trace documented by teleseismic P-wave tomography (Figure 11a), whereas subduction beneath the Southern Apennines mainly involved Ionian oceanic crust (Figure 11b). On the northeastern boundary of the Adriatic microplate, the Adriatic crust underthrust beneath the Dinarides is connected with a NE-dipping high-velocity anomaly interpreted as the Dinaric slab (Figure 11a). The ophiolitic rocks of the Sava and Vardar units exposed farther east (dashed green lines in Figure 11a) are likely relics of older, Mesozoic subduction zones (Sun et al., 2019).

During the progressive northward motion of the Adriatic microplate in the Cenozoic (Dewey et al., 1989; Jolivet et al., 2003), the Apenninic and Dinaric slabs have likely interacted with the SE-dipping Alpine slab to the North (W. Q. Ji et al., 2019; Malusà et al., 2016b, 2018). It has been suggested that the interaction between the northward shifting Apenninic slab and the Central Alps slab may have controlled the location of the northern tip of the Ligurian-Provençal basin during Apenninic slab retreat and associated Neogene ex-

Figure 10. Upper mantle velocity structure in the broader Alpine region. (a) Absolute P velocities at 50 km depth according to the 3-D Pn tomography model of Sun et al. (2019). Belts of yellow-to-orange colors indicate the lateral extent of continental subduction (numbers 1–4 indicate features discussed in the main text). (b, c and d) V_p anomalies in the teleseismic tomography model of Zhao et al. (2016b) at 100, 200, and 300-km depth. Low-velocity anomalies A and B (yellow-to-red colors) are detected on both sides of the Alpine slab, which is underlined by a laterally continuous high-velocity anomaly (blue colors). (e) Representative cross-sections (see locations in (b)—green solid lines) of the teleseismic tomography model of Zhao et al. (2016b), showing the attitude of the Alpine, Apenninic, and Dinaric slabs. (f) Seismic events used for the tomography models of Sun et al. (2019) (green box) and Zhao et al. (2016b) (purple dots).

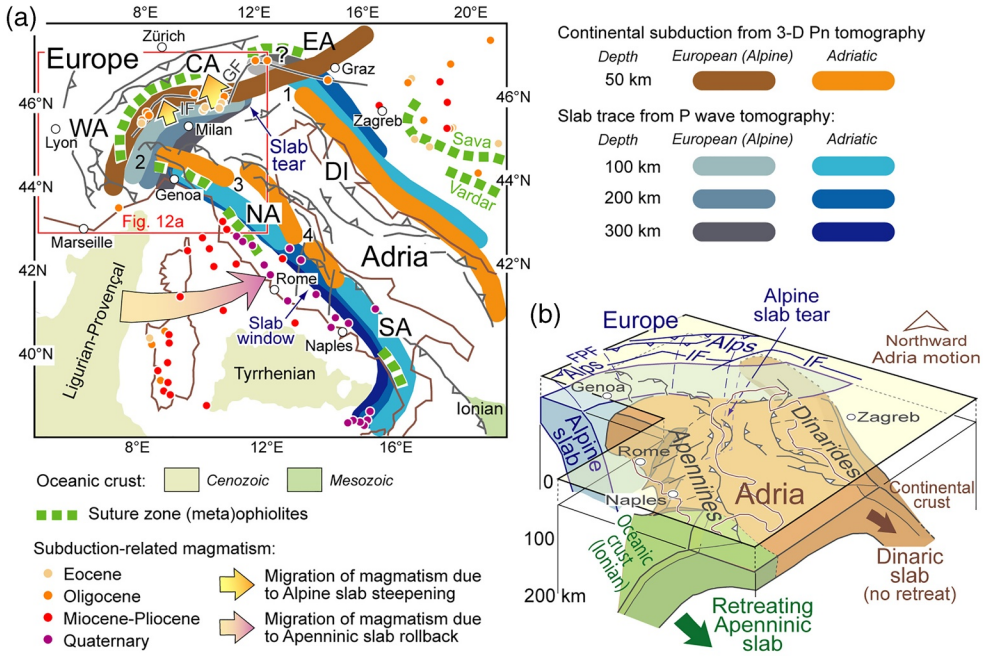

Figure 11. Interpretive slab structure beneath the Alpine region as constrained by recent tomography studies. (a) Tectonic sketch map showing the relations among slab structure (Sun et al., 2019), distribution of orogenic magmatism (Carminati & Doglioni, 2012; W. Q. Ji et al. 2019; Kovacs et al., 2007) and accreted (meta)ophiolites (Bigi et al., 1990; Ustaszewski et al., 2008). The present-day slab traces at 100, 200, and 300-km depth are based on the P-wave tomography models of Zhao et al. (2016b) and Piromallo and Morelli (2003) (which was only considered outside of the well-resolved areas of the Zhao et al. (2016b)'s model). Numbers 1–4 (same as in Figure 10a) indicate features discussed in the main text. The question mark indicates the controversial high-velocity anomaly beneath the remnants of the former Alpine subduction zone. IF, Insubric Fault; GF, Giudicarie Fault; other acronyms as in Figure 10a (b) Cartoon summarizing the relationships between the Alpine slab and the Apenninic and Dinaric slabs (modified after Sun et al., 2019).

tension in the Apenninic backarc region (Malusà et al., 2016b). At the transition between the Eastern Alps and the Dinarides, the NE-dipping high-velocity anomaly detected in the 100–200 km depth range beneath the remnants of the former Alpine subduction zone (question mark in Figure 11a) may also provide evidence of the interaction between different slabs. This enigmatic feature may either represent the northern edge of the Dinaric slab, or the overturned remnants of the Alpine slab, or a combination of the two slabs (Kästle et al., 2020; Rosenberg et al., 2018; Salimbeni et al., 2013; Schmid et al., 2013; Sun et al., 2019; Zhao et al., 2016b). Further constraints to the complicated slab structure in that region are expected in the next future from the AlpArray experiment (e.g., Paffrath et al., 2020; Plomerova et al., 2020).

To the West of the Giudicarie Fault, subducted continental material imaged by Pn tomography is clearly connected with the SE-dipping high-velocity anomaly of the Alpine slab, which is continuously imaged from the Western to the Central Alps (Figure 11a). To the east of the Giudicarie Fault, this high-velocity anomaly shows a systematic northward step, interpreted by W. Q. Ji et al. (2019) as the evidence of a vertical tear in the Alpine slab (Figure 11), possibly formed after the onset of Dinaric subduction in the Eocene (e.g., Carminati et al., 2012). According to W. Q. Ji et al. (2019), the interaction between the Alpine and Dinaric slabs, and the consequent progressive steepening of the Alpine slab would explain the timing, distribution and geochemistry of Periadriatic magmatism in the absence of slab breakoff, providing a viable alternative to the classic slab-breakoff model of Periadriatic magmatism proposed by von Blanckenburg and Davies (1995).

Farther South, at the transition between the Alpine and Apenninic slabs, previous tomography models (e.g., Piromallo and Morelli, 2003) have suggested the occurrence of a major slab gap. This gap would have allowed the development of an asthenospheric toroidal flow compensating the long-recognized retreat of

the Apenninic slab (Faccenna & Becker, 2010; Salimbeni et al., 2013; Vignaroli et al., 2008), which is attested to by a progressive migration of Cenozoic orogenic magmatism across the Mediterranean (Figure 11a) (e.g., Carminati & Doglioni, 2012; Lustrino et al., 2011). However, the slab structure revealed by the CIFALPS experiment shows no evidence of a major gap between the Alps and the Apennines at upper mantle depths (Figure 11b). This finding has major implications for the interpretation of the seismic anisotropy pattern at the scale of the broader Alpine region, as described below.

9.4. Polyphase Development of Anisotropic Mantle Fabrics

In Figure 12a, shear wave splitting measurements on CIFALPS data (Salimbeni et al., 2018) and from previous work (Barruol et al., 2004, 2011; Salimbeni et al., 2008, 2013) are plotted on the 150-km depth slice of the Zhao et al. (2016b)'s tomography model as segments parallel to the fast axis and scaled with the delay time. Because the Alpine and Adriatic slabs are both very steep, any depth slice of the Zhao et al. (2016b)'s model would provide similar relationships between velocity anomalies and anisotropy. These relationships reveal a polyphase development of anisotropic mantle fabrics in the Alpine region, which may either reflect fossil or active mantle flows (Salimbeni et al., 2018). Note that the shear wave splitting measurements indicated by the purple segments in Figure 12a integrate the seismic anisotropy over the uppermost 300 km and are mainly due to the lattice-preferred-orientation of olivine crystals in the mantle (Savage & Sheehan, 2000; Piromallo et al., 2006). In order to discriminate upper mantle and crustal contributions to the observed seismic anisotropy, S wave anisotropy measurements from local earthquakes (Baccheschi et al., 2019) are also shown in Figure 12a and are indicated by different shades of green for different depth ranges. However, the contribution of crustal anisotropy to the total seismic anisotropy is minor, as highlighted by the different scales adopted for the different splitting measurements (Figure 12a). This negligible contribution of crustal anisotropy to total shear-wave splitting measured on SKS phases is confirmed at the scale of the greater Alps by preliminary results from the AlpArray seismic experiment (Link et al., 2020).

According to Salimbeni et al. (2018), shear wave splitting measurements plotting on the high-velocity anomalies of the Zhao et al. (2016b)'s model may reflect fossil fabrics in the lithospheric mantle of the Alpine and Apenninic slabs (1 in Figure 12a). Fossil fabrics within slabs are generally considered a negligible source of anisotropy (Audet, 2013; Long & Silver, 2008, 2009). However, a fossil fabric defined by olivine crystallographic preferred orientation (CPO) can be preserved in the oceanic lithosphere since the time of plate formation (Mercier et al., 2008) and is generally aligned with the direction of plate spreading (Shinohara et al., 2008). In the Alpine region, fossil fabrics acquired during Tethyan rifting are described in several mantle slivers accreted in the Alpine and Apenninic orogenic belts (e.g., Nicolas et al., 1972; Vissers et al., 1995). They include coarse-grained spinel lherzolite tectonites with olivine CPO consistent with deformation by dislocation creep (Tommasi et al., 1999; Vauchez et al., 2012). This tectonite fabric, developed at 900°C–1000°C and ~1.4 GPa during low-angle simple shearing and asymmetric rifting in the Jurassic (Hoogerduijn Strating et al., 1993), may characterize a thick slab section (Figure 12b). It is generally overprinted by spinel-, plagioclase-, hornblende-, and chlorite-bearing mylonites, and by serpentine mylonites developed as a result of strain localization during progressive mantle exhumation toward the Tethys seafloor (Piccardo & Vissers, 2007). Because these fabrics can survive subsequent deformation at eclogitic depths within the Alpine subduction channel (Hermann et al., 2000; Scambelluri et al., 1995), they are also likely preserved in low-strain domains within the slab. Their present-day attitude depends on: (i) the direction of plate spreading, (ii) the trench orientation relative to the paleomargin, and (iii) the present-day slab dip (Figure 12b). The spreading direction in the Jurassic was likely perpendicular to the trend of the European and Adriatic paleomargins, which is constrained by stratigraphic, tectonic and thermochronologic data (e.g., Fantoni & Franciosi, 2010; Guillot et al., 2009b; Lemoine et al., 1986; Malusà et al., 2016a, 2016b; Winterer & Bosellini, 1981), whereas the orientations of the Alpine and Apenninic trenches and the dip angle of the Alpine and Apenninic slabs are well constrained by paleotectonic reconstructions (Jolivet et al., 2003; Malusà et al., 2015; Vignaroli et al., 2008) and available tomography models. Based on the above constraints, the fossil fabrics acquired during Tethyan rifting should be marked, in the Alpine region, by slab-parallel to oblique fast axis directions (Figure 12b), which are indeed observed in the map of Figure 12a (Salimbeni et al., 2018). In the Northern Apennines, slab-parallel fast-axis directions are detected at depths as shallow as 20 km (green segments in Figure 12a) (Baccheschi et al., 2019).

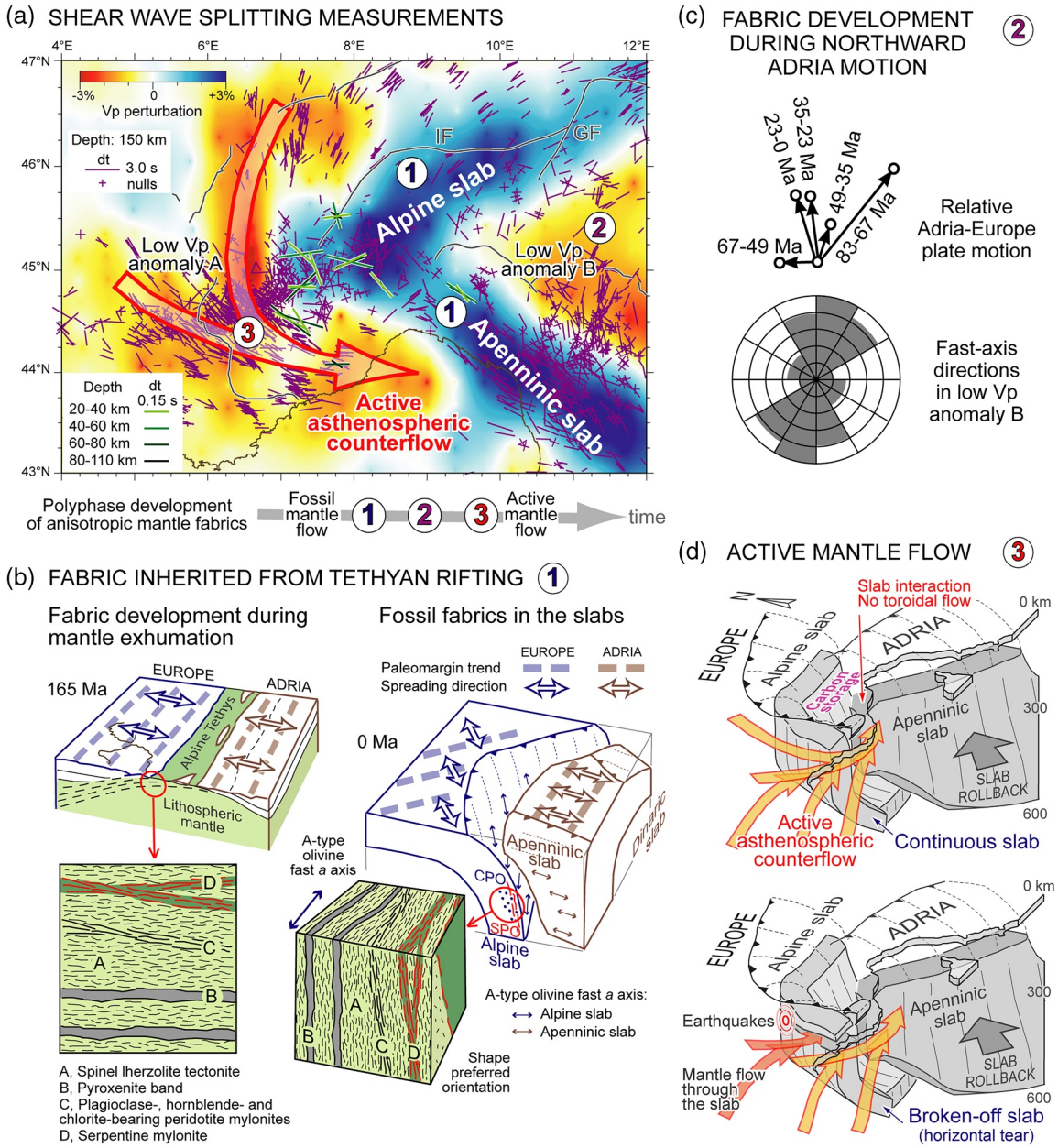

Figure 12. Polyphase development of anisotropic mantle fabrics in the Alpine region. (a) Map of single SKS splitting measurements (in purple) (Barruol et al., 2004, 2011; Salimbeni et al. 2008, 2013, 2018) and S-wave anisotropy measurements from local earthquakes (in green) (Baccheschi et al., 2019). Measurements are plotted on the 150-km depth slice of the tomography model of Zhao et al. (2016b) (GF, Giudicarie Fault; IF, Insubric Fault). Segments are parallel to the fast-velocity axis and scaled with delay time (note the different scales for SKS and S waves). Numbers 1–3 indicate different anisotropic fabrics as described in (b) to (d): fabric 1 is found in correspondence with the high V_p anomalies marking the Alpine and Apenninic slabs; fabrics 2 and 3 are from low V_p anomalies B and A, respectively. No toroidal mantle flow is observed around the northern tip of the Apenninic slab. (b) Anisotropic mantle fabric 1 inherited from Tethyan rifting. To the left, as observed in outcrops of exhumed mantle rocks within the Alpine orogenic wedge (e.g., Erro-Tobbio unit). To the right, expected attitude of fabric 1 in the Alpine and Apenninic slabs, based on the direction of plate spreading, trench orientation (Malusà et al., 2015, 2016b) and slab dip. CPO, crystallographic preferred orientation; SPO, shape preferred orientation. (c) Fast-axis directions of anisotropic mantle fabric 2 as compared to the direction of relative Adria-Europe plate motion (Dewey et al., 1989; arrows are scaled with distance; numbers indicate the age in Ma). (d) Alternative slab structures beneath the Alpine region (i.e., continuous vs. broken-off Alpine slab) and expected patterns of active asthenospheric mantle flows resulting from Apenninic slab rollback (fabric 3). Slab breakoff beneath the Western Alps (e.g. Kästle et al., 2020) would imply mantle flow through the slab and anomalously deep earthquakes beneath the northern Po Plain, unlike observed. Note the different origin of the low V_p anomaly A (explained by a vertical component of active asthenospheric counterflow by Salimbeni et al., 2018) and the low V_p anomaly B (explained by the presence of carbon-rich melts released from the Alpine slab by Malusà et al., 2018).

The low V_p anomaly region to the North of the Apenninic slab shows instead NNW-SSE to NE-SW fast-axis directions (2 in Figure 12a) that are consistent with the direction of relative Adria-Europe plate motion inferred from magnetic anomalies since the Late Cretaceous (Figure 12c) (Dewey et al., 1989; Jolivet & Faccenna, 2000). This suggests that the anisotropic fabric in that region may have formed during post-Jurassic Adria-Europe convergence, and possibly before the onset of Apenninic slab rollback (Salimbeni et al., 2018). If this interpretation is correct, fast-axis directions consistent with Adria-Europe plate motion should be also recorded by seismic stations in the Adriatic Sea (Molinari et al., 2018). WNW-ESE fast-axis directions parallel to the Jurassic spreading directions are poorly represented beneath the Adriatic microplate, which provides support for the hypothesis of asymmetric Tethyan rifting as already proposed on a geologic basis (e.g., Lemoine et al., 1986; Malusà et al., 2015; Manatschal & Müntener, 2009). In fact, asymmetric rifting implies that, during lithospheric extension, tectonite fabrics should be best developed within the Tethys oceanic lithosphere and the European subcontinental mantle but should not be expected in the Adriatic subcontinental mantle (Figure 12b), in line with the results reported in Figure 12a.

Finally, the low V_p anomaly region to the west of the Alpine and Apenninic slabs shows a continuous trend of fast-axis directions (3 in Figure 12a) that follows the arc of the Western Alps down to the Ligurian coast, where this trend merges with a WNW-ESE trend of fast-axis directions already described in SE France by Barruol et al. (2004). This seismic anisotropy pattern has a clear asthenospheric origin. It shows different directions compared to Pn anisotropy that samples the shallow lithospheric mantle (Díaz et al., 2013) and azimuthal anisotropy from noise and surface waves that samples a maximum depth of 120–125 km (Fry et al., 2010; H. Zhu & Tromp, 2013). Since its first detection, the anisotropy trend 3 was interpreted as an effect of asthenospheric flow due to the eastward retreat of the Apenninic slab (Barruol et al., 2004; Jolivet et al., 2009; Lucente et al., 2006), an interpretation confirmed by the CIFALPS experiment (Salimbeni et al., 2018). This continuous trend of fast-axis directions provides additional evidence against the hypothesis of Alpine slab breakoff. In fact, slab breakoff would imply a mantle flow through the slab that should be revealed by slab-perpendicular fast-axis directions (Figure 12d). These slab-perpendicular fast axes are not observed in Figure 12a.

9.5. Contrasting Origin of the Low-Velocity Anomalies in the Alpine Upper Mantle

The observed correspondence between the continuous trend of fast-axis directions and the low V_p anomaly in the European upper mantle provides pinpoints for further interpretation of the upper mantle structure beneath the Alpine region. This low V_p anomaly may either attest to the presence of fluids or have a thermal origin. The former hypothesis can be excluded in light of the location and the depth of the low V_p anomaly with respect to the nearby slabs (Figures 10e and 11). On the other hand, a potential thermal origin may be related to asthenospheric upwelling, possibly due to the counterflow induced by Apenninic slab retreat in the absence of an adequate mass compensation by a toroidal mantle flow around the northern tip of the retreating slab (Salimbeni et al., 2018). An efficient toroidal mantle flow would compensate the effects of slab retreat on the adjoining mantle by transferring asthenospheric material from the rear of the Apenninic slab toward a supraslab position (Faccenna & Becker, 2010; Salimbeni et al., 2013; Vignaroli et al., 2008). However, seismic anisotropy data are not supportive of an efficient toroidal flow beneath the Po Plain (Figure 12a). Recent tomography models show no major gap in the slab structure between the Alps and the Apennines (Figure 11), and the absence of enough space between the two slabs may preclude flow around the northern tip of the Apenninic slab during its rollback, with major implications for the asthenospheric mantle flow farther west. In fact, the absence of an efficient toroidal flow implies that Apenninic slab rollback may have induced not only a suction effect and an asthenospheric counterflow at the rear of the unbroken Western Alps slab (Barruol et al., 2004; Jolivet et al., 2009), but also a component of asthenospheric upwelling to compensate the lack of mantle material transferred from the rear to the front of the Apenninic slab (Salimbeni et al., 2018). Although the magnitude of mantle upwelling is probably much smaller than the magnitude of the horizontal component of the mantle flow (Figure 12d), the vertical component associated with mantle flow may have led to a temperature increase in the upper mantle, which may explain the low V_p anomaly imaged by P-wave tomography (Zhao et al., 2016b).

The low V_p anomaly B located atop the Alpine slab beneath the Po Plain may instead attest to the impact of slab released fluids, as first suggested by Giacomuzzi et al. (2011). This topic has been recently addressed

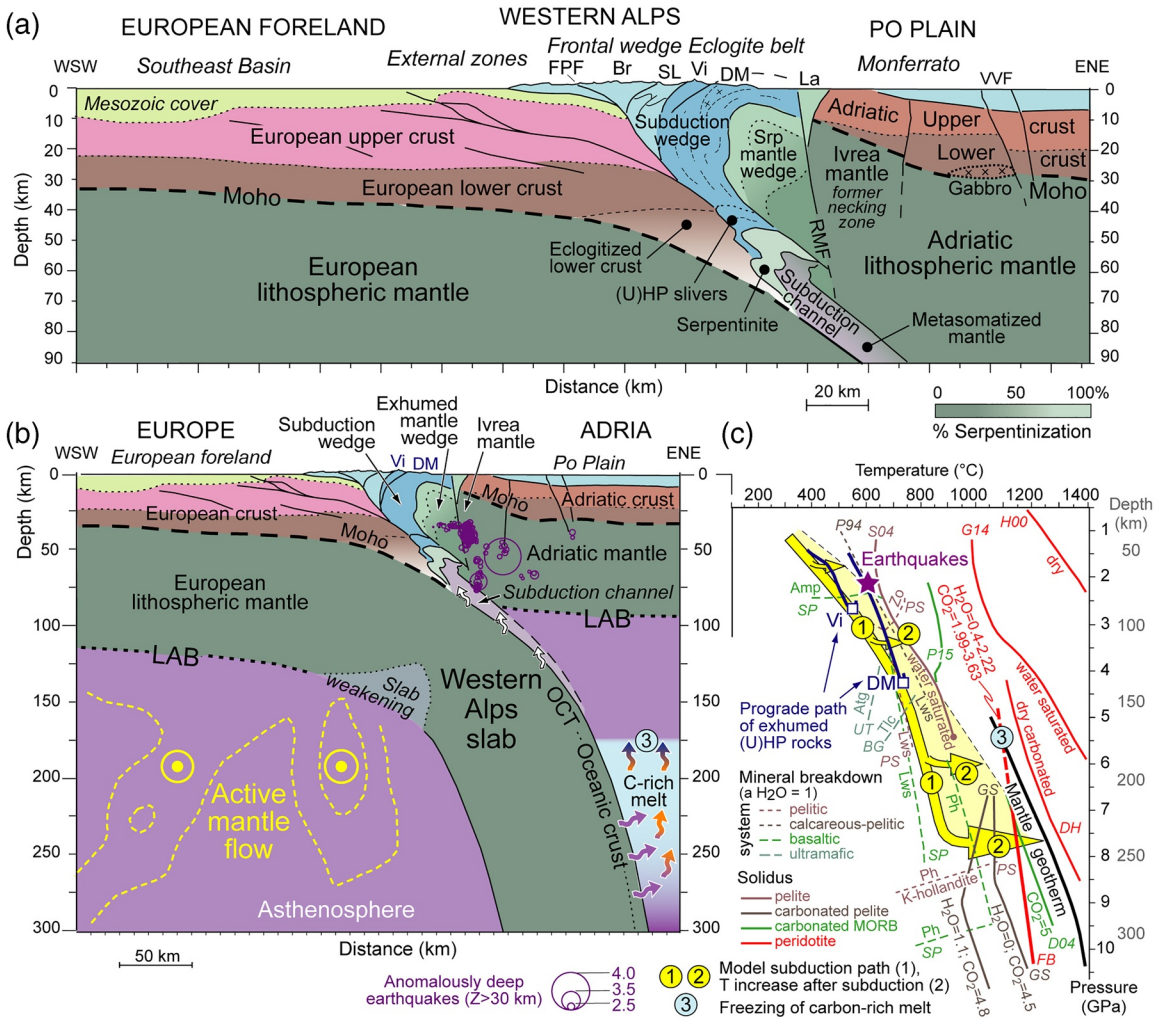

Figure 13. Geologic cross-sections based on geophysical constraints along the CIFALPS transect (Beller et al., 2018; Lyu et al., 2017; Malusà et al., 2017; Salimbeni et al., 2018; Solarino et al., 2018; Zhao et al., 2015, 2016b, 2020). (a) Lithospheric-scale cross-section showing the serpentinized mantle wedge beneath the Dora-Maira (U)HP dome (DM) (Solarino et al., 2018) and the slivers of serpentinite and (U)HP rocks exhumed along the subduction channel (Zhao et al., 2020) (the amount of serpentinization is inferred from seismic velocities, see Figure 4). The Ivrea mantle, representing the former necking zone of the southern Tethyan margin, is juxtaposed against serpentinized mantle-wedge rocks along the Rivoli-Marene deep Fault (RMF). Other acronyms: Br, Briançonnais; FPF, Frontal Pennine Fault; LA, Lanzo; SL, Schistes lustrés; Vi, Viso; VVF, Villalvernia-Varzi Fault. (b) Cross-section at upper-mantle scale. Active mantle flow beneath the European foreland, likely triggered by Apenninic slab rollback (Salimbeni et al., 2018), promote thermal weakening of the overlying Alpine slab, which is unbroken (Zhao et al., 2016b). Carbon-rich melt released from the Alpine slab may determine supersolidus conditions in the overlying mantle-wedge peridotite, and the resulting network of carbonate-silicate melt is solidified at ~180 km depth (Malusà et al., 2018). White arrows indicate potential fluid flow in the subduction channel. Anomalously deep earthquakes with hypocentral depth > 30 km (in purple) mainly originate in the Adriatic lithospheric mantle. Acronyms: OCT, ocean-continent transition; LAB, lithosphere-asthenosphere boundary (after Lyu et al., 2017; Malusà et al., 2018). (c) Subduction paths in the southern Western Alps and associated mineral reactions (modified after Malusà et al., 2018); depth (*y*-axis) as in (b); DM, Dora-Maira; Vi, Viso. Cold subduction (yellow path 1, after Syracuse et al., 2010) favors the preservation of carbonates and hydrous minerals to asthenospheric depths. The temperature increase after subduction cessation (2) is consistent with the occurrence of anomalously deep earthquakes in peridotites of the Adriatic upper plate (purple star). Increasing temperatures induce: (i) dehydration reactions with fluids possibly rising along the subduction channel; and (ii) melting of metasediments and carbonated metabasics, with carbon-rich melts that determine supersolidus conditions in the mantle-wedge peridotite, at depth greater than 180 km (freezing point 3). Keys to solidus curves (continuous lines): in brown, wet solidus and second critical end-point of pelite (S04, Schmidt et al., 2004); in gray, carbonated pelite solidi with bulk H_2O and CO_2 contents in wt% (GS, Grassi & Schmidt, 2011a, 2011b); in green, part of the solidus of carbonated basaltic eclogite (D04, Dasgupta et al., 2004) and hydrated and carbonated gabbro (P15, Poli, 2015); in red, solidi of dry peridotite (H00, Hirschmann, 2000), water saturated peridotite (G14, Green et al., 2014), dry carbonated peridotite (DH, Dasgupta & Hirschmann, 2006) and potassium-rich hydrated carbonated peridotite (FB, as compiled by Grassi & Schmidt, 2011a, 2011b). Keys to mineral breakdown curves (dashed lines): parts of amphibole-, zoisite-, lawsonite- and phengite-out curves in basalts (SP, Schmidt & Poli, 1998) and pelites/greywakes (PS, Poli & Schmidt, 2002), part of the lawsonite-out curve in a CASH system (P94, Pawley, 1994); part of antigorite- and talc-out curves in ultramafic system (UT, Ulmer & Trommsdorff, 1999; BG, Bose & Ganguly, 1995).

by Malusà et al. (2018), who combined geodynamic reconstructions with geophysical imaging and petrological modeling to reveal large-scale carbon processes associated with the complex slab configuration of the Alpine region. According to Malusà et al. (2018), the low-velocity anomaly in the upper mantle beneath the Po Plain would be generated by extraction of carbon-rich melts from the asthenosphere, favored by the breakdown of slab carbonates and hydrous minerals after cold Alpine subduction. Carbonates and hydrous minerals (e.g., phengite) can escape breakdown if the geothermal gradient during subduction is sufficiently low (Figure 13c) and can be dragged into the upper mantle by the downgoing slab (1 in Figure 13c). After subduction, the slab is progressively thermally reequilibrated toward ambient mantle conditions, with a temperature increase (2 in Figure 13c) that may promote dehydration reactions and carbonate breakdown. Consequent generation of carbon-rich supercritical fluids at the slab interface triggers melting in the overlying mantle wedge, with low density and low viscosity carbon-rich melts rising in the Adriatic asthenosphere (Figure 13b) to be finally frozen at ~180 km depth (3 in Figure 13b), where the mantle geotherm crosses the carbonated hydrous peridotite solidus (3 in Figure 13c). This implies sequestration of carbon in the upper mantle without immediate release (Malusà et al., 2018).

The low-velocity anomalies A and B located on either side of the Alpine slab may thus have different origins, that is asthenospheric upwelling to the west (Salimbeni et al., 2018; Zhao et al., 2016b) and fluids released from the Alpine slab to the east (Malusà et al., 2018). This makes numerical modeling exercises applied to the analysis of sub-lithospheric mantle convection (e.g., Sternai et al., 2019) more challenging than expected, because the commonly assumed relationships between seismic velocity, temperature and rock density (e.g., Simmons et al., 2010) are not necessarily met. This may explain why both the tomography models of Lippitsch et al. (2003) and Zhao et al. (2016b), when analyzed in terms of mantle convection modeling (Sternai et al., 2019), point to positive dynamic uplift in the Po Plain that is at odds with observations. If not properly accounted for, the different origins of the different low-velocity anomalies in the Alpine region may preclude a reliable quantification of the contribution from mantle convection to the measured uplift rates (e.g., Nocquet et al., 2016; Serpelloni et al., 2013; Walpersdorf et al., 2015).

10. Interpretive Cross-Sections at Lithospheric and Upper-Mantle Scales

Based on the geophysical constraints provided by the CIFALPS experiment, interpretive cross-sections at the scale of the lithosphere and the upper mantle are shown in Figure 13. In the southern Western Alps, the uppermost 20–25 km of the European lower plate consists of a mainly granitic upper crust and associated sedimentary cover (Figure 13a). These upper crustal rocks rest on top of a relatively homogeneous lower crust, likely consisting of granulitic rocks of felsic to intermediate composition (Solarino et al., 2018). At depths >40 km beneath the Alpine subduction wedge, the European lower crust is progressively eclogitized, but seismically distinguishable from the underlying mantle lithosphere down to depths of ~75 km (Solarino et al., 2018; Zhao et al., 2015). The eastward-dipping European Moho is located at 30–40 km depth beneath the Southeast basin and the External zone, reaching ~75 km depth beneath the Dora-Maira and the western Po Plain (Zhao et al., 2015, 2020). The main NE-SW trending Moho step detected to the NW of the Belledonne and Mont Blanc massifs (Lu et al., 2018; Zhao et al., 2020) is not observed in the southern Western Alps, where the European Moho shows a more continuous profile (Figure 13a). No deep seismicity is observed along the European Moho or along its continuation at depth, as expected since subduction is no longer active (Malusà et al., 2017) (Figure 13b).

On the upper-plate side of the orogen, the mainly gneissic and anisotropic Adriatic upper crust is 10–15 km thick beneath the Po Plain and the Monferrato thrust sheets (Figure 13a). At the western tip of the Adriatic upper plate, the westward pinching Adriatic lower crust has a more heterogeneous composition compared to the lower crust of the European plate, and locally includes granulitic metapelites and underplated gabbro (Solarino et al., 2018). The eastward-dipping Adriatic Moho is located at ~30 km depth under the Monferrato and at much shallower depth of 10–15 km in correspondence with the former necking zone of the southern Tethyan margin (Zhao et al., 2015). In the Adriatic lithospheric mantle, the dry to partly serpentinized peridotites of the former necking zone are underthrust by the peridotites of the European lithospheric mantle (Zhao et al., 2020) (Figure 13a).

The Alpine subduction wedge is apparently thicker in the northern Western Alps compared to the southern Western Alps (Zhao et al., 2020). In the southern Western Alps, the subduction wedge includes pervasively fractured Schistes lustrés and Briançonnais rocks of the doubly-vergent Frontal wedge, exposed beside (U)HP metaophiolites and poorly fractured granitic gneisses of the Dora-Maira dome. A body of mantle-wedge rocks with variable degrees of serpentinization, ranging from >90% in the uppermost part of the body to <30% at depth >30 km, is inferred under the Dora-Maira at depths as shallow as ∼10 km. Similar bodies are not imaged beneath the eclogitic domes exposed farther north (i.e., the Gran Paradiso and Monte Rosa domes) (Solarino et al., 2018; Zhao et al., 2020). The body of mantle-wedge rocks under the Dora-Maira is virtually aseismic (Eva et al., 2020), consistent with the fact that serpentinization promotes aseismic deformation. To the east, these mantle-wedge rocks are delimited by an active left-lateral fault in the lithospheric mantle (Rivoli-Marene deep fault, RMF in Figure 13a) that is marked by the alignment of anomalously deep earthquake hypocenters (Malusà et al., 2017). Therefore, based on the cross-section of Figure 13a, three different types of mantle rocks may contribute to the Ivrea gravity anomaly in the southern Western Alps: (i) to the west, mantle-wedge rocks emplaced at shallow crustal depth syn or post exhumation of the Dora-Maira (U)HP rocks; (ii) to the east, dry to partly serpentinized peridotites exhumed along the former necking zone of the southern Tethyan margin; (iii) in between, mantle rocks of the Lanzo massif that underwent Alpine subduction and were later exhumed and accreted against the Adriatic upper plate when the Dora-Maira (U)HP rocks were still buried at mantle depths (e.g., Angiboust & Glodny, 2020; Rubatto & Hermann, 2001; Rubatto et al., 2008).

In the underlying subduction channel, slivers of eclogitic metasediments and other (U)HP rocks are documented starting from depths ∼40 km (Solarino et al., 2018). Serpentinites likely mark the subduction channel in the depth range between ∼45 and ∼70 km (Zhao et al., 2020) and are replaced at greater depth by metasomatized mantle peridotites likely affected by infiltration of slab fluids. At either side of the Alpine subduction wedge, different tectonic styles characterize the lower and upper plate lithosphere. The former is cut by hinterland-dipping thrusts rooted in the Alpine subduction wedge, whereas the latter is cut by near-vertical faults (Figure 13a).

At the upper-mantle scale (Figure 13b), the CIFALPS results indicate that the lithosphere-asthenosphere boundary is located at ∼110 km depth beneath the European foreland and is approximately parallel to the eastward dipping European Moho, which suggests a ∼110 km thick and eastward-dipping European lithosphere (Lyu et al., 2017). Beneath the Po Plain, the Adriatic lithosphere-asthenosphere boundary is located at ∼100 km depth (Malusà et al., 2018). The Western Alps slab is apparently continuous beneath the western Po Plain, possibly reaching ∼300 km in length (Zhao et al., 2016b). It includes not only European lithosphere, but also Tethys lithosphere and the lithosphere of the adjoining ocean-continent transition zone (OCT in Figure 13b) (Malusà et al., 2018), all showing a tectonite fabric that is not documented in the Adriatic subcontinental mantle (Salimbeni et al., 2018). The asthenosphere at the rear of the Western Alps slab is affected by slab-parallel mantle flow likely triggered by Apenninic slab rollback (Barruol et al., 2004; Salimbeni et al., 2018). This flow may have induced weakening of the overlying Alpine slab (Figure 13b). In a supraslab position, independent circulations may have controlled slab-to-mantle exchanges at different depth ranges, with cold subduction possibly favoring long-term sequestration of carbon in the asthenospheric mantle (Malusà et al., 2018).

11. Geodynamic Evolution and Progressive Development of the Deep Alpine Structure

The deep Alpine structure revealed by the CIFALPS experiments was acquired during different steps of the complex evolution of the Adria-Europe plate boundary zone. It results from a combination of pre-Alpine tectonic inheritance, impact of Tethyan rifting, accommodation of Adria-Europe convergence by Alpine subduction, and activity of nearby subduction zones after Alpine subduction cessation and continent-continent collision.

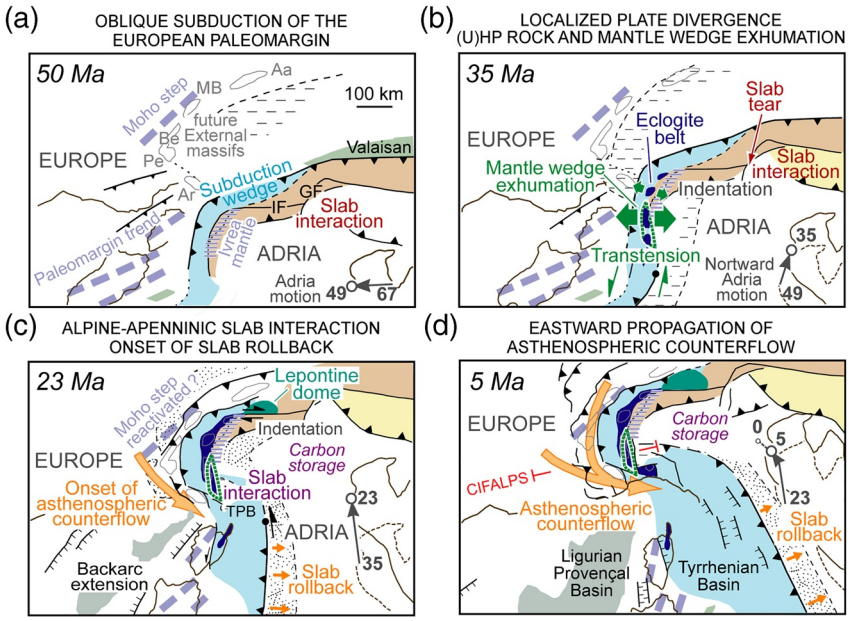

Figure 14. Cenozoic evolution of the Adria-Europe plate boundary zone in four steps (modified after Malusà et al., 2015) showing the progressive development of crustal and upper mantle structures revealed by geophysical experiments. (a) 50 Ma—oblique subduction of the European paleomargin beneath Adria. The European plate includes a Moho step near the future External massifs (likely an inheritance of pre-Alpine tectonics); the Adriatic plate includes the Ivrea mantle (former necking zone of the southern margin of the Tethys). Subduction of Tethys ocean lithosphere is almost completed; the SE-dipping Alpine slab starts interacting with the NE-dipping Dinaric slab. (b) 35 Ma—northward Adria motion induces tearing of the Alpine slab beneath the Eastern Alps, indentation of Adriatic lithosphere beneath the Alpine subduction wedge in the Central Alps, and transtension in the Western Alps, leading to mantle-wedge and (U)HP rock exhumation (the exhumed mantle wedge of the southern Western Alps is juxtaposed against the previously exhumed Ivrea mantle). (c) 23 Ma—onset of Alpine-Apenninic slab interaction and Apenninic slab rollback inducing extension in the Apenninic backarc. The lack of a toroidal mantle flow around the northern tip of the Apenninic slab starts to be compensated by SE-ward directed counter flow in the asthenospheric mantle beneath the European foreland. The Moho step near the future External massifs is possibly reactivated by flexural loading. Carbon-rich melts are realeased from the Alpine slab due to progressive thermal re-equilibration of the slab after subduction cessation, carbon starts to be stored in the overlying asthenospheric mantle. (d) 5 Ma—further Apenninic slab retreat determines the E-ward propagation of the asthenospheric counterflow toward the Ligurian Alps, with consequent tilting of the Tertiary Piedmont basin (TPB) succession. Other keys as in Figure 1.

11.1. Pre-Alpine Inheritance and Tethyan Rifting

Tethyan rifting marking the onset of the Alpine tectonic cycle likely reactivated former Paleozoic suture zones (Bergomi et al., 2017; Guillot et al., 2009b). We infer that the different composition of the upper and lower crust in the Adriatic and European plates may be partly inherited from different pre-Alpine evolutions (Solarino et al., 2018). Many Variscan lineaments were re-activated during the opening of the Alpine Tethys (Malusà et al., 2016a), and a Variscan inheritance may be also suggested for the Moho step detected by Lu et al. (2018) and Zhao et al. (2020) to the NW of the Belledonne and Mont Blanc massifs. During the opening of the Alpine Tethys, the Ivrea mantle rocks were exhumed to shallow crustal depths in the necking zone of the southern Tethyan margin (Manatschal & Müntener, 2009). This process may have also led to the westward thinning of the Adriatic lower crust along the CIFALPS transect (Figure 13a). Subcontinental mantle rocks were exhumed to the Tethys seafloor at this stage and underwent serpentinization by seafloor hydrothermal activity and seawater alteration (Deschamps et al., 2013). Due to the low spreading rates characterizing the Alpine Tethys, serpentinization may have occurred over a thickness of 2–4 km reaching extents of 70%–80% (e.g., Rouméjon & Cannat, 2014). During lithospheric extension, mantle peridotites now belonging to the Alpine slab likely acquired a tectonite fabric controlled by the direction of Jurassic spreading. All of these features were already present during the early stages of oblique Alpine subduction

(Figure 14a) and may have controlled the propagation of deformation during subduction and subsequent continent-continent collision.

11.2. Alpine Subduction and Exhumation

During Alpine subduction, abyssal serpentinites formed at the Tethys seafloor were either stacked in the subduction wedge or dragged into the Alpine subduction channel. Subducted European lower crust underwent progressive eclogitization, whereas upper-crust slivers were stacked in the subduction wedge (Solarino et al., 2018; Zhao et al., 2015). Aqueous fluids released from the slab at sub-arc depths promoted serpentinization in the subduction wedge and along the plate interface above the subduction channel. The resulting serpentinized plate interface may have favored the subduction of European continental lithosphere and the formation of continental (U)HP rocks (Zhao et al., 2020). Northward Adria motion in the late Eocene and associated localized divergence in the western segment of the Alpine subduction zone may have triggered, according to Malusà et al. (2011, 2015), the fast exhumation of buoyant (U)HP rocks now exposed in the Dora-Maira massif (Figure 14b). Along the CIFALPS transect, serpentinized mantle-wedge rocks may have followed the exhumation path of buoyant (U)HP rocks toward the Earth's surface to be finally emplaced beneath the Dora-Maira dome (Liao et al., 2018b; Solarino et al., 2018), also favoring the final exhumation of continental (U)HP rocks across the upper crust where eclogitized continental-crust rocks may become neutrally buoyant (Schwartz et al., 2001). During transtension, subducted abyssal and deeper mantle-wedge serpentinites likely moved upwards along the subduction channel, which became much thicker compared to the previous stages of plate convergence (Liao et al., 2018b; Zhao et al., 2020). Subducted abyssal serpentinites may also form the uppermost part of the serpentinized mantle wedge beneath the Dora-Maira, where the degree of serpentinization of the precursor peridotite may reach as high as 90%. The exhumed mantle-wedge rocks and the Ivrea mantle rocks were thus juxtaposed at shallow crustal levels in the late Eocene (Solarino et al., 2018). In the northern Western Alps, mantle-wedge exhumation was likely precluded by the lower amount of divergence due to the coeval indentation of Adria beneath the Central Alps (Liao et al., 2018b), also associated with back-folding of (U)HP domes (Keller et al., 2005) and backthrusting of Southalpine units (Zanchetta et al., 2015). At a broader scale, the interaction between the Dinaric slab and the Alpine slab may have led to the formation, beneath the Giudicarie Fault, of a vertical tear in the Alpine slab (Zhao et al., 2016b) with major implications for the development of Periadriatic magmatism (W. Q. Ji et al. 2019).

11.3. Post-subduction Evolution

After cessation of Alpine subduction, Neogene retreat of the Apenninic slab likely induced a counterflow in the asthenospheric mantle at the rear of the Alpine slab (Barruol et al., 2004; Salimbeni et al., 2018). Interaction between the northward shifting Apenninic slab and the SW-dipping Alpine slab may have controlled the location of the northern tip of the scissor-type Ligurian-Provençal basin opening in the Apenninic back-arc (Malusà et al., 2016b). In the southern Western Alps, the northward motion of the Adriatic microplate was accommodated by strike-slip activity along the Rivoli-Marene deep fault (Eva et al., 2015), located at the eastern boundary of the exhumed mantle wedge. In the Adriatic mantle lithosphere, earthquakes occurrence down to depths of ~75 km indicates that geothermal gradients in the upper plate have remained low (<8°C/km) and substantially similar to the gradients experienced by the Dora-Maira (U)HP rocks during their prograde path (Figure 13c) (Malusà et al., 2017). Thermal re-equilibration of the Alpine slab toward ambient mantle conditions promoted the generation of carbon-rich supercritical fluids and carbon storage in the Alpine upper mantle. The Moho step in the European foreland was possibly reactivated as a result of flexural loading by the leading edge of the Adriatic microplate (Figure 14c). During the final collision stages (Figure 14d), the Ivrea mantle acted as a rigid buttress constraining crustal shortening to the lower plate, which may have favored the formation of the Jura fold-and-thrust belt to the NW of the Alps (Liao et al., 2018a), whereas the eastward propagation of the asthenospheric counterflow toward the Ligurian Alps led to the northward tilting of the Tertiary Piedmont basin succession.

12. Conclusions and Open Questions

The CIFALPS experiment has allowed a major step forward in our understanding of the deep structure of the southern Western Alps and of the broader Alpine region more generally. Major tectonic features at the scale of the lithosphere and the upper mantle are now constrained in a compelling way by the integration of independent tomographic methods that exploit different information from high-resolution seismic data sets. The application of a wide range of tomographic methods to the analysis of a single fossil subduction zone and the joint interpretation with geological and petrophysical data make the CIFALPS experiment a reference case that could be exported to other study areas. Major results include:

(i) the first seismic evidence of European crust subducted into the Adriatic upper mantle, right beneath the place where coesite was first recognized in continental (U)HP rocks in the Alps
(ii) evidence of the major involvement of the mantle wedge during crucial steps of (U)HP rock exhumation
(iii) the first high-resolution image of a fossil subduction channel providing evidence of a serpentinized plate interface that favors continental subduction
(iv) evidence of a continuous slab beneath the Western and Central Alps, ruling out the classic hypothesis of slab breakoff magmatism right in the place where the slab-breakoff model was first proposed; however, this does not exclude that slab breakoff magmatism may have affected other regions on Earth
(v) evidence of a polyphase development of anisotropic mantle fabrics, either representing active mantle flows inducing localized weakening of the overlying lithosphere, or fossil fabrics inherited from previous rifting stages

Open questions remain to be addressed, concerning for example the upper mantle structure at the transition between the different slabs imaged beneath the broader Alpine region, the impact of slab-parallel mantle flow on the overlying lithosphere, or the lateral continuity of the finest geologic structures recognized in the fossil subduction channel along the CIFALPS transect. New constraints to the complicated slab structure at the transition between the Eastern Alps and the Dinarides are expected from the Swath-D AlpArray complementary experiment (Heit et al., 2018). Additional insights on the deep tectonic structure of the western Alpine region will be provided by the CIFALPS-2 experiment, a passive seismic survey that crosscuts the northern Western Alps across the Gran Paradiso massifs and the Ivrea body, reaching as far south as the Ligurian Sea.

Data Availability Statement

Data are available through Zhao et al. (2015, 2016b), Lyu et al. (2017), Salimbeni et al. (2018), Solarino et al. (2018), Sun et al. (2019), and Zhao et al. (2020).

Acknowledgments
The authors thank Rixiang Zhu, Yi Chen, Qin Wang, and Helle Pedersen for support and fruitful discussions. This research was supported by CAS program (GJHZ1776), NSFC (Grants nos. 41625016, 41888101, and 91755000), National Key R&D Program of China (Grant no. 2017YFC0601206), Agence Nationale de la Recherche (contract ANR-15-CE31-0015), and Labex OSUG@2020 (Investissement d'Avenir, ANR-10-LABX-56). The authors have no conflict of interest to declare.

References

Agard, P., Monié, P., Jolivet, L., & Goffé, B. (2002). Exhumation of the Schistes Lustrés complex: In situ laser probe 40Ar/39Ar constraints and implications for the Western Alps. *Journal of Metamorphic Geology*, *20*(6), 599–618.

Agard, P., Yamato, P., Jolivet, L., & Burov, E. (2009). Exhumation of oceanic blueschists and eclogites in subduction zones: Timing and mechanisms. *Earth-Science Reviews*, *92*(1–2), 53–79.

Amato, A., Margheriti, L., Azzara, R., Basili, A., Chiarabba, C., Ciaccio, M. G., & Nostro, C. (1998). Passive seismology and deep structure in central Italy. In *Geodynamics of lithosphere & Earth's mantle* (pp. 479–493). Basel: Birkhäuser.

Angiboust, S., & Glodny, J. (2020). Exhumation of eclogitic ophiolitic nappes in the W. Alps: New age data and implications for crustal wedge dynamics. *Lithos*, *353*, 105374.

Argand, E. (1911). I. Les nappes de recouvrement des Alpes pennines et leurs prolongements structuraux (No. 31-33). *Kommission bei A. Francke (vorm. Schmid & Francke)*.

Argand, E. (1916). Sur l'arc des Alpes occidentales. *G. Bridel*.

Audet, P. (2013). Seismic anisotropy of subducting oceanic uppermost mantle from fossil spreading. *Geophysical Research Letters*, *40*(1), 173–177.

Baccheschi, P., Salimbeni, S., Solarino, S., Eva, E., Malusà, M. G., Guillot, S., & Margheriti, L. (2019). Anisotropic structure beneath the Western Alps as inferred by the analysis of anomalously deep earthquakes. *Geophysical Research Abstracts*, *21*, EGU2019–16944.

Barfety, J. C., Lemoine, M., Mercier, D., Polino, R., Nievergelt, P., Bertrand, J., et al. (1996). *Carte Géologique de France (1/50.000), Feuille Briançon (823)*. Orléans: Bureau de Recherche Geologiques et Minieres.

Barruol, G., Bonnin, M., Pedersen, H., Bokelmann, G. H., & Tiberi, C. (2011). Belt-parallel mantle flow beneath a halted continental collision: The Western Alps. *Earth and Planetary Science Letters*, *302*(3–4), 429–438.

Barruol, G., Deschamps, A., & Coutant, O. (2004). Mapping upper mantle anisotropy beneath SE France by SKS splitting indicates Neogene asthenospheric flow induced by Apenninic slab roll-back and deflected by the deep Alpine roots. *Tectonophysics*, *394*(1–2), 125–138.

Bellahsen, N., Mouthereau, F., Boutoux, A., Bellanger, M., Lacombe, O., Jolivet, L., & Rolland, Y. (2014). Collision kinematics in the western external Alps. *Tectonics*, *33*(6), 1055–1088.

Beller, S., Monteiller, V., Operto, S., Nolet, G., Paul, A., & Zhao, L. (2018). Lithospheric architecture of the South-Western Alps revealed by multiparameter teleseismic full-waveform inversion. *Geophysical Journal International*, *212*(2), 1369–1388.

Beltrando, M., Compagnoni, R., & Lombardo, B. (2010). (Ultra-) High-pressure metamorphism and orogenesis: An Alpine perspective. *Gondwana Research*, *18*(1), 147–166.

Bergomi, M. A., Dal Piaz, G. V., Malusà, M. G., Monopoli, B., & Tunesi, A. (2017). The Grand St Bernard-Briançonnais nappe system and the Paleozoic inheritance of the Western Alps unraveled by zircon U-Pb dating. *Tectonics*, *36*(12), 2950–2972.

Bergomi, M. A., Zanchetta, S., & Tunesi, A. (2015). The tertiary dike magmatism in the Southern Alps: Geochronological data and geodynamic significance. *International Journal of Earth Sciences*, *104*(2), 449–473.

Bernoulli, D., Caron, C., Homewood, P., Kälin, O., & Van Stujvenberg, J. (1979). Evolution of continental margins in the Alps. *Schweizerische mineralogische und petrographische Mitteilungen*, *59*, 165–170.

Bertrand, J. M., Guillot, F., Leterrier, J., Perruchot, M. P., Aillères, L., & Macaudière, J. (1998). Granitoïdes de la Zone Houillère Briançonnaise en Savoie et en Val d'Aoste (Alpes Occidentales): géologie et géochronologie U-Pb sur zircon. *Geodinamica Acta*, *11*(1), 33–49.

Béthoux, N., Sue, C., Paul, A., Virieux, J., Fréchet, J., Thouvenot, F., & Cattaneo, M. (2007). Local tomography and focal mechanisms in the South-western Alps: Comparison of methods and tectonic implications. *Tectonophysics*, *432*, 1–19.

Bezacier, L., Reynard, B., Bass, J. D., Wang, J., & Mainprice, D. (2010). Elasticity of glaucophane, seismic velocities and anisotropy of the subducted oceanic crust. *Tectonophysics*, *494*(3–4), 201–210.

Bezacier, L., Reynard, B., Cardon, H., Montagnac, G., & Bass, J. D. (2013). High-pressure elasticity of serpentine and seismic properties of the hydrated mantle wedge. *Journal of Geophysical Research: Solid Earth*, *118*(2), 527–535.

Bigi, G., Cosentino, D., Parotto, M., Sartori, R., & Scandone, P. (1990). Structural model of Italy and gravity map. Sheets 1-9, 1:500.000. Progetto Finalizzato Geodinamica C.N.R. *Quaderni Ricerca Scientifica*, *3*, 114.

Bistacchi, A., Dal Piaz, G., Massironi, M., Zattin, M., & Balestrieri, M. (2001). The Aosta–Ranzola extensional fault system and Oligocene–Present evolution of the Austroalpine–Penninic wedge in the northwestern Alps. *International Journal of Earth Sciences*, *90*(3), 654–667.

Bocquet, J. (1971). Cartes de répartition de quelques minéraux du métamorphisme alpin dans les Alpes franco italiennes. *Eclogae Geol. Helv.*, *64*, 71–103.

Bocquet, J., Delaloye, M., Hunziker, J. C., & Krummenacher, D. (1974). K-Ar and Rb-Sr dating of blue amphiboles, micas, and associated minerals from the Western Alps. *Contributions to Mineralogy and Petrology*, *47*(1), 7–26.

Bodin, T., Sambridge, M., Rawlinson, N., & Arroucau, P. (2012). Transdimensional tomography with unknown data noise. *Geophysical Journal International*, *189*(3), 1536–1556.

Bodin, T., Sambridge, M., Tkalčić, H., Arroucau, P., Gallagher, K., & Rawlinson, N. (2012b). Transdimensional inversion of receiver functions and surface wave dispersion. *Journal of Geophysical Research*, *117*(B2). https://doi.org/10.1029/2011JB008560

Bodin, T., Yuan, H., & Romanowicz, B. (2014). Inversion of receiver functions without deconvolution—application to the Indian craton. *Geophysical Journal International*, *196*(2), 1025–1033.

Bose, K., & Ganguly, J. (1995). Experimental and theoretical studies of the stabilities of talc, antigorite and phase A at high pressures with applications to subduction processes. *Earth and Planetary Science Letters*, *136*(3–4), 109–121.

Boudier, F. (1978). Structure and petrology of the Lanzo peridotite massif (Piedmont Alps). *The Geological Society of America Bulletin*, *89*(10), 1574–1591.

Brandmayr, E., Blagoeva, R., Zuri, M., Romanelli, F., Doglioni, C., & Panza, G. F. (2010). The lithosphere in Italy: Structure and seismicity (No. IC--2010/020). *Journal of the Virtual Explorer*, *36*. https://doi.org/10.3809/jvirtex.2010.00224

Brouwer, F. M., Van De Zedde, D. M. A., Wortel, M. J. R., & Vissers, R. L. M. (2004). Late-orogenic heating during exhumation: Alpine PTt trajectories and thermomechanical models. *Earth and Planetary Science Letters*, *220*(1–2), 185–199.

Brouwer, F., Vissers, R., & Lamb, W. (2002). Structure and metamorphism of the Gran Paradiso massif, western Alps, Italy. *Contributions to Mineralogy and Petrology*, *143*(4), 450–470.

Brownlee, S. J., Hacker, B. R., Salisbury, M., Seward, G., Little, T. A., Baldwin, S. L., & Abers, G. A. (2011). Predicted velocity and density structure of the exhuming Papua New Guinea ultrahigh-pressure terrane. *Journal of Geophysical Research*, *116*(B8).

Caby, R. (1975). Geodynamic implications of transverse folding in the Western Alps for the Alpine fold belt. *Nature*, *256*(5513), 114–117.

Caby, R. (1996). Low-angle extrusion of high-pressure rocks and the balance between outward and inward displacements of Middle Penninic units in the western Alps. *Eclogae Geologicae Helvetiae*, *89*(1), 229–268.

Campillo, M., & Paul, A. (2003). Long-range correlations in the diffuse seismic coda. *Science*, *299*(5606), 547–549.

Capponi, G., & Crispini, L. (2002). Structural and metamorphic signature of alpine tectonics in the Voltri Massif (Ligurian Alps, North-Western Italy). *Eclogae Geologicae Helvetiae*, *95*(1), 31–42.

Carminati, E., & Doglioni, C. (2012). Alps vs. Apennines: The paradigm of a tectonically asymmetric Earth. *Earth-Science Reviews*, *112*(1–2), 67–96.

Carminati, E., Lustrino, M., & Doglioni, C. (2012). Geodynamic evolution of the central and western Mediterranean: Tectonics vs. igneous petrology constraints. *Tectonophysics*, *579*, 173–192.

Carminati, E., Wortel, M. J. R., Spakman, W., & Sabadini, R. (1998). The role of slab detachment processes in the opening of the western–central Mediterranean basins: Some geological and geophysical evidence. *Earth and Planetary Science Letters*, *160*(3–4), 651–665.

Cattaneo, M., Augliera, P., Parolai, S., & Spallarossa, D. (1999). Anomalously deep earthquakes in northwestern Italy. *Journal of Seismology*, *3*(4), 421–435.

Chevrot, S., Villaseñor, A., Sylvander, M., Benahmed, S., Beucler, E., Cougoulat, G., & Grimaud, F. (2014). High-resolution imaging of the Pyrenees and Massif Central from the data of the PYROPE and IBERARRAY portable array deployments. *Journal of Geophysical Research: Solid Earth*, *119*(8), 6399–6420.

Chopin, C. (1984). Coesite and pure pyrope in high-grade blueschists of the Western Alps: A first record and some consequences. *Contributions to Mineralogy and Petrology*, *86*(2), 107–118.

Chopin, C., Henry, C., & Michard, A. (1991). Geology and petrology of the coesite-bearing terrain, Dora Maira massif, Western Alps. *European Journal of Mineralogy*, *3*(2), 263–291.

Christensen, N. I. (1989). Seismic velocities. In R. S. Carmichael (Ed.), *Practical handbook of physical properties of rocks and minerals* (p. 741). Boca Raton, FL: CRC Press.

Closs, H., & Labrouste, Y. (Eds.). (1963). Rechèrches séismologiques dans les Alpes occidentales au moyen de grandes explosions en 1956, 1958 et 1960. Mémoires collectif du groupe d'etude des explosions alpines, Année géophysique internationale, *12-2*, 233–235.

Cotte, N., Pedersen, H. A., & TOR Working Group. (2002). Sharp contrast in lithospheric structure across the Sorgenfrei–Tornquist Zone as inferred by Rayleigh wave analysis of TOR1 project data. *Tectonophysics*, *360*(1–4), 75–88.
Coward, M., & Dietrich, D. (1989). Alpine tectonics—An overview. *Geological Society, London, Special Publications*, *45*(1), 1–29.
Dal Piaz, G. V. (2001). History of tectonic interpretations of the Alps. *Journal of Geodynamics*, *32*(1–2), 99–114.
Dal Piaz, G. V., Bistacchi, A., & Massironi, M. (2003). Geological outline of the Alps. *Episodes*, *26*(3), 175–180.
Dal Piaz, G. V., & Ernst, W. G. (1978). Areal geology and petrology of eclogites and associated metabasites of the Piemonte ophiolite nappe, breuil—St. Jacques area, Italian Western Alps. *Tectonophysics*, *51*(1–2), 99–126.
Dal Piaz, G. V., & Lombardo, B. (1986). Early Alpine eclogite metamorphism in the Penninic Monte Rosa-Gran Paradiso basement nappes of the northwestern Alps. *Geological Society of America Memoir*, *164*, 249–265.
Dal Zilio, L. (2020). Slab rollback Orogeny model for the evolution of the Central Alps: Seismo-Thermo-Mechanical test. In *Cross-scale modeling of mountain building and the seismic cycle: From Alps to Himalaya* (pp. 45–66). Dordrecht: Springer.
Dando, B. D. E., Stuart, G. W., Houseman, G. A., Hegedüs, E., Brückl, E., & Radovanović, S. (2011). Teleseismic tomography of the mantle in the Carpathian-Pannonian region of central Europe. *Geophysical Journal International*, *186*(1), 11–31.
Dasgupta, R., & Hirschmann, M. M. (2006). Melting in the Earth's deep upper mantle caused by carbon dioxide. *Nature*, *440*(7084), 659–662.
Davies, J. H., & von Blanckenburg, F. (1995). Slab breakoff: A model of lithosphere detachment and its test in the magmatism and deformation of collisional orogens. *Earth and Planetary Science Letters*, *129*(1–4), 85–102.
De Paoli, M. C., Clarke, G. L., & Daczko, N. R. (2012). Mineral equilibria modeling of the granulite–eclogite transition: Effects of whole-rock composition on metamorphic facies type-assemblages. *Journal of Petrology*, *53*(5), 949–970.
Deschamps, F., Godard, M., Guillot, S., & Hattori, K. (2013). Geochemistry of subduction zone serpentinites: A review. *Lithos*, *178*, 96–127.
Deville, E., Fudral, S., Lagabrielle, Y., Marthaler, M., & Sartori, M. (1992). From oceanic closure to continental collision: A synthesis of the "Schistes lustrés" metamorphic complex of the Western Alps. *The Geological Society of America Bulletin*, *104*(2), 127–139.
Dewey, J. F., Helman, M. L., Knott, S. D., Turco, E., & Hutton, D. H. W. (1989). Kinematics of the western Mediterranean. *Geological Society, London, Special Publications*, *45*(1), 265–283.
Dewey, J. F., Pitman, W. C., Ryan, W. B., & Bonnin, J. (1973). Plate tectonics and the evolution of the Alpine system. *The Geological Society of America Bulletin*, *84*(10), 3137–3180.
Diaz, J., Gil, A., & Gallart, J. (2013). Uppermost mantle seismic velocity and anisotropy in the Euro-Mediterranean region from Pn and Sn tomography. *Geophysical Journal International*, *192*(1), 310–325.
Diehl, T., Husen, S., Kissling, E., & Deichmann, N. (2009). High-resolution 3-DP-wave model of the Alpine crust. *Geophysical Journal International*, *179*(2), 1133–1147.
Dolomieu de, D. G. (1791). Sur un genre de pierres calcaires très peu effervescentes avec les acides et phosphorescentes par la collision. *Journal de Physique*, t. XXXIX.
Dost, B. (1990). Upper mantle structure under western Europe from fundamental and higher mode surface waves using the NARS array. *Geophysical Journal International*, *100*(1), 131–151.
Dumont, T., Schwartz, S., Guillot, S., Simon-Labric, T., Tricart, P., & Jourdan, S. (2012). Structural and sedimentary records of the Oligocene revolution in the Western Alps. *Journal of Geodynamics*, *56–57*, 18–38.
Dumont, T., Simon-Labric, T., Authemayou, C., & Heymes, T. (2011). Lateral termination of the north-directed Alpine orogeny and onset of westward escape in the Western Alpine arc: Structural and sedimentary evidence from the external zone. *Tectonics*, *30*(5). https://doi.org/10.1029/2010TC002836
Dziewonski, A. M., & Anderson, D. L. (1981). Preliminary reference Earth model. *Physics of the Earth and Planetary Interiors*, *25*(4), 297–356.
Ernst, W. G. (1971). Metamorphic zonations on presumably subducted lithospheric plates from Japan, California and the Alps. *Contributions to Mineralogy and Petrology*, *34*(1), 43–59.
Ernst, W. G. (1973). Interpretative synthesis of metamorphism in the Alps. *The Geological Society of America Bulletin*, *84*(6), 2053–2078.
Eva, E., Malusà, M. G., & Solarino, S. (2015). A seismotectonic picture of the inner southern Western Alps based on the analysis of anomalously deep earthquakes. *Tectonophysics*, *661*, 190–199.
Eva, E., Malusà, M. G., & Solarino, S. (2020). Seismotectonics at the transition between opposite-dipping slabs (western Alpine region). *Tectonics*, *39*, 1–20.e2020TC006086. https://doi.org/10.1029/2020TC006086
Evans, B. W. (2004). The serpentinite multisystem revisited: chrysotile is metastable. *International Geology Review*, *46*(6), 479–506.
Ewing, T. A., Rubatto, D., & Hermann, J. (2014). Hafnium isotopes and Zr/Hf of rutile and zircon from lower crustal metapelites (Ivrea–Verbano Zone, Italy): Implications for chemical differentiation of the crust. *Earth and Planetary Science Letters*, *389*, 106–118.
Faccenna, C., & Becker, T. W. (2010). Shaping mobile belts by small-scale convection. *Nature*, *465*(7298), 602–605.
Faccenna, C., Becker, T. W., Auer, L., Billi, A., Boschi, L., Brun, J. P., & Piromallo, C. (2014). Mantle dynamics in the Mediterranean. *Reviews of Geophysics*, *52*(3), 283–332.
Fantoni, R., & Franciosi, R. (2010). Tectono-sedimentary setting of the Po Plain and Adriatic foreland. *Rendiconti Lincei*, *21*(1), 197–209.
Federico, L., Capponi, G., Crispini, L., & Scambelluri, M. (2004). Exhumation of alpine high-pressure rocks: Insights from petrology of eclogite clasts in the Tertiary Piedmontese basin (Ligurian Alps, Italy). *Lithos*, *74*(1–2), 21–40.
Ferrara, G., Hirt, B., Jäger, E., & Niggli, E. (1962). Rb-Sr and U-Pb age determinations on the pegmatite of I Mondei (Penninic Camughera-Moncucco-Complex, Italian Alps and some gneisses from the neighborhood). *Eclogae Geologicae Helvetiae*, *55*.
Forcella, F., Mottana, A., & Pasquarè, G. (1973). Il massiccio cristallino interno di Valosio (Gruppo di Voltri, Provincia di Alessandria). *Memorie della Società Geologica Italiana*, *12*, 485–528.
Fox, M., Herman, F., Kissling, E., & Willett, S. D. (2015). Rapid exhumation in the Western Alps driven by slab detachment and glacial erosion. *Geology*, *43*(5), 379–382.
Frei, W., Heitzmann, P., & Lehner, P. (1990). Swiss NFP-20 research program of the deep structure of the Alps. *Mémoires de la Société géologique de France*, *156*(1833), 29–46.
Frey, M., Hunziker, J. C., Frank, W., Bocquet, J., Dal Piaz, G. V., Jager, E., & Niggli, E. (1974). Alpine metamorphism of the Alps: A review. *Schweizerische Mineralogische und Petrographische Mitteilungen*, *54*, 247–290.
Fry, B., Deschamps, F., Kissling, E., Stehly, L., & Giardini, D. (2010). Layered azimuthal anisotropy of Rayleigh wave phase velocities in the European Alpine lithosphere inferred from ambient noise. *Earth and Planetary Science Letters*, *297*(1–2), 95–102.
Gabudianu Radulescu, I., Rubatto, D., Gregory, C., & Compagnoni, R. (2009). The age of HP metamorphism in the Gran Paradiso Massif, Western Alps: A petrological and geochronological study of "silvery micaschists". *Lithos*, *110*(1–4), 95–108.
Ganne, J., Bertrand, J. M., Fudral, S., Marquer, D., & Vidal, O. (2007). Structural and metamorphic evolution of the Ambin massif (western Alps): Toward a new alternative exhumation model for the Brianconnais domain. *Bulletin de la Societe Geologique de France*, *178*(6), 437–458.

Garzanti, E., Radeff, G., & Malusà, M. G. (2018). Slab breakoff: A critical appraisal of a geological theory as applied in space and time. *Earth-Science Reviews*, *177*, 303–319.

Geissler, W. H., Sodoudi, F., & Kind, R. (2010). Thickness of the central and eastern European lithosphere as seen by S receiver functions. *Geophysical Journal International*, *181*(2), 604–634.

Giacomuzzi, G., Chiarabba, C., & De Gori, P. (2011). Linking the Alps and Apennines subduction systems: New constraints revealed by high-resolution teleseismic tomography. *Earth and Planetary Science Letters*, *301*(3–4), 531–543.

Goffé, B., Bousquet, R., Henry, P., & Le Pichon, X. (2003). Effect of the chemical composition of the crust on the metamorphic evolution of orogenic wedges. *Journal of Metamorphic Geology*, *21*(2), 123–141.

Grassi, D., & Schmidt, M. W. (2011a). The melting of carbonated pelites from 70 to 700 km depth. *Journal of Petrology*, *52*(4), 765–789.

Grassi, D., & Schmidt, M. W. (2011b). Melting of carbonated pelites at 8–13 GPa: Generating K-rich carbonatites for mantle metasomatism. *Contributions to Mineralogy and Petrology*, *162*(1), 169–191.

Green, D. H., Hibberson, W. O., Rosenthal, A., Kovács, I., Yaxley, G. M., Falloon, T. J., & Brink, F. (2014). Experimental study of the influence of water on melting and phase assemblages in the upper mantle. *Journal of Petrology*, *55*(10), 2067–2096.

Groppo, C., Ferrando, S., Gilio, M., Botta, S., Nosenzo, F., Balestro, G., et al. (2019). What's in the sandwich? New P–T constraints for the (U) HP nappe stack of southern Dora-Maira Massif (Western Alps). *European Journal of Mineralogy*, *31*(4), 665–683.

Groupe de Recherche Géofrance 3D. (1997). Géofrance 3D: l'imagerie géologique et géophysique du sous-sol de la France. *Mémoires de la Société géologique de France*, *172*, 53–71.

Guillot, S., di Paola, S., Ménot, R. P., Ledru, P., Spalla, M. I., Gosso, G., & Schwartz, S. (2009b). Suture zones and importance of strike-slip faulting for Variscan geodynamic reconstructions of the External Crystalline Massifs of the western Alps. *Bulletin de la Societe Geologique de France*, *180*(6), 483–500.

Guillot, S., Hattori, K., Agard, P., Schwartz, S., & Vidal, O. (2009a). Exhumation processes in oceanic and continental subduction contexts: A review. *Subduction zone geodynamics* (pp. 175–205). New York, NY: Springer.

Hacker, B. R., & Abers, G. A. (2004). Subduction factory 3: An excel worksheet and macro for calculating the densities, seismic wave speeds, and H_2O contents of minerals and rocks at pressure and temperature. *Geochemistry, Geophysics, Geosystems*, *5*(1). https://doi.org/10.1029/2003GC000614

Hacker, B. R., Abers, G. A., & Peacock, S. M. (2003). Subduction factory 1. Theoretical mineralogy, densities, seismic wave speeds, and H_2O contents. *Journal of Geophysical Research*, *108*(B1). https://doi.org/10.1029/2001JB001127

Hacker, B. R., Kelemen, P. B., & Behn, M. D. (2015). Continental lower crust. *Annual Review of Earth and Planetary Sciences*, *43*, 167–205.

Handy, M. R., Schmid, S. M., Bousquet, R., Kissling, E., & Bernoulli, D. (2010). Reconciling plate-tectonic reconstructions of Alpine Tethys with the geological–geophysical record of spreading and subduction in the Alps. *Earth-Science Reviews*, *102*(3–4), 121–158.

Handy, M. R., Ustaszewski, K., & Kissling, E. (2015). Reconstructing the Alps–Carpathians–Dinarides as a key to understanding switches in subduction polarity, slab gaps and surface motion. *International Journal of Earth Sciences*, *104*(1), 1–26.

Hawkesworth, C. J., Waters, D. J., & Bickle, M. J. (1975). Plate tectonics in the Eastern Alps. *Earth and Planetary Science Letters*, *24*(3), 405–413.

Hearn, T. M. (1999). Uppermost mantle velocities and anisotropy beneath Europe. *Journal of Geophysical Research*, *104*(B7), 15123–15139.

Heit, B., Weber, M., Haberland, C., Tilmann, F., Hemmleb, S., Schwarz, S., & Pesaresi, D. (2018). The AlpArray SWATH-D experiment – A dense seismic array in the Central, Eastern and Southern Alps. *Geophysical Research Abstracts*, *20*, EGU2018–11509.

Henry, C., Michard, A., & Chopin, C. (1993). Geometry and structural evolution of ultra-high-pressure and high-pressure rocks from the Dora-Maira massif, Western Alps, Italy. *Journal of Structural Geology*, *15*, 965–965.

Hermann, J., Müntener, O., & Scambelluri, M. (2000). The importance of serpentinite mylonites for subduction and exhumation of oceanic crust. *Tectonophysics*, *327*(3–4), 225–238.

Hetényi, G., Cattin, R., Brunet, F., Bollinger, L., Vergne, J., Nábělek, J. L., & Diament, M. (2007). Density distribution of the India plate beneath the Tibetan plateau: Geophysical and petrological constraints on the kinetics of lower-crustal eclogitization. *Earth and Planetary Science Letters*, *264*(1–2), 226–244.

Hetényi, G., Molinari, I., Clinton, J., Bokelmann, G., Bondár, I., Crawford, W. C., et al. (2018). The AlpArray seismic network: A large-scale European experiment to image the Alpine Orogen. *Surveys in Geophysics*, *39*(5), 1009–1033.

Hilairet, N., Daniel, I., & Reynard, B. (2006). Equation of state of antigorite, stability field of serpentines, and seismicity in subduction zones. *Geophysical Research Letters*, *33*(2).

Hilairet, N., Reynard, B., Wang, Y., Daniel, I., Merkel, S., Nishiyama, N., & Petitgirard, S. (2007). High-pressure creep of serpentine, interseismic deformation, and initiation of subduction. *Science*, *318*(5858), 1910–1913.

Hirschmann, M. M. (2000). Mantle solidus: Experimental constraints and the effects of peridotite composition. *Geochemistry, Geophysics, Geosystems*, *1*(10). https://doi.org/10.1029/2000GC000070

Hoogerduijn Strating, E., Rampone, E., Piccardo, G. B., Drury, M. R., & Vissers, R. L. M. (1993). Subsolidus emplacement of mantle peridotites during incipient oceanic rifting and opening of the Mesozoic Tethys (Voltri Massif, NW Italy). *Journal of Petrology*, *34*(5), 901–927.

Hua, Y., Zhao, D., & Xu, Y. (2017). P wave anisotropic tomography of the Alps. *Journal of Geophysical Research: Solid Earth*, *122*(6), 4509–4528.

Jamieson, R. A., & Beaumont, C. (2013). On the origin of orogens. *The Geological Society of America Bulletin*, *125*(11—12), 1671–1702.

Ji, S., Li, A., Wang, Q., Long, C., Wang, H., Marcotte, D., & Salisbury, M. (2013). Seismic velocities, anisotropy, and shear-wave splitting of antigorite serpentinites and tectonic implications for subduction zones. *Journal of Geophysical Research: Solid Earth*, *118*(3), 1015–1037.

Ji, S., Shao, T., Michibayashi, K., Oya, S., Satsukawa, T., Wang, Q., et al. (2015). Magnitude and symmetry of seismic anisotropy in mica-and amphibole-bearing metamorphic rocks and implications for tectonic interpretation of seismic data from the southeast Tibetan Plateau. *Journal of Geophysical Research: Solid Earth*, *120*(9), 6404–6430.

Ji, W. Q., Malusà, M. G., Tiepolo, M., Langone, A., Zhao, L., & Wu, F. Y. (2019). Synchronous Periadriatic magmatism in the Western and Central Alps in the absence of slab breakoff. *Terra Nova*, *31*(2), 120–128.

Jolivet, L., & Faccenna, C. (2000). Mediterranean extension and the Africa-Eurasia collision. *Tectonics*, *19*(6), 1095–1106.

Jolivet, L., Faccenna, C., Goffé, B., Burov, E., & Agard, P. (2003). Subduction tectonics and exhumation of high-pressure metamorphic rocks in the Mediterranean orogens. *American Journal of Science*, *303*(5), 353–409.

Jolivet, L., Faccenna, C., & Piromallo, C. (2009). From mantle to crust: Stretching the Mediterranean. *Earth and Planetary Science Letters*, *285*(1–2), 198–209.

Karato, S. I. (2010). Rheology of the Earth's mantle: A historical review. *Gondwana Research*, *18*(1), 17–45.

Kästle, E. D., El-Sharkawy, A., Boschi, L., Meier, T., Rosenberg, C., Bellahsen, N., et al. (2018). Surface wave tomography of the alps using ambient-noise and earthquake phase velocity measurements. *Journal of Geophysical Research: Solid Earth*, *123*(2), 1770–1792.

Kästle, E. D., Rosenberg, C., Boschi, L., Bellahsen, N., Meier, T., & El-Sharkawy, A. (2020). Slab break-offs in the Alpine subduction zone. *International Journal of Earth Sciences*, 1–17. https://doi.org/10.1007/s00531-020-01821-z

Keller, L. M., Hess, M., Fügenschuh, B., & Schmid, S. M. (2005). Structural and metamorphic evolution of the Camughera–Moncucco, Antrona and Monte Rosa units southwest of the Simplon line, Western Alps. *Eclogae Geologicae Helvetiae*, *98*(1), 19–49.

Kennett, B. L., Engdahl, E. R., & Buland, R. (1995). Constraints on seismic velocities in the Earth from traveltimes. *Geophysical Journal International*, *122*(1), 108–124.

Kerckhove, C. (1969). La 'zone du Flysch' dans les nappes de l'Embrunais-Ubaye (Alpes occidentales). *Geologie Alpine*, *45*, 5–204.

Kern, H., Jin, Z., Gao, S., Popp, T., & Xu, Z. (2002). Physical properties of ultrahigh-pressure metamorphic rocks from the Sulu terrain, eastern central China: Implications for the seismic structure at the Donghai (CCSD) drilling site. *Tectonophysics*, *354*(3–4), 315–330.

Khazanehdari, J., Rutter, E. H., & Brodie, K. H. (2000). High-pressure-high-temperature seismic velocity structure of the midcrustal and lower crustal rocks of the Ivrea-Verbano zone and Serie dei Laghi, NW Italy. *Journal of Geophysical Research*, *105*(B6), 13843–13858.

Kilian, W., & Revil, J. (1903). *Contributions à la connaissance de la zone du Briançonnais, le Jurassique supérieur*. De Alliers Frères, 31 p.

Kissling, E. (1988). Geotomography with local earthquake data. *Reviews of Geophysics*, *26*(4), 659–698.

Kissling, E. (1993). Deep structure of the Alps—What do we really know?. *Physics of the Earth and Planetary Interiors*, *79*(1–2), 87–112.

Kissling, E., & Schlunegger, F. (2018). Rollback orogeny model for the evolution of the Swiss Alps. *Tectonics*, *37*(4), 1097–1115.

Kissling, E., Schmid, S. M., Lippitsch, R., Ansorge, J., & Fügenschuh, B. (2006). Lithosphere structure and tectonic evolution of the Alpine arc: New evidence from high-resolution teleseismic tomography. *Geological Society, London, Memoirs*, *32*, 129–145.

Koulakov, I., Kaban, M. K., Tesauro, M., & Cloetingh, S. A. P. L. (2009). P-and S-velocity anomalies in the upper mantle beneath Europe from tomographic inversion of ISC data. *Geophysical Journal International*, *179*(1), 345–366.

Kovács, I., Csontos, L., Szabó, C., Bali, E., Falus, G., Benedek, K., & Zajacz, Z. (2007). Paleogene-early Miocene igneous rocks and geodynamics of the Alpine-Carpathian-Pannonian-Dinaric region: An integrated approach. *Geological Society of America Special Paper*, *418*, 93–112.

Lagabrielle, Y., & Cannat, M. (1990). Alpine Jurassic ophiolites resemble the modern central Atlantic basement. *Geology*, *18*(4), 319–322.

Lagabrielle, Y., & Lemoine, M. (1997). Alpine, Corsican and Apennine ophiolites: The slow-spreading ridge model. *Comptes Rendus de l'Academie des Sciences – Series IIA: Earth and Planetary Science*, *325*(12), 909–920.

Lanari, P., Guillot, S., Schwartz, S., Vidal, O., Tricart, P., Riel, N., & Beyssac, O. (2012). Diachronous evolution of the alpine continental subduction wedge: evidence from P–T estimates in the Briançonnais Zone houillère (France–Western Alps). *Journal of Geodynamics*, *56*, 39–54.

Langston, C. A. (1979). Structure under Mount Rainier, Washington, inferred from teleseismic body waves. *Journal of Geophysical Research*, *84*(B9), 4749–4762.

Lapen, T. J., Johnson, C. M., Baumgartner, L. P., Mahlen, N. J., Beard, B. L., & Amato, J. M. (2003). Burial rates during prograde metamorphism of an ultra-high-pressure terrane: An example from Lago di Cignana, western Alps, Italy. *Earth and Planetary Science Letters*, *215*(1–2), 57–72.

Lardeaux, J. M., Schwartz, S., Tricart, P., Paul, A., Guillot, S., Béthoux, N., & Masson, F. (2006). A crustal-scale cross-section of the south-western Alps combining geophysical and geological imagery. *Terra Nova*, *18*(6), 412–422.

Larose, E., Margerin, L., Derode, A., van Tiggelen, B., Campillo, M., Shapiro, N., et al. (2006). Correlation of random wavefields: An interdisciplinary review. *Geophysics*, *71*(4), SI11–SI21.

Laubscher, H. P. (1974). Evoluzione e struttura delle Alpi. *Le Scienze*, *72*, 264–275.

Lemoine, M., Bas, T., Arnaud-Vanneau, A., Arnaud, H., Dumont, T., Gidon, M., et al. (1986). The continental margin of the Mesozoic Tethys in the Western Alps. *Marine and Petroleum Geology*, *3*(3), 179–199.

Lenze, A., & Stöckhert, B. (2007). Microfabrics of UHP metamorphic granites in the Dora Maira Massif, western Alps – No evidence of deformation at great depth. *Journal of Metamorphic Geology*, *25*(4), 461–475.

Liao, J., Gerya, T., & Malusà, M. G. (2018a). 3D modeling of crustal shortening influenced by along-strike lithological changes: Implications for continental collision in the Western and Central Alps. *Tectonophysics*, *746*, 425–438.

Liao, J., Malusà, M. G., Zhao, L., Baldwin, S. L., Fitzgerald, P. G., & Gerya, T. (2018b). Divergent plate motion drives rapid exhumation of (ultra) high pressure rocks. *Earth and Planetary Science Letters*, *491*, 67–80.

Liati, A., & Froitzheim, N. (2006). Assessing the Valais ocean, Western Alps: U-Pb SHRIMP zircon geochronology of eclogite in the Balma unit, on top of the Monte Rosa nappe. *European Journal of Mineralogy*, *18*(3), 299–308.

Ligorria, J. P., & Ammon, C. J. (1999). Iterative deconvolution and receiver-function estimation. *Bulletin of the Seismological Society of America*, *89*(5), 1395–1400.

Link, F., & Rümpker, G. (2020). The mantle flow below the Alps from isolated mantle anisotropy based on differential Ps – XKS Splitting. *Geophysical Research Abstracts*, *22*, EGU2020–2810.

Lippitsch, R., Kissling, E., & Ansorge, J. (2003). Upper mantle structure beneath the Alpine orogen from high-resolution teleseismic tomography. *Journal of Geophysical Research: Solid Earth*, *108*(B8). https://doi.org/10.1029/2002JB002016

Lombardo, B., Nervo, R., Compagnoni, R., Messiga, B., Kienast, J. R., Mével, C., et al. (1978). Osservazioni preliminari sulle ofiolite metamorfiche del Monviso (Alpi Occidentali). *Rendiconti della Societa Italiana di Mineralogia e Petrologia*, *34*, 253–305.

Long, M. D., & Silver, P. G. (2008). The subduction zone flow field from seismic anisotropy: A global view. *Science*, *319*(5861), 315–318.

Long, M. D., & Silver, P. G. (2009). Shear wave splitting and mantle anisotropy: Measurements, interpretations, and new directions. *Surveys in Geophysics*, *30*(4–5), 407–461.

Lucente, F. P., Margheriti, L., Piromallo, C., & Barruol, G. (2006). Seismic anisotropy reveals the long route of the slab through the western-central Mediterranean mantle. *Earth and Planetary Science Letters*, *241*(3–4), 517–529.

Lugeon, M. (1901). Les grandes nappes de recouvrement des Alpes du Chablais et de la Suisse. *Bulletin de la Société Géologique de France*, *50*, 723–825.

Lugeon, M. (1902). Les grandes dislocations et la naissance des Alpes suisses. *Eclogae Geologicae Helvetiae*, *7*, 335–346.

Lu, Y., Stehly, L., Brossier, R., & Paul, A. (2020). Imaging Alpine crust using ambient noise wave-equation tomography. *Geophysical Journal International*, *22*, 69–85.

Lu, Y., Stehly, L., & Paul, A., & AlpArray Working Group. (2018). High-resolution surface wave tomography of the European crust and uppermost mantle from ambient seismic noise. *Geophysical Journal International*, *214*(2), 1136–1150.

Lustrino, M., Duggen, S., & Rosenberg, C. L. (2011). The Central-Western Mediterranean: anomalous igneous activity in an anomalous collisional tectonic setting. *Earth-Science Reviews*, *104*(1–3), 1–40.

Lyon-Caen, H., & Molnar, P. (1989). Constraints on the deep structure and dynamic processes beneath the Alps and adjacent regions from an analysis of gravity anomalies. *Geophysical Journal International*, *99*(1), 19–32.

Lyu, C., Pedersen, H. A., Paul, A., Zhao, L., & Solarino, S. (2017). Shear wave velocities in the upper mantle of the Western Alps: New constraints using array analysis of seismic surface waves. *Geophysical Journal International*, *210*(1), 321–331.

Macera, P., Gasperini, D., Ranalli, G., & Mahatsente, R. (2008). Slab detachment and mantle plume upwelling in subduction zones: An example from the Italian South-Eastern Alps. *Journal of Geodynamics*, *45*(1), 32–48.

Maffione, M., Speranza, F., Faccenna, C., Cascella, A., Vignaroli, G., & Sagnotti, L. (2008). A synchronous Alpine and Corsica-Sardinia rotation. *Journal of Geophysical Research*, *113*(B3). https://doi.org/10.1029/2007JB005214

Mainprice, D., Barruol, G., & Ismail, W. B. (2000). The seismic anisotropy of the Earth's mantle: From single crystal to polycrystal. *Geophysical Monograph – American Geophysical Union*, *117*, 237–264.

Malusà, M. G., Anfinson, O. A., Dafov, L. N., & Stockli, D. F. (2016b). Tracking Adria indentation beneath the Alps by detrital zircon U-Pb geochronology: Implications for the Oligocene–Miocene dynamics of the Adriatic microplate. *Geology*, *44*(2), 155–158.

Malusà, M. G., & Balestrieri, M. L. (2012). Burial and exhumation across the Alps–Apennines junction zone constrained by fission-track analysis on modern river sands. *Terra Nova*, *24*(3), 221–226.

Malusà, M. G., Danišík, M., & Kuhlemann, J. (2016a). Tracking the Adriatic-slab travel beneath the Tethyan margin of Corsica–Sardinia by low-temperature thermochronometry. *Gondwana Research*, *31*, 135–149.

Malusà, M. G., Faccenna, C., Baldwin, S. L., Fitzgerald, P. G., Rossetti, F., Balestrieri, M. L., & Piromallo, C. (2015). Contrasting styles of (U) HP rock exhumation along the Cenozoic Adria-Europe plate boundary (Western Alps, Calabria, Corsica). *Geochemistry, Geophysics, Geosystems*, *16*(6), 1786–1824.

Malusà, M. G., Faccenna, C., Garzanti, E., & Polino, R. (2011). Divergence in subduction zones and exhumation of high pressure rocks (Eocene Western Alps). *Earth and Planetary Science Letters*, *310*(1–2), 21–32.

Malusà, M. G., Frezzotti, M. L., Ferrando, S., Brandmayr, E., Romanelli, F., & Panza, G. F. (2018). Active carbon sequestration in the Alpine mantle wedge and implications for long-term climate trends. *Scientific Reports*, *8*(1), 1–8.

Malusà, M. G., Polino, R., & Martin, S. (2005). The Gran San Bernardo nappe in the Aosta valley (western Alps): A composite stack of distinct continental crust units. *Bulletin de la Societe Geologique de France*, *176*(5), 417–431.

Malusà, M. G., Polino, R., & Zattin, M. (2009). Strain partitioning in the axial NW Alps since the Oligocene. *Tectonics*, *28*(3).

Malusà, M. G., Zhao, L., Eva, E., Solarino, S., Paul, A., Guillot, S., et al. (2017). Earthquakes in the western Alpine mantle wedge. *Gondwana Research*, *44*, 89–95.

Manatschal, G. (2004). New models for evolution of magma-poor rifted margins based on a review of data and concepts from West Iberia and the Alps. *International Journal of Earth Sciences*, *93*(3), 432–466.

Manatschal, G., & Bernoulli, D. (1999). Architecture and tectonic evolution of nonvolcanic margins: Present-day Galicia and ancient Adria. *Tectonics*, *18*(6), 1099–1119.

Manatschal, G., & Müntener, O. (2009). A type sequence across an ancient magma-poor ocean–continent transition: The example of the western Alpine Tethys ophiolites. *Tectonophysics*, *473*(1–2), 4–19.

Marschall, H. R., & Schumacher, J. C. (2012). Arc magmas sourced from mélange diapirs in subduction zones. *Nature Geoscience*, *5*(12), 862–867.

Martini, J. (1972). Le métamorphisme dans les chaînes alpines externes et ses implications dans l'orogenèse. *Schweizerische Mineralogische und Petrographische Mitteilungen*, *52*, 257–276.

Masson, H., Bussy, F., Eichenberger, M., Giroud, N., Meilhac, C., & Presniakov, S. (2008). Early Carboniferous age of the Versoyen ophiolites and consequences: Non-existence of a "Valais ocean"(Lower Penninic, western Alps). *Bulletin de la Societe Geologique de France*, *179*(4), 337–355.

Mechie, J., Yuan, X., Schurr, B., Schneider, F., Sippl, C., Ratschbacher, L., et al. (2012). Crustal and uppermost mantle velocity structure along a profile across the Pamir and southern Tien Shan as derived from project TIPAGE wide-angle seismic data. *Geophysical Journal International*, *188*(2), 385–407.

Mercier, J. P., Bostock, M. G., Audet, P., Gaherty, J. B., Garnero, E. J., & Revenaugh, J. (2008). The teleseismic signature of fossil subduction: Northwestern Canada. *Journal of Geophysical Research*, *113*(B4).

Michard, A., Avigad, D., Goffé, B., & Chopin, C. (2004). The high-pressure metamorphic front of the south Western Alps (Ubaye-Maira transect, France, Italy). *Schweizerische Mineralogische und Petrographische Mitteilungen*, *84*, 215–235.

Milnes, A. G. (1974). Structure of the Pennine Zone (Central Alps): A new working hypothesis. *The Geological Society of America Bulletin*, *85*(11), 1727–1732.

Mitterbauer, U., Behm, M., Brückl, E., Lippitsch, R., Guterch, A., Keller, G. R., et al. (2011). Shape and origin of the East-Alpine slab constrained by the ALPASS teleseismic model. *Tectonophysics*, *510*(1–2), 195–206.

Mohn, G., Manatschal, G., Müntener, O., Beltrando, M., & Masini, E. (2010). Unraveling the interaction between tectonic and sedimentary processes during lithospheric thinning in the Alpine Tethys margins. *International Journal of Earth Sciences*, *99*(1), 75–101.

Molinari, I., Argnani, A., Morelli, A., & Basini, P. (2015). Development and testing of a 3D seismic velocity model of the Po Plain sedimentary basin, Italy. *Bulletin of the Seismological Society of America*, *105*(2A), 753–764.

Molinari, I., Dasović, I., Stipčević, J., Šipka, V., Jarić, D., Kissling, E., et al. (2018). Investigation of the central Adriatic lithosphere structure with the AlpArray-CASE seismic experiment. *Geofizika*, *35*(2), 103–128.

Molinari, I., & Morelli, A. (2011). EPcrust: A reference crustal model for the European Plate. *Geophysical Journal International*, *185*(1), 352–364.

Nicolas, A., Bouchez, J. L., & Boudier, F. (1972). Interprétation cinématique des déformations plastiques dans le massif de lherzolite de Lanzo (Alpes piemontaises)—Comparaison avec d'autres massifs. *Tectonophysics*, *14*(2), 143–171.

Nicolas, A., Hirn, A., Nicolich, R., & Polino, R. (1990a). Lithospheric wedging in the western Alps inferred from the ECORS-CROP traverse. *Geology*, *18*(7), 587–590.

Nicolas, A., Polino, R., Hirn, A., & Nicolich, R. (1990b). ECORS-CROP traverse and deep structure of the western Alps: A synthesis. *Mémoires de la Société géologique de France*, *156*(1833), 15–27.

Nocquet, J. M., Sue, C., Walpersdorf, A., Tran, T., Lenôtre, N., Vernant, P., et al. (2016). Present-day uplift of the western Alps. *Scientific Reports*, *6*(1), 1–6.

O'Brien, P. J. (2001). Subduction followed by collision: Alpine and Himalayan examples. *Physics of the Earth and Planetary Interiors*, *127*(1–4), 277–291.

Oxburgh, E. R. (1972). Flake tectonics and continental collision. *Nature*, *239*(5369), 202–204.

Paffrath, M., & Friederich, W., & the AlpArray Working Group. (2020). Teleseismic P-wave travel time tomography of the Alpine upper mantle using AlpArray seismic network data. *Geophysical Research Abstracts*, *22*, EGU2020–13779.

Paquette, J. L., Montel, J. M., & Chopin, C. (1999). U-Th-Pb dating of the Brossasco ultrahigh-pressure metagranite, Dora-Maira massif, western Alps. *European Journal of Mineralogy*, *11*(1), 69–77.

Paul, A., Cattaneo, M., Thouvenot, F., Spallarossa, D., Béthoux, N., & Fréchet, J. (2001). A three-dimensional crustal velocity model of the southwestern Alps from local earthquake tomography. *Journal of Geophysical Research*, *106*(B9), 19367–19389.

Pawley, A. R. (1994). The pressure and temperature stability limits of lawsonite: implications for H 2 O recycling in subduction zones. *Contributions to Mineralogy and Petrology*, *118*(1), 99–108.

Peacock, S. M., & Hyndman, R. D. (1999). Hydrous minerals in the mantle wedge and the maximum depth of subduction thrust earthquakes. *Geophysical Research Letters*, *26*(16), 2517–2520.

Peccerillo, A., & Frezzotti, M. L. (2015). Magmatism, mantle evolution and geodynamics at the converging plate margins of Italy. *Journal of the Geological Society*, *172*(4), 407–427.

Pera, E., Mainprice, D., & Burlini, L. (2003). Anisotropic seismic properties of the upper mantle beneath the Torre Alfina area (Northern Apennines, Central Italy). *Tectonophysics*, *370*(1–4), 11–30.

Pfiffner, O. A. (2014). *Geology of the Alps*. New York, NY: John Wiley & Sons.

Pfiffner, O. A., Schlunegger, F., & Buiter, S. J. H. (2002). The Swiss Alps and their peripheral foreland basin: Stratigraphic response to deep crustal processes. *Tectonics*, *21*(2), 3–1.

Piana Agostinetti, N., Salimbeni, S., Pondrelli, S., Malusà, M. G., Zhao, L., Eva, E., et al. (2017). Mantle wedge anisotropy beneath the Western Alps: Insights from Receiver Function analysis. *Geophysical Research Abstracts*, *19*, EGU2017–12545.

Piccardo, G. B. (2003). Mantle processes during ocean formation: petrologic records in peridotites from the Alpine-Apennine ophiolites. *Episodes*, *26*(3), 193–199.

Piccardo, G. B., & Vissers, R. L. M. (2007). The pre-oceanic evolution of the Erro-Tobbio peridotite (Voltri Massif, Ligurian Alps, Italy). *Journal of Geodynamics*, *43*(4–5), 417–449.

Piccardo, G. B., Zanetti, A., & Müntener, O. (2007). Melt/peridotite interaction in the Southern Lanzo peridotite: Field, textural and geochemical evidence. *Lithos*, *94*(1–4), 181–209.

Piromallo, C., Becker, T. W., Funiciello, F., & Faccenna, C. (2006). Three-dimensional instantaneous mantle flow induced by subduction. *Geophysical Research Letters*, *33*(8). https://doi.org/10.1029/2005GL025390

Piromallo, C., & Faccenna, C. (2004). How deep can we find the traces of Alpine subduction?. *Geophysical Research Letters*, *31*(6).

Piromallo, C., & Morelli, A. (2003). P wave tomography of the mantle under the Alpine-Mediterranean area. *Journal of Geophysical Research: Solid Earth*, *108*(B2). https://doi.org/10.1029/2002JB001757

Plomerová, J., Žlebčíková, H., Hetényi, G., Vecsey, L., Babuška, V., The AlpArray-EASI Working Group, and the AlpArray Working Group. (2020). Tomography image of double high-velocity heterogeneity beneath the Eastern Alps from the AlpArray data. *Geophysical Research Abstracts*, *22*, EGU2020–7728.

Poli, S. (2015). Carbon mobilized at shallow depths in subduction zones by carbonatitic liquids. *Nature Geoscience*, *8*(8), 633–636.

Poli, S., & Schmidt, M. W. (2002). Petrology of subducted slabs. *Annual Review of Earth and Planetary Sciences*, *30*(1), 207–235.

Polino, R., & Lemoine, M. (1984). Détritisme mixte d'origine continentale et océanique dans les sédiments jurassico-crétacés supra-ophiolitiques de la Téthys ligure: la série du Lago Nero (Alpes Occidentales franco-italiennes). Comptes-rendus des séances de l'Académie des sciences. Série 2. *Mécanique-physique, chimie, sciences de l'univers, sciences de la terre*, *298*(8), 359–364.

Polino, R., Malusà M. G., Martin, S., Carraro, F., Gianotti, F., Bonetto, F., et al. (2012). *Carta Geologica d'Italia alla Scala 1:50.000—Foglio 090 Aosta*. Roma: Regione Autonoma Valle d'Aosta—ISPRA.

Qorbani, E., Bianchi, I., & Bokelmann, G. (2015). Slab detachment under the Eastern Alps seen by seismic anisotropy. *Earth and Planetary Science Letters*, *409*, 96–108.

Quick, J. E., Sinigoi, S., & Mayer, A. (1994). Emplacement dynamics of a large mafic intrusion in the lower crust, Ivrea-Verbano Zone, northern Italy. *Journal of Geophysical Research*, *99*(B11), 21559–21573.

Ramsay, J. G. (1963). Stratigraphy, structure and metamorphism in the Western Alps. *Proceedings of the Geologists' Association*, *74*(3), 357–IN12.

Reinecke, T. (1991). Very-high-pressure metamorphism and uplift of coesite-bearing metasediments from the Zermatt-Saas zone, Western Alps. *European Journal of Mineralogy*, 7–18.

Reynard, B. (2013). Serpentine in active subduction zones. *Lithos*, *178*, 171–185.

Rosenberg, C. L., Schneider, S., Scharf, A., Bertrand, A., Hammerschmidt, K., Rabaute, A., & Brun, J. P. (2018). Relating collisional kinematics to exhumation processes in the Eastern Alps. *Earth-Science Reviews*, *176*, 311–344.

Rossi, M., Mosca, P., Polino, R., Rogledi, S., & Biffi, U. (2009). New outcrop and subsurface data in the Tertiary Piedmont Basin (NW-Italy): Unconformity-bounded stratigraphic units and their relationships with basin-modification phases. *Rivista Italiana di Paleontologia e Stratigrafia*, *115*(3), 305–335.

Rouméjon, S., & Cannat, M. (2014). Serpentinization of mantle-derived peridotites at mid-ocean ridges: Mesh texture development in the context of tectonic exhumation. *Geochemistry, Geophysics, Geosystems*, *15*(6), 2354–2379.

Roure, F., Bergerat, F., Damotte, B., Mugnier, J. L., & Polino, R. (1996). The ECORS-CROP Alpine Seismic Traverse. *Mémoires de la Société géologique de France*, *1833*, 170.

Rubatto, D., Gebauer, D., & Fanning, M. (1998). Jurassic formation and Eocene subduction of the Zermatt–Saas-Fee ophiolites: Implications for the geodynamic evolution of the Central and Western Alps. *Contributions to Mineralogy and Petrology*, *132*(3), 269–287.

Rubatto, D., & Hermann, J. (2001). Exhumation as fast as subduction?. *Geology*, *29*(1), 3–6.

Rubatto, D., Müntener, O., Barnhoorn, A., & Gregory, C. (2008). Dissolution-reprecipitation of zircon at low-temperature, high-pressure conditions (Lanzo Massif, Italy). *American Mineralogist*, *93*(10), 1519–1529.

Rudnick, R. L., & Fountain, D. M. (1995). Nature and composition of the continental crust: A lower crustal perspective. *Reviews of Geophysics*, *33*(3), 267–309.

Salimbeni, S., Malusà, M. G., Zhao, L., Guillot, S., Pondrelli, S., Margheriti, L., et al. (2018). Active and fossil mantle flows in the western Alpine region unraveled by seismic anisotropy analysis and high-resolution P wave tomography. *Tectonophysics*, *731*, 35–47.

Salimbeni, S., Pondrelli, S., & Margheriti, L. (2013). Hints on the deformation penetration induced by subductions and collision processes: Seismic anisotropy beneath the Adria region (Central Mediterranean). *Journal of Geophysical Research: Solid Earth*, *118*(11), 5814–5826.

Salimbeni, S., Pondrelli, S., Margheriti, L., Park, J., & Levin, V. (2008). SKS splitting measurements beneath Northern Apennines region: A case of oblique trench-retreat. *Tectonophysics*, *462*(1–4), 68–82.

Savage, M. K. (1999). Seismic anisotropy and mantle deformation: What have we learned from shear wave splitting? *Reviews of Geophysics*, *37*(1), 65–106.

Savage, M. K., & Sheehan, A. F. (2000). Seismic anisotropy and mantle flow from the Great Basin to the Great Plains, western United States. *Journal of Geophysical Research*, *105*(B6), 13715–13734.

Scafidi, D., Solarino, S., & Eva, C. (2006). Structure and properties of the Ivrea body and of the Alps-Apennines system as revealed by local earthquake tomography. *Bollettino di Geofisica Teorica*, *47*, 497–514.

Scafidi, D., Solarino, S., & Eva, C. (2009). P wave seismic velocity and Vp/Vs ratio beneath the Italian peninsula from local earthquake tomography. *Tectonophysics*, *465*(1–4), 1–23.

Scambelluri, M., Müntener, O., Hermann, J., Piccardo, G. B., & Trommsdorff, V. (1995). Subduction of water into the mantle: History of an Alpine peridotite. *Geology*, *23*(5), 459–462.

Schaltegger, U., & Brack, P. (2007). Crustal-scale magmatic systems during intracontinental strike-slip tectonics: U, Pb and Hf isotopic constraints from Permian magmatic rocks of the Southern Alps. *International Journal of Earth Sciences*, *96*(6), 1131–1151.

Schlunegger, F., & Castelltort, S. (2016). Immediate and delayed signal of slab breakoff in Oligo/Miocene Molasse deposits from the European Alps. *Scientific Reports*, *6*, 31010.

Schlunegger, F., & Kissling, E. (2015). Slab rollback orogeny in the Alps and evolution of the Swiss Molasse basin. *Nature Communications*, *6*(1), 1–10.

Schmid, S. M., Fügenschuh, B., Kissling, E., & Schuster, R. (2004). Tectonic map and overall architecture of the Alpine orogen. *Eclogae Geologicae Helvetiae*, *97*(1), 93–117.

Schmid, S. M., & Kissling, E. (2000). The arc of the western Alps in the light of geophysical data on deep crustal structure. *Tectonics*, *19*(1), 62–85.

Schmid, S. M., Kissling, E., Diehl, T., van Hinsbergen, D. J., & Molli, G. (2017). Ivrea mantle wedge, arc of the Western Alps, and kinematic evolution of the Alps–Apennines orogenic system. *Swiss Journal of Geosciences*, *110*(2), 581–612.

Schmid, S. M., Pfiffner, O. A., Froitzheim, N., Schönborn, G., & Kissling, E. (1996). Geophysical-geological transect and tectonic evolution of the Swiss-Italian Alps. *Tectonics*, *15*(5), 1036–1064.

Schmid, S. M., Scharf, A., Handy, M. R., & Rosenberg, C. L. (2013). The Tauern Window (Eastern Alps, Austria): A new tectonic map, with cross-sections and a tectonometamorphic synthesis. *Swiss Journal of Geosciences*, *106*(1), 1–32.

Schmidt, M. W., & Poli, S. (1998). Experimentally based water budgets for dehydrating slabs and consequences for arc magma generation. *Earth and Planetary Science Letters*, *163*(1–4), 361–379.

Schmidt, M. W., Vielzeuf, D., & Auzanneau, E. (2004). Melting and dissolution of subducting crust at high pressures: The key role of white mica. *Earth and Planetary Science Letters*, *228*(1–2), 65–84.

Schwartz, S., Allemand, P., & Guillot, S. (2001). Numerical model of the effect of serpentinites on the exhumation of eclogitic rocks: Insights from the Monviso ophiolitic massif (Western Alps). *Tectonophysics*, *342*(1–2), 193–206.

Schwartz, S., Guillot, S., Reynard, B., Lafay, R., Debret, B., Nicollet, C., et al. (2013). Pressure–temperature estimates of the lizardite/antigorite transition in high pressure serpentinites. *Lithos*, *178*, 197–210.

Schwartz, S., Lardeaux, J. M., Guillot, S., & Tricart, P. (2000). Diversité du métamorphisme éclogitique dans le massif ophiolitique du Monviso (Alpes occidentales, Italie). *Geodinamica Acta*, *13*(2–3), 169–188.

Schwartz, S., Tricart, P., Lardeaux, J. M., Guillot, S., & Vidal, O. (2009). Late tectonic and metamorphic evolution of the Piedmont accretionary wedge (Queyras Schistes lustrés, western Alps): Evidences for tilting during Alpine collision. *The Geological Society of America Bulletin*, *121*(3–4), 502–518.

Serpelloni, E., Faccenna, C., Spada, G., Dong, D., & Williams, S. D. (2013). Vertical GPS ground motion rates in the Euro-Mediterranean region: New evidence of velocity gradients at different spatial scales along the Nubia-Eurasia plate boundary. *Journal of Geophysical Research: Solid Earth*, *118*(11), 6003–6024.

Shapiro, N. M., Campillo, M., Stehly, L., & Ritzwoller, M. H. (2005). High-resolution surface-wave tomography from ambient seismic noise. *Science*, *307*(5715), 1615–1618.

Shinohara, M., Fukano, T., Kanazawa, T., Araki, E., Suyehiro, K., Mochizuki, M., et al. (2008). Upper mantle and crustal seismic structure beneath the Northwestern Pacific Basin using a seafloor borehole broadband seismometer and ocean bottom seismometers. *Physics of the Earth and Planetary Interiors*, *170*(1–2), 95–106.

Silver, P. G., Mainprice, D., Ismail, W. B., Tommasi, A., & Barruol, G. (1999). Mantle structural geology from seismic anisotropy. *Special Publication – Geochemical Society*, *6*, 79–103.

Simmons, N. A., Forte, A. M., Boschi, L., & Grand, S. P. (2010). GyPSuM: A joint tomographic model of mantle density and seismic wave speeds. *Journal of Geophysical Research*, *115*(B12).

Sinclair, H. D. (1997). Flysch to molasse transition in peripheral foreland basins: The role of the passive margin versus slab breakoff. *Geology*, *25*(12), 1123–1126.

Solarino, S., Kissling, E., Sellami, S., Smriglio, G., Thouvenot, F., Granet, M., et al. (1997). Compilation of a recent seismicity data base of the greater Alpine region from several seismological networks and preliminary 3D tomographic results. *Annals of Geophysics*, *40*(1), 161–174.

Solarino, S., Malusà, M. G., Eva, E., Guillot, S., Paul, A., Schwartz, S., et al. (2018). Mantle wedge exhumation beneath the Dora-Maira (U) HP dome unraveled by local earthquake tomography (Western Alps). *Lithos*, *296*, 623–636.

Spada, M., Bianchi, I., Kissling, E., Agostinetti, N. P., & Wiemer, S. (2013). Combining controlled-source seismology and receiver function information to derive 3-D Moho topography for Italy. *Geophysical Journal International*, *194*(2), 1050–1068.

Spakman, W., & Wortel, R. (2004). A tomographic view on western Mediterranean geodynamics. In *The TRANSMED Atlas: The Mediterranean region from crust to mantle* (pp. 31–52). New York, NY: Springer.

Stampfli, G. M., Borel, G. D., Marchant, R., & Mosar, J. (2002). Western Alps geological constraints on western Tethyan reconstructions. *Journal of the Virtual Explorer*, *8*, 77.

Stampfli, G. M., Mosar, J., Marquer, D., Marchant, R., Baudin, T., & Borel, G. (1998). Subduction and obduction processes in the Swiss Alps. *Tectonophysics*, *296*(1–2), 159–204.

Sternai, P., Sue, C., Husson, L., Serpelloni, E., Becker, T. W., Willett, S. D., & Valla, P. (2019). Present-day uplift of the European Alps: Evaluating mechanisms and models of their relative contributions. *Earth-Science Reviews*, *190*, 589–604.

Sue, C., Delacou, B., Champagnac, J. D., Allanic, C., Tricart, P., & Burkhard, M. (2007). Extensional neotectonics around the bend of the Western/Central Alps: An overview. *International Journal of Earth Sciences*, *96*(6), 1101–1129.

Sue, C., Thouvenot, F., Fréchet, J., & Tricart, P. (1999). Widespread extension in the core of the western Alps revealed by earthquake analysis. *Journal of Geophysical Research*, *104*(B11), 25611–25622.

Sun, W., & Kennett, B. L. N. (2016a). Uppermost mantle structure of the Australian continent from Pn traveltime tomography. *Journal of Geophysical Research: Solid Earth*, *121*(3), 2004–2019.

Sun, W., & Kennett, B. L. N. (2016b). Uppermost mantle P wavespeed structure beneath eastern China and its surroundings. *Tectonophysics*, *683*, 12–26.

Sun, W., Zhao, L., Malusà, M. G., Guillot, S., & Fu, L. Y. (2019). 3-D Pn tomography reveals continental subduction at the boundaries of the Adriatic microplate in the absence of a precursor oceanic slab. *Earth and Planetary Science Letters*, *510*, 131–141.

Syracuse, E. M., van Keken, P. E., & Abers, G. A. (2010). The global range of subduction zone thermal models. *Physics of the Earth and Planetary Interiors*, *183*(1–2), 73–90.

Tardy, M., Bethoux, N., Lardeaux, J. M., & Paul, A. (1999). The Géofrance 3D project in the western Alps: A synthesis. Documents du BRGM. *Géologie régionale et générale*, *293*, 52–63.

Thöni, M. (2006). Dating eclogite-facies metamorphism in the Eastern Alps – Approaches, results, interpretations: A review. *Mineralogy and Petrology*, *88*(1–2), 123–148.

Thouvenot, F., Paul, A., Frechet, J., Béthoux, N., Jenatton, L., & Guiguet, R. (2007). Are there really superposed Mohos in the southwestern Alps? New seismic data from fan-profiling reflections. *Geophysical Journal International*, *170*(3), 1180–1194.

Thouvenot, F., Paul, A., Senechal, G., Hirn, A., & Nicolich, R. (1990). ECORS-CROP wide-angle reflection seismics: Constraints on deep interfaces beneath the Alps. In Deep structure of the Alps (156, pp. 97–106).

Thouvenot, F., Senechal, G., Truffert, C., & Guellec, S. (1996). Comparison between two techniques of line-drawing migration (ray-tracing and common tangent method). *Memoires de la Societe Geologique de France*, 53–60.

Tommasi, A., Tikoff, B., & Vauchez, A. (1999). Upper mantle tectonics: Three-dimensional deformation, olivine crystallographic fabrics and seismic properties. *Earth and Planetary Science Letters*, *168*(1–2), 173–186.

Tricart, P. (1984). From passive margin to continental collision; a tectonic scenario for the Western Alps. *American Journal of Science*, *284*(2), 97–120.

Trümpy, R. (1960). Paleotectonic evolution of the Central and Western Alps. *The Geological Society of America Bulletin*, *71*(6), 843–907.

Ulmer, P., & Trommsdorff, V. (1999). Phase relations of hydrous mantle subducting to 300 km. *Geological Society London Special Publications*, *6*, 259–281.

Ustaszewski, K., Schmid, S. M., Fügenschuh, B., Tischler, M., Kissling, E., & Spakman, W. (2008). A map-view restoration of the Alpine-Carpathian-Dinaridic system for the Early Miocene. *Swiss Journal of Geosciences*, *101*(1), 273–294.

Vauchez, A., Tommasi, A., & Mainprice, D. (2012). Faults (shear zones) in the Earth's mantle. *Tectonophysics*, *558*, 1–27.

Vignaroli, G., Faccenna, C., Jolivet, L., Piromallo, C., & Rossetti, F. (2008). Subduction polarity reversal at the junction between the Western Alps and the Northern Apennines, Italy. *Tectonophysics*, *450*(1–4), 34–50.

Vissers, R. L. M., Drury, M. R., Hoogerduijn, E. H., Spiers, C. J., & Van der Wal, D. (1995). Mantle shear zones and their effect on lithosphere strength during continental breakup. *Tectonophysics*, *249*(3–4), 155–171.

von Blanckenburg, F., & Davies, J. H. (1995). Slab breakoff: A model for syncollisional magmatism and tectonics in the Alps. *Tectonics*, *14*(1), 120–131.

Wagner, M., Kissling, E., & Husen, S. (2012). Combining controlled-source seismology and local earthquake tomography to derive a 3-D crustal model of the western Alpine region. *Geophysical Journal International*, *191*(2), 789–802.

Waldhauser, F., Lippitsch, R., Kissling, E., & Ansorge, J. (2002). High-resolution teleseismic tomography of upper-mantle structure using an a priori three-dimensional crustal model. *Geophysical Journal International*, *150*(2), 403–414.

Walpersdorf, A., Sue, C., Baize, S., Cotte, N., Bascou, P., Beauval, C., et al. (2015). Coherence between geodetic and seismic deformation in a context of slow tectonic activity (SW Alps, France). *Journal of Geodynamics*, *85*, 58–65.

Wang, Q., Ji, S., Salisbury, M. H., Xia, B., Pan, M., & Xu, Z. (2005). Pressure dependence and anisotropy of P-wave velocities in ultrahigh-pressure metamorphic rocks from the Dabie–Sulu orogenic belt (China): Implications for seismic properties of subducted slabs and origin of mantle reflections. *Tectonophysics*, *398*(1–2), 67–99.

Watanabe, T., Shirasugi, Y., Yano, H., & Michibayashi, K. (2011). Seismic velocity in antigorite-bearing serpentinite mylonites. *Geological Society, London, Special Publications*, *360*(1), 97–112.

Weiss, T., Siegesmund, S., Rabbel, W., Bohlen, T., & Pohl, M. (1999). Seismic velocities and anisotropy of the lower continental crust: A review. In *Seismic exploration of the deep continental crust* (pp. 97–122). Basel: Birkhäuser.

Winterer, E. L., & Bosellini, A. (1981). Subsidence and sedimentation on Jurassic passive continental margin, Southern Alps, Italy. *AAPG Bulletin*, *65*(3), 394–421.

Wortel, M. J. R., & Spakman, W. (1992). Structure and dynamics of subducted lithosphere in the Mediterranean region. *Proceedings of the Koninklijke Nederlandse Akademie Van Wetenschappen*, *95*(3), 325–347.

Wortel, M. J. R., & Spakman, W. (2000). Subduction and slab detachment in the Mediterranean-Carpathian region. *Science*, *290*(5498), 1910–1917.

Yoshino, T., Nishihara, Y., & Karato, S. I. (2007). Complete wetting of olivine grain boundaries by a hydrous melt near the mantle transition zone. *Earth and Planetary Science Letters*, *256*(3–4), 466–472.

Yuan, H., & Bodin, T. (2018). A probabilistic shear wave velocity model of the crust in the central West Australian craton constrained by transdimensional inversion of ambient noise dispersion. *Tectonics*, *37*(7), 1994–2012.

Zanchetta, S., Garzanti, E., Doglioni, C., & Zanchi, A. (2012). The Alps in the Cretaceous: A doubly vergent pre-collisional orogen. *Terra Nova*, *24*(5), 351–356.

Zanchetta, S., Malusà, M. G., & Zanchi, A. (2015). Precollisional development and Cenozoic evolution of the Southalpine retrobelt (European Alps). *Lithosphere*, *7*(6), 662–681.

Zhao, L., Malusà, M. G., Yuan, H., Paul, A., Guillot, S., Lu, Y., et al. & CIFALPS Group, & AlpArray Working Group. (2020). Evidence for a serpentinized plate interface favoring continental subduction. *Nature Communications*, *11*, 2171. https://doi.org/10.1038/s41467-020-15904-7

Zhao, L., Paul, A., Guillot, S., Solarino, S., Malusà, M. G., Zheng, T., et al. (2015). First seismic evidence for continental subduction beneath the Western Alps. *Geology*, *43*(9), 815–818.

Zhao, L., Paul, A., Malusà, M. G., Xu, X., Zheng, T., Solarino, S., et al. (2016b). Continuity of the Alpine slab unraveled by high-resolution P wave tomography. *Journal of Geophysical Research*, *121*, 8720–8737.

Zhao, L., Paul, A., & Solarino, S. (2016a). RESIF 2016 Seismic network YP: CIFALPS temporary experiment (China–Italy–France Alps seismic transect). *RESIF – Réseau Sismologique et géodésique Français*. https://doi.org/10.15778/RESIF.YP2012

Zhu, H., & Tromp, J. (2013). Mapping tectonic deformation in the crust and upper mantle beneath Europe and the North Atlantic Ocean. *Science*, *341*(6148), 871–875.

Zhu, L. (2000). Crustal structure across the San Andreas Fault, southern California from teleseismic converted waves. *Earth and Planetary Science Letters*, *179*(1), 183–190.